Informes Técnicos Ciemat

1178
Agosto, 2009

Report on Thermo-Hydro-Mechanical Laboratory Tests Performed by CIEMAT on Febex Bentonite 2004-2008

M. V. Villar
R. Gómez-Espina

Departamento de Medio Ambiente

Toda correspondencia en relación con este trabajo debe dirigirse al Servicio de Información y Documentación, Centro de Investigaciones Energéticas, Medioambientales y Tecnológicas, Ciudad Universitaria, 28040-MADRID, ESPAÑA.

Las solicitudes de ejemplares deben dirigirse a este mismo Servicio.

Los descriptores se han seleccionado del Thesauro del DOE para describir las materias que contiene este informe con vistas a su recuperación. La catalogación se ha hecho utilizando el documento DOE/TIC-4602 (Rev. 1) Descriptive Cataloguing On-Line, y la clasificación de acuerdo con el documento DOE/TIC.4584-R7 Subject Categories and Scope publicados por el Office of Scientific and Technical Information del Departamento de Energía de los Estados Unidos.

Catálogo general de publicaciones oficiales
http://www.060.es

Depósito Legal: M -14226-1995
ISSN: 1135 - 9420
NIPO: 471-09-051-9

Editorial CIEMAT

CLASIFICACIÓN DOE Y DESCRIPTORES

S58
BENTONITE; TESTING; LABORATORY EQUIPMENT; RADIOACTIVE WASTE STORAGE; PERMEABILITY; HYDRAULIC CONDUCTIVITY;TEMPERATURE GRADIENTS.

Report on Thermo-Hydro-Mechanical Laboratory Tests Performed by CIEMAT on Febex Bentonite 2004-2008

Villar, M. V.; Gómez-Espina, R.
67 pp. 70 fig. 35 refs.

Abstract:

The results of the laboratory studies performed by CIEMAT with the FEBEX bentonite in the context of WP3.2 of the NF-PRO Project and of the Agreement ENRESA-CIEMAT Anexo V are presented and analysed in this report. They refer to the effect of the hydraulic gradient on the permeability of bentonite, the effect of the thermal gradient on the hydration kinetics of bentonite, and the repercussion of temperature on the hydro-mechanical properties of bentonite (swelling, permeability and water retention capacity). In all the cases the bentonite has been used compacted to densities expected in the engineered barrier of a high-level radioactive waste repository. The existence of threshold and critical hydraulic gradients has been observed, both of them dependent on bentonite density and water pressures. After more than seven years of hydration, the 40-cm high bentonite columns are far from full saturation, the thermal gradient additionally delaying the process, which is very slow. Temperatures below 100°C slightly decrease the swelling and the water retention capacity of the bentonite and increase its permeability. The information obtained improves the knowledge on the behaviour of expansive clay and will help the development of constitutive models and the interpretation of the results obtained in the mock-up and the in situ tests.

Informe sobre los Ensayos Termo-Hidro-Mecánicos Realizados en CIEMAT con la Bentonita Febex 2004-2008

Villar, M. V.; Gómez-Espina, R.
67 pp. 70 fig. 35 refs.

Resumen:

Se presentan y analizan los resultados de los trabajos de laboratorio llevados a cabo por CIEMAT con la bentonita FEBEX en el marco del WP3.2 del proyecto NF-PRO y del Acuerdo ENRESA-CIEMAT Anexo V. Se refieren al efecto del gradiente hidráulico sobre la permeabilidad de la bentonita, el efecto del gradiente térmico sobre la cinética de hidratación de la bentonita y a la influencia de la temperatura sobre las propiedades hidro-mecánicas de la bentonita (hinchamiento, permeabilidad y retención de agua). En todos los casos se ha utilizado la bentonita compactada a las densidades esperables en la barrera de ingeniería de un almacenamiento de residuos radiactivos de alta actividad. Se ha puesto de manifiesto la existencia de gradientes hidráulicos umbrales y críticos cuyos valores dependen de la densidad de la bentonita y de las presiones de agua. Columnas de bentonita de 40 cm de altura que se han estado hidratando durante más de siete años todavía están lejos de la saturación total, dada la lentitud del proceso, especialmente cuando hay un gradiente térmico. La temperatura por debajo de 100°C disminuye ligeramente la capacidad de hinchamiento y de retención de agua de la bentonita, y aumenta su permeabilidad. La información obtenida mejora el conocimiento sobre el comportamiento de la arcilla expansiva y ayudará al desarrollo de modelos constitutivos y a la interpretación de resultados obtenidos en ensayos en maqueta e in situ.

–CONTENTS–

REPORT ON THERMO-HYDRO-MECHANICAL LABORATORY TESTS PERFORMED BY CIEMAT ON FEBEX BENTONITE 2004-2008

1 INTRODUCTION

The design of high-level radioactive waste (HLW) repositories in deep geological media includes the construction of a barrier around the waste containers constituted by a sealing material. Bentonite has been chosen as sealing material in most disposal concepts because of its low permeability, swelling capacity and retention properties, among other features. The behaviour of a HLW repository is determined, to a large extent, by the characteristics of the design and construction of the engineered barriers and especially by the changes that may occur in the mechanical, hydraulic, and geochemical properties as a result of the combined effects of heat generated by the radioactive decay and of the water and solutes supplied by the surrounding rock. Therefore, it is considered of fundamental importance for the evaluation of long-term behaviour that the processes taking place in the near field be understood and quantified.

Thanks to the integration between the basic laboratory research and the work at different scales (up to the dimensions of a real repository gallery), the knowledge about the thermal, hydraulic and mechanical (THM) behaviour of the clay barrier under the conditions of a Deep Geological Repository has considerably improved. This integration has allowed the development, application and calibration of numerical models that consider in a coupled way the relevant processes that control the system performance. Thus, in the last years and in the context of various projects, different laboratory and numerical methods have been evaluated; a methodology has been developed to appropriately characterise the barrier material; a comprehensive data base for several bentonites (particularly the FEBEX and MX-80 bentonites) has been obtained, what has allowed the definition of the constitutive equations of the material; and the THM behaviour of the bentonite has been modelled, the main interaction processes being detected.

However, the same projects that allowed this progress in our knowledge of THM processes showed also that there were still processes and parameters that were not been taken properly into account: the effects of scale, the possible hydraulic threshold, the evolution of microstructure, the geochemical processes that modify the solid and the water interacting with THM properties, etc.

A series of processes that take place in the near field of a HLW repository relevant for the Performance Assesment exercises and that still were not well known was selected by CIEMAT for its study and evaluation in WP3.2 of NF_PRO. Taking into account those, the following objectives were proposed and intended to be accomplished by means of laboratory tests:

- To improve the understanding of water flow under low hydraulic gradients, determining the existence of threshold or critical gradients for different bentonite dry densities.

- To evaluate the parameters and processes influencing the hydration kinetics in the clay barrier and to understand it, especially with respect to its long-time evolution.

- To determine the impact of temperature on the hydro-mechanical properties of the bentonite and the reversibility of the modifications observed.

2 MATERIAL: THE FEBEX BENTONITE

The tests have been performed with a bentonite from the Cortijo de Archidona deposit (Almería, Spain) which was selected by ENRESA as suitable material for the backfilling and sealing of HLW repositories. It is the same clay material used in the FEBEX Project to manufacture the blocks of the mock-up (Madrid, Spain) and the *in situ* (Grimsel Test Site, Switzerland) tests. The processing at the factory consisted on disaggregation and gently grinding, drying at 60°C and sieving by 5 mm. This granulated material, without further treatment, has been used in all the tests described in this report.

The physico-chemical properties of the FEBEX bentonite, as well as its most relevant thermo-hydro-mechanical and geochemical characteristics obtained during the projects FEBEX I and II are summarised in the final reports of the project (ENRESA 2000, 2006) and are shown in detail in ENRESA (1998), Villar (2000, 2002), Lloret *et al*. (2002, 2004), Fernández (2003) and Missana *et al*. (2004). Several laboratories participated in these characterisation tasks. A summary of the results obtained is gathered below.

The mineralogical composition of the FEBEX bentonite was analysed by X-ray diffraction. The montmorillonite content is higher than 90 percent (92±3 %). The smectitic phases are actually made up of a smectite-illite mixed layer, with 10-15 percent of illite layers. Besides, the bentonite contains variable quantities of quartz (2±1 %), plagioclase (2±1 %), K-felspar, calcite and opal-CT (cristobalite-trydimite, 2±1 %). By weight from dense concentrates and SEM observation, the following minerals have been identified: mica (biotite, sericite, muscovite), chlorite, non-differentiated silicates (Al, K, Fe, Mg, Mn), augite-diopside, hypersthene, hornblende, oxides (ilmenite, rutile, magnetite, Fe-oxides), phosphates (apatite, xenotime, monacite) and other non differentiated minerals of titanium and rare earth. Their contribution to the bentonite composition is around 0.8 percent.

The mineralogical composition was also observed and quantified by optical microscopy study of thin sections. The textural heterogeneity itself is the main feature that can be described in the sample. The FEBEX bentonite is mainly composed of clay aggregates. The remaining elements of the texture are glassy materials, volcanic rock fragments and individual accessory minerals (quartz and felspars). Calcite is usually present as esparitic crystals replacing felspars, but it has been observed also as isolated micritic cements.

Table I shows the average content values of the exchangeable cations along with the cation exchange capacity (CEC), as determined by different methods and laboratories.

The chemical composition of an aqueous extract of bentonite/water ratio of 1/4 is presented in Table II. The content of chlorides and sulphates is worthy of mention.

Table I: Average values of exchangeable cations and cation exchange complex (CEC) as determined by different methods (meq/100g)

	CSIC-Zaidín[a]	CIEMAT[b]	CIEMAT[c]
Ca^{2+}	43 ± 5	42 ± 3	35 ± 2
Mg^{2+}	32 ± 3	32 ± 2	31 ± 3
Na^{+}	24 ± 4	25 ± 2	27 ± 0
K^{+}	2.1 ± 0.2	2.5 ± 0.3	2.6 ± 0.4
Sum of exchangeable cations	101 ± 4		96 ± 0
CEC[3]		102 ± 4	

[a]Determined by displacement by 1M NH_4AcO at pH 7 after washing of soluble salts (ENRESA 2000), the values are recalculated to give a sum of cations equal to CEC; [b]Determined by displacement by 0.5M $CsNO_3$ at pH 7 (Fernández 2003); [c]Determined by NaAcO/NH_4AcO pH=8.2 (ENRESA 2000)

Table II: Solubilised elements in the 1/4 bentonite/water aqueous extract as determined by two laboratories. Concentrations are related to the dry mass of clay (mmol/100 g, dried at 110ºC)

	pH	Cl^-	SO_4^{2-}	HCO_3^-	Na^+	K^+	Mg^{2+}	Ca^{2+}	Al^{3+}	SiO_2
CIEMAT[a]	8.73	1.98	0.98	1.18	5.02	0.073	0.055	0.050	0.013	0.145
UAM[b]	7.93	2.03	1.84	1.56	6.04	0.062	0.146	0.067		

[a]Fernández 2003. Sr^{2+} and Fe^{3+} were found in concentrations lower than 10^{-3} mmol/100g
[b]ENRESA 2000. As, V, Br, Sr, Ti, Mn, Fe, Ni, Cu, Zn and Y in concentrations lower than 10^{-3} mmol/100g

The liquid limit of the bentonite is 102±4 percent, the plastic limit 53±3 percent, the specific gravity 2.70±0.04, and 67±3 percent of particles are smaller than 2 μm. The hygroscopic water content in equilibrium with the laboratory atmosphere (relative humidity 50±10 %, temperature 21±3 °C, total suction about 100 MPa) is 13.7±1.3 percent. The value obtained for the external specific surface area using nitrogen adsorption technique (single point BET method) is 32±3 m^2/g and the total specific surface area obtained using the Keeling hygroscopicity method is about 725 m^2/g. The analysis of the mercury intrusion data reveals that the intra-aggregate pores (smaller than 0.006 μm) represent the 73-78 percent of total pore volume when the bentonite is compacted at a dry density of 1.7 g/cm^3.

The saturated hydraulic conductivity to deionised water (k_w, m/s) of samples of untreated FEBEX bentonite compacted at different dry densities is exponentially related to dry density (ρ_d, g/cm^3). A distinction may be made between two different empirical fittings depending on the density interval:

for dry densities of less than 1.47 g/cm^3:

$$\log k_w = -6.00\ \rho_d - 4.09 \quad [1]$$

for dry densities in excess of 1.47 g/cm^3:

$$\log k_w = -2.96\ \rho_d - 8.57 \quad [2]$$

The determinations were done at room temperature. The variation in the experimental values with respect to these fittings is smaller for low densities than it is for higher values, with an average –in absolute values– of 30 percent.

The swelling pressure (P_s, MPa) of FEBEX samples compacted with their hygroscopic water content and flooded with deionised water up to saturation at room temperature and constant volume conditions can be related to dry density (ρ_d, g/cm^3) through the following equation:

$$\ln P_s = 6.77\ \rho_d - 9.07 \qquad [3]$$

In this case, the difference between experimental values and this fitting is, on average, 25 percent. This dispersion, which is wider for higher dry densities, is due both to the natural variability of bentonite and to the measurement method used, which does not allow high degrees of accuracy.

In unconfined conditions, the relationship between suction (s, MPa) and water content (w, %) changes, taking into account the initial dry density (ρ_{d0}, g/cm^3), may be fitted to the following equation:

$$w = (45.1\ \rho_{d0}\text{-}39.2) - (18.8\rho_{d0}\text{-}20.34) \log s \qquad [4]$$

The retention curve of the bentonite was also determined in samples compacted to different dry densities under different temperatures (Lloret *et al*. 2004, Villar & Lloret, 2004). The volume of the samples remained constant during the determinations, since they were confined in constant volume cells. To impose the different relative humidities, *i.e*. total suctions, the cells were placed in desiccators with sulphuric acid solutions of various concentrations. The data from these laboratory determinations are shown in Figure 1. Following an approach similar to that presented by Sánchez (2004) to fit the data from these laboratory determinations, the empirical Equation 4 can be obtained:

$$w = (a + b\,n)\left[1 + \left(\frac{s}{P_0\, e^{-\eta(n-n_0)}\, e^{-\alpha(T-T_0)}}\right)^{\frac{1}{1-\lambda}}\right]^{-\lambda} \qquad [5]$$

where w is the water content in percentage, n the porosity, s the suction in MPa, and T the temperature in ºC. The values of parameters a, b, P_0, η, n_0, α, T_0 and λ are indicated in Table III. The differences between measured values and the estimated values using Equation 5 are smaller than 2 percent in terms of water content. This equation has been modified with the results obtained in this investigation, as shown in section 5.3.4.

Table III: Values of parameters in Equation 5

a	b	P_0 (MPa)	λ	η	n_0	α (1/ºC)	T_0 (ºC)
10.96	41.89	12.68	0.211	7.97	0.4	0.00647	20

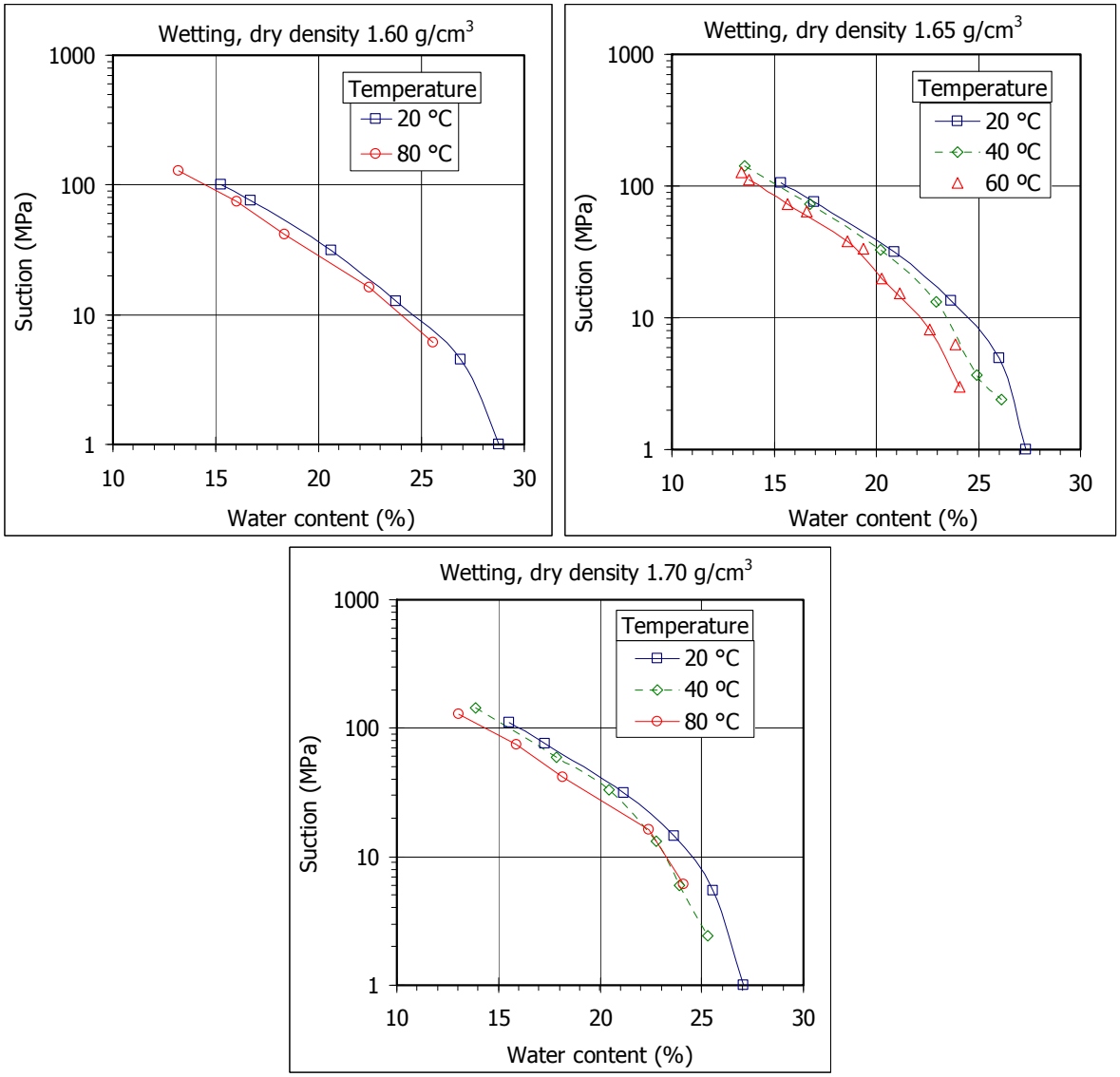

Figure 1: Water retention curves at different temperatures and for different bentonite densities obtained during the FEBEX project

The thermal conductivity (λ, W/m·K) of the compacted bentonite at laboratory temperature is related to the degree of saturation (S_r) through the following expression:

$$\lambda = \frac{A_1 - A_2}{1 + e^{(S_r - x_0)/dx}} + A_2 \qquad [6]$$

where A_1 represents the value of λ for S_r=0, A_2 the value of λ for S_r=1, x_0 the degree of saturation for which thermal conductivity is the average of the two extreme values and dx is a parameter. This equation was chosen because it accurately represents the behaviour of conductivity versus water content (degree of saturation), which are directly related but not in a linear fashion (Villar 2000, 2002). The empirical fitting obtained, with r^2 of 0.923, gives the following values for each parameter:

$$A_1 = 0.57 \pm 0.02$$
$$A_2 = 1.28 \pm 0.03$$
$$x_0 = 0.65 \pm 0.01$$
$$dx = 0.100 \pm 0.016$$

Some isothermal infiltration tests and heat flow tests at constant overall water content were performed during FEBEX I project and they were backanalysed using CODEBRIGHT (Lloret *et al*. 2002, Pintado *et al*. 2002). It is possible to fit the experimental data using a cubic law for the relative permeability ($k_r = S_r^3$) and a value of 0.8 for the tortuosity factor (τ).

3 EFFECT OF HYDRAULIC GRADIENT ON BENTONITE PERMEABILITY

3.1 Introduction

The application of Darcy's law for the calculation of the coefficient of permeability requires that the velocity of the flow be proportional to the hydraulic gradient, that is to say, that the value of the coefficient obtained be independent of the hydraulic gradient applied during the determination. This means that the relationship between flow and hydraulic gradient is linear, and that this linear relationship crosses the origin (Figure 2). For different reasons, this condition may not be fulfilled, thus invalidating the use of Darcy's expression. Furthermore, the values of bentonite permeability are frequently obtained under high hydraulic gradients, necessary to induce a measurable flow in such low permeability materials.

In fact, the values of hydraulic head applied to determine Equation 1 and Equation 2 were between 7000 cm, for clay dry densities of 1.30 g/cm^3, and 66000 cm, for dry densities of 1.84 g/cm^3. The backpressure applied in all the cases was of 6000 cm (600 kPa). Taking into account that the length of the specimen is 2.5 cm, the average hydraulic gradient was 15200. All the samples were tested with at least two different hydraulic gradients suitable for their dry density, in other words, sufficiently high so as to provide a measurable flow. The values of hydraulic conductivity obtained during FEBEX I for the two hydraulic gradients applied in each test are represented in Figure 3 (Villar 2000). The points joined by lines correspond to the same test; *i.e*. to the measurements performed on a specific sample of a given dry density. It may be observed that, although there may be some difference between the value of conductivity obtained with the different gradients for the same sample, such variations are probably the result of the experimental method, since there is no trend for one variable with respect to the other. This would confirm the independence of the flow observed from the hydraulic gradient applied, and therefore the validity of Darcy's law for the calculation of the coefficient of permeability, at least in the range of gradients that was considered (Lloret *et al*. 2004).

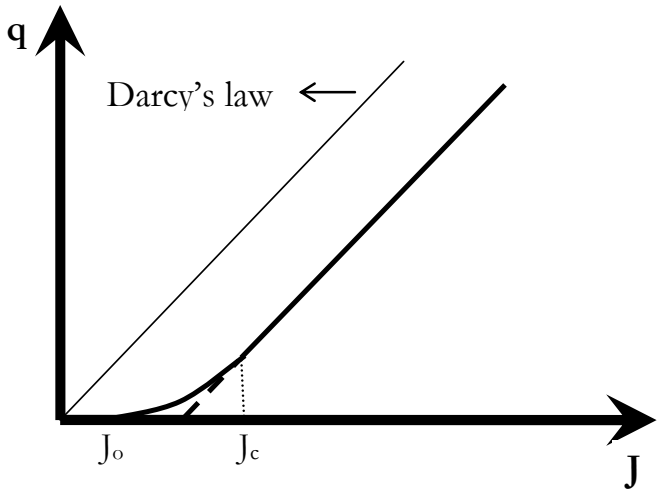

Figure 2: Relationship between flow (q) and hydraulic gradient (J) according to Darcy's law and possible deviations (J_o: threshold gradient; J_c: critical gradient)

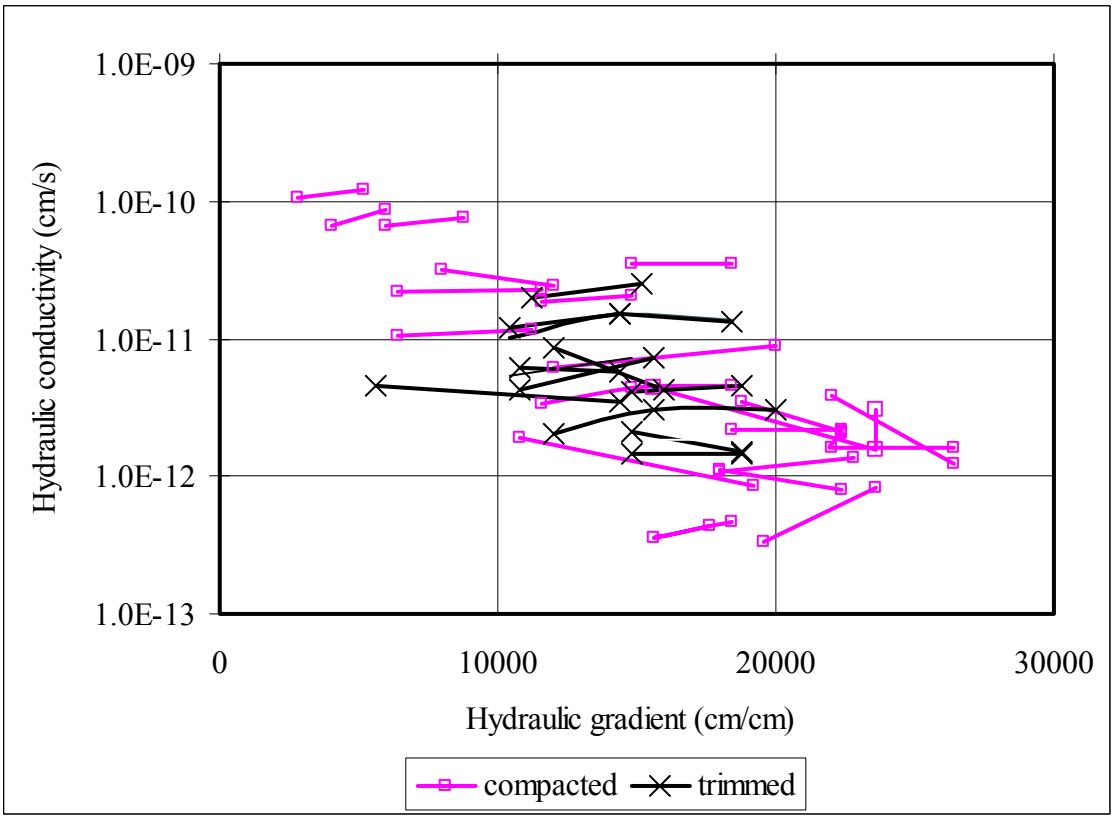

Figure 3: Variation in hydraulic conductivity obtained for different samples versus the hydraulic gradient applied for its determination as a function of the kind of sample preparation (points joined by lines correspond to the same sample) (Lloret *et al.* 2004)

It may also be appreciated in Figure 3 that, as the permeability of the sample decreases, *i.e.* as its dry density increases, the value of the hydraulic gradients applied for performance of the measurement increases, this being necessary in order to be able to measure very low flows. However, it was not possible to determine whether no flow occurs in the case of lower hydraulic gradients, or whether it is simply not possible to measure it with the available

technique. Consequently, it was not established whether or not the critical hydraulic gradient pointed out by several authors exists, below which the relation between flow and gradient in clays deviates from linearity (Figure 2, Olsen 1962, Yong *et al*. 1986). If a threshold gradient exists, it would be lower for samples of lower dry density. This would appear to be confirmed by the fact that lower hydraulic gradients need to be applied in samples with lower dry densities, although as explained above, this might be due simply to the fact that for these densities flows are larger and easier to measure.

In order to deepen in the investigation of the existence of a threshold gradient, the values of flow rate for the two hydraulic gradients applied in each of the tests mentioned above were plotted in Figure 4 and Figure 5, the latter being an enlargement of the former. Again, the points joined by lines correspond to the same test; *i.e*. to the measurements performed on a specific sample of a given dry density. If we assume that the relationship between gradient and flow is linear, and we extrapolate these lines towards flow 0, despite the variation found among the different tests, we would observe a trend to find gradients higher than 0 to have a measurable flow, around 5000, and even higher in the case of the highest densities (Figure 5). However, this aspect should be confirmed with more refined and specific tests.

To clarify the effect of hydraulic gradient on the value of hydraulic conductivity, the hydraulic conductivity of FEBEX clay samples has been measured under low hydraulic gradients and injection pressures. The methodology followed and the results obtained are presented below.

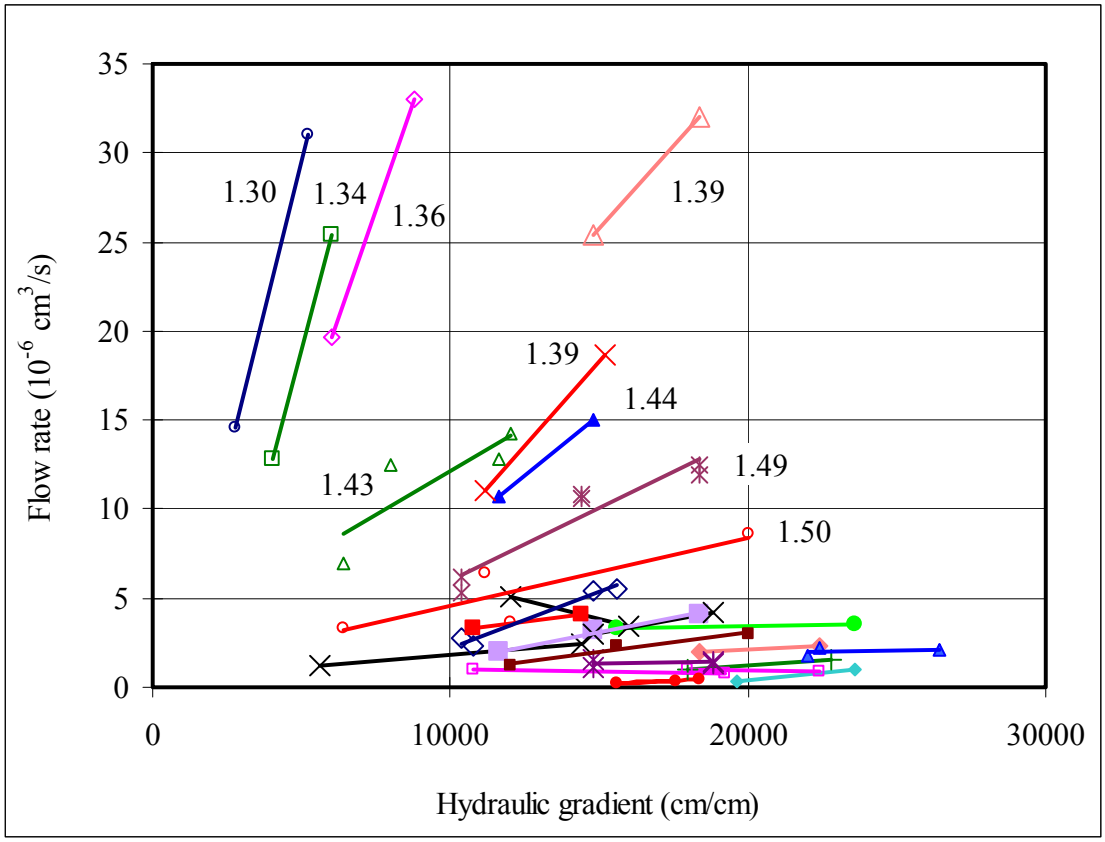

Figure 4: Variation in flow rate obtained for different samples versus hydraulic gradient (points joined by lines correspond to the same specimen, whose dry density is indicated in g/cm^3) (Lloret *et al.* 2004)

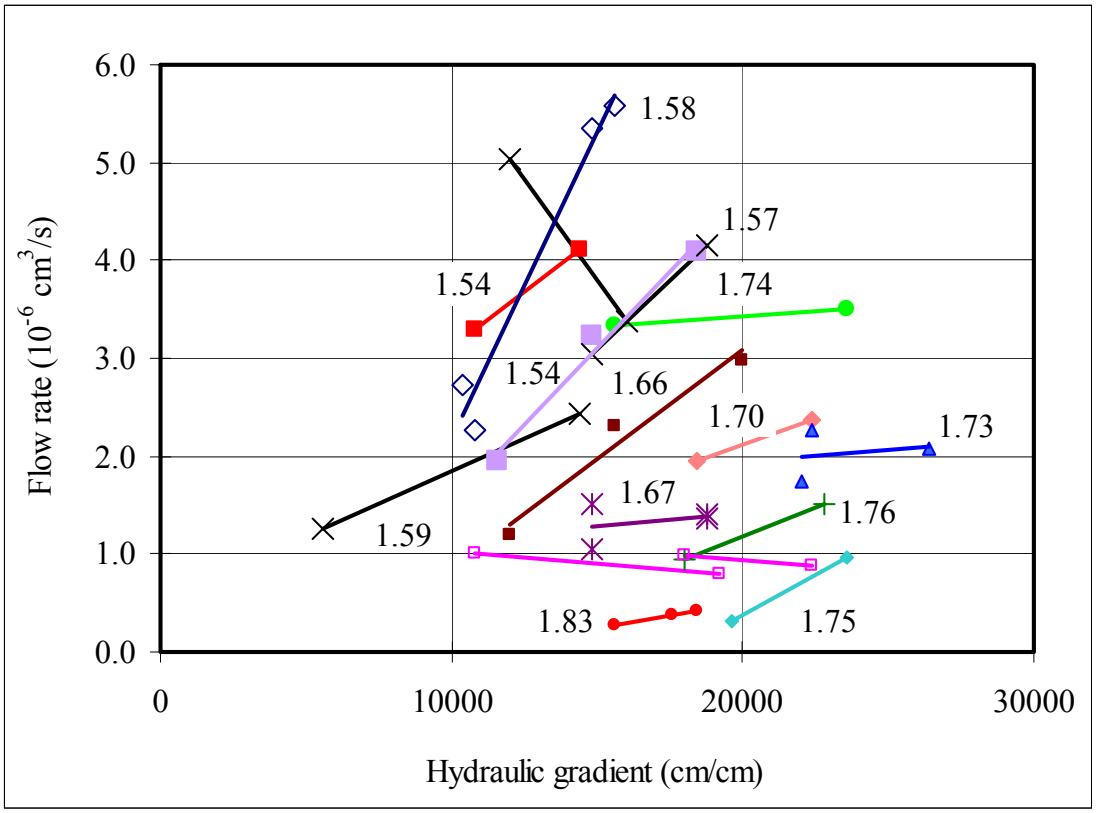

Figure 5: Variation in flow rate obtained for different samples of high density versus hydraulic gradient (points joined by lines correspond to the same specimen, whose dry density is indicated in g/cm^3) (Lloret *et al.* 2004)

3.2 Methodology

The granulated clay with its hygroscopic water content was compacted inside stainless steel cells by applying uniaxial pressure, the dimensions of the specimens being 5.0 cm in diameter and 2.5 cm in height.

The sample is saturated with deionised water injected at a pressure of 0.6 MPa by the upper and lower surfaces through porous stones. An automatic pressure/volume controller manufactured by GDS Instruments Limited is used to saturate the sample. Once the specimen is saturated, a pressure/volume controller is connected to the bottom inlet and another one to the upper outlet (Figure 6). These controllers allow the fixing of pressure with an accuracy of 1 kPa and the measurement of water volume changes resolved to 1 mm^3. Other kind of devices –such as hydraulic pumps– have also been used to keep pressure. To measure the water outflow automatic volume change apparatuses have been used in some occasions. A combination of different pressures was applied in order to obtain different hydraulic gradients, the pressure at the bottom of the sample being always higher than on top. Every hydraulic gradient is kept up to stabilisation of the outflow. To calculate hydraulic conductivity (k_w) Darcy's law is applied, using the water outflow (J) measured in the upper outlet by the automatic pressure/volume controller in a long period of time in which the water flow is constant:

$$k_w = \frac{J \times l}{A \times \Delta P} \qquad [7]$$

where ΔP is the hydraulic head in cm of water, A is the surface area of the cell (19.63 cm^2) and l the length of the specimen (2.50 cm).

At the end of the test, the sample is weighed, measured and oven-dried at 110°C to check the actual water content and dry density.

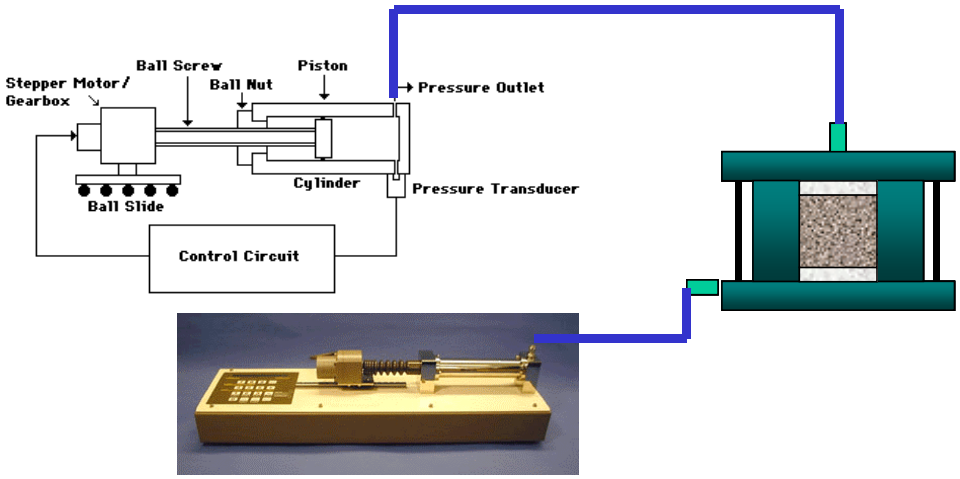

Figure 6: Setup for the measurement of permeability under low hydraulic gradients

3.3 Results

Three tests to determine the permeability under low hydraulic gradients have been finished, for dry densities of 1.40 (2 tests) and 1.50 g/cm^3. Tests with samples of dry density 1.55 and 1.65 g/cm^3 are in course. A summary of the tests performed and in course is shown in Table IV. The hydraulic gradients applied range from 200 to 2400 and the injection pressures, from 200 to 7200 kPa. These hydraulic gradients are much lower than the ones used to determine Equations 1 and 2, which were between 7000 and 66000.

The permeability coefficients have been computed from the water outflow, which is the standard procedure. However, in some cases they have also been calculated from the water inflow, just in order to check if the values obtained are similar, which should be the case if the samples are fully saturated.

In the figures shown below and corresponding to the results of these tests, the temperature indicated corresponds to the average value in the laboratory during each determination. The time indicated is the time elapsed since the sample was put into the cell for saturation.

Table IV: Summary of the permeability tests performed under low hydraulic gradients (hygroscopic initial water content)

Reference	Nominal ρ_d (g/cm^3)	Actual ρ_d (g/cm^3)	Compaction P (MPa)	Final w (%)	Final S_r (%)	Duration (days)
Grad1.4	1.40	1.40	4.8	37.0	108	564
Grad1.4_2	1.40	1.37	6.6	38.6	107	573
Grad1.5	1.50	1.49	8.8	33.2	111	416
Grad1.55	1.55		5.5			>1500
Grad1.65	1.65		21.3			>1500

3.3.1 Dry density 1.4 g/cm^3

The results of a test performed with a sample of nominal dry density 1.40 g/cm^3 (test Grad1.4) are shown in Figure 7. A uniaxial pressure of 4.8 MPa was applied to manufacture the sample. The actual dry density of the specimen –checked after disassembling– was 1.40 g/cm^3 and the final water content was 37.0 percent, what gives a final degree of saturation of 108 percent.

The hydraulic gradients applied were between 200 and 2400, with maximum injection pressures of 1200 kPa, and the average value of permeability found was $5.0 \cdot 10^{-13}$ m/s. This value is in the order of the value obtained using Equation 1 ($3.2 \cdot 10^{-13}$ m/s). Table V summarises the results of the measurements performed. It was not possible to get a measurable flow for hydraulic gradients below 200 if the injection pressure was lower than 350-400 kPa. There is not a clear trend of the values as a function of the hydraulic gradients applied in the measurement (Figure 7). Flow shows an approximately linear relation with hydraulic gradient, although with a large dispersion for gradients below 1000.

Test Grad1.4 went on for 564 days, but no trend of permeability over time was found (Figure 8). However, the repercussion of the laboratory temperature on the values obtained is noticeable.

Table V: Minimum injection pressures and hydraulic gradients applied to get measurable flow and permeabilities obtained in test Grad1.4 for different backpressures

Backpressure (kPa)	Minimum injection pressure (kPa)	Minimum hydraulic gradient	k_w (m/s)
300	350	200	$7.3 \cdot 10^{-13}$
350	<450	<400	$2.1 \cdot 10^{-13}$
400	<450	<200	$2.5 \cdot 10^{-13}$
600	<1000	<1600	$5.8 \cdot 10^{-13}$

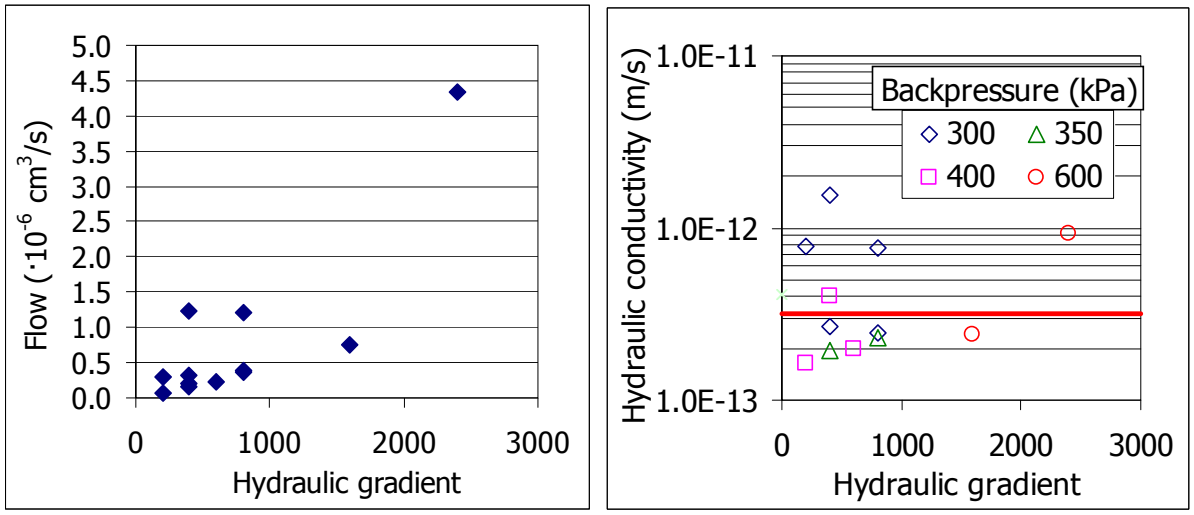

Figure 7: Flows and hydraulic conductivity obtained under low hydraulic gradients for a FEBEX sample compacted at nominal dry density 1.40 g/cm^3 (test Grad1.4). The horizontal line stands for the value obtained during FEBEX I with higher pressures

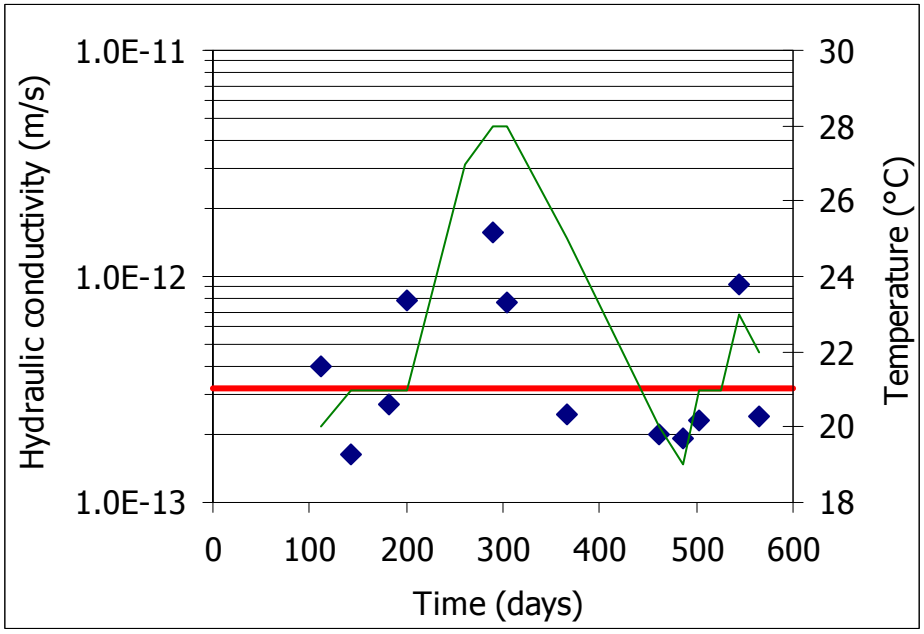

Figure 8: Evolution over time of the hydraulic conductivity measured under different low hydraulic gradients of a specimen of FEBEX clay compacted at dry density 1.40 g/cm^3 (test Grad1.4). The temperature during the determination is indicated by a continuous line. The horizontal line stands for the value obtained during FEBEX I with higher pressures

Another test with the same nominal dry density has been finished (test Grad1.4_2). A uniaxial pressure of 6.6 MPa was applied to manufacture this sample. The actual dry density of the specimen –checked after disassembling– was 1.37 g/cm^3 and the final water content was 38.6 percent, what gives a final degree of saturation of 107 percent.

The hydraulic gradients applied were between 200 and 2000, with maximum injection pressures of 800 kPa, and the average value of permeability found was $6.6 \cdot 10^{-13}$ m/s. This value is consistent with those obtained in test Grad1.4 and it is only slightly higher than the value obtained using Equation 1 ($4.9 \cdot 10^{-13}$ m/s). Table VI shows the injection pressures and

hydraulic gradients that had to be applied to get measurable flow for different backpressures, along with the average hydraulic conductivity values obtained for each backpressure. It was not possible to get a measurable flow for hydraulic gradients below 400 if the injection pressure was lower than 550-600 kPa. The values of hydraulic conductivity and flow measured are shown in Figure 9, where the linear relationship between flow and hydraulic gradient can be observed, what confirms the validity of Darcy's law in this range of pressures. Consequently, there is not a clear trend of the permeability values as a function of the hydraulic gradients applied in the measurement. Another measurement was performed at the end of the test under a hydraulic gradient similar to those applied during FEBEX I, 5333, and an injection pressure of 600 kPa. The hydraulic conductivity value obtained was $5.4 \cdot 10^{-13}$ m/s, *i.e.* in the order of the values obtained under lower hydraulic gradients.

Table VI: Minimum injection pressures and hydraulic gradients applied to get measurable flow and permeabilities obtained in test Grad1.4_2 for different backpressures

Backpressure (kPa)	Minimum injection pressure (kPa)	Minimum hydraulic gradient	k_w (m/s)
300	500	800	$6.9 \cdot 10^{-13}$
400	600	800	$5.1 \cdot 10^{-13}$
450	550	400	$6.8 \cdot 10^{-13}$
500	600	400	$7.4 \cdot 10^{-13}$
550	>600	>200	

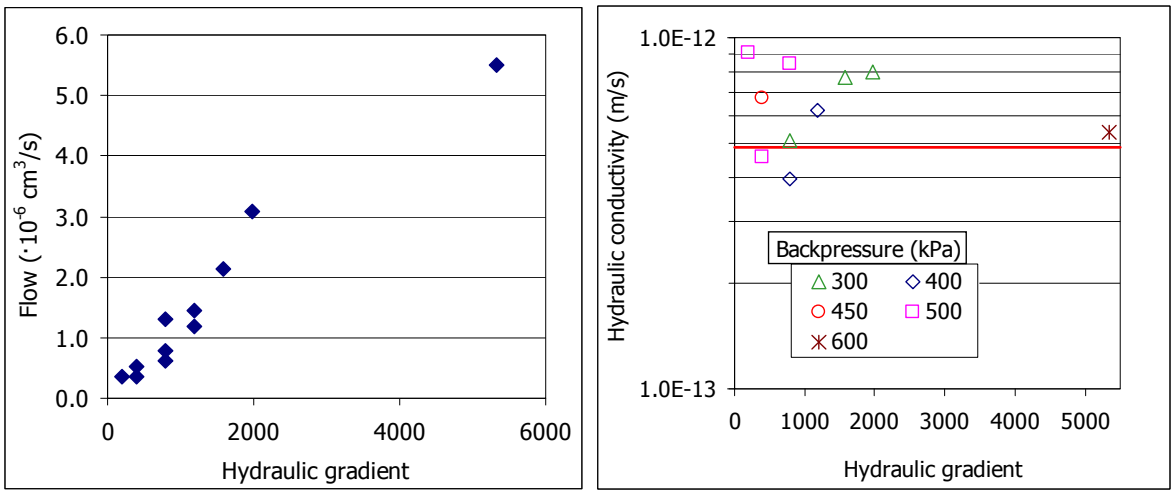

Figure 9: Flows and hydraulic conductivity obtained under low hydraulic gradients for a FEBEX sample compacted at nominal dry density 1.40 g/cm^3 (test Grad1.4_2).The horizontal line stands for the value obtained during FEBEX I with higher pressures

Test Grad1.4_2 went on for 573 days, but no steady evolution of permeability over time was found (Figure 10). The hydraulic conductivity has been also calculated using the water inflow values, and the values thus obtained are plotted in the figure as well. It can be observed that, up to 300 days of testing, the values calculated from the inflow were higher than those calculated from the outflow. Afterwards, both values are similar, what points to a perfect saturation of the clay.

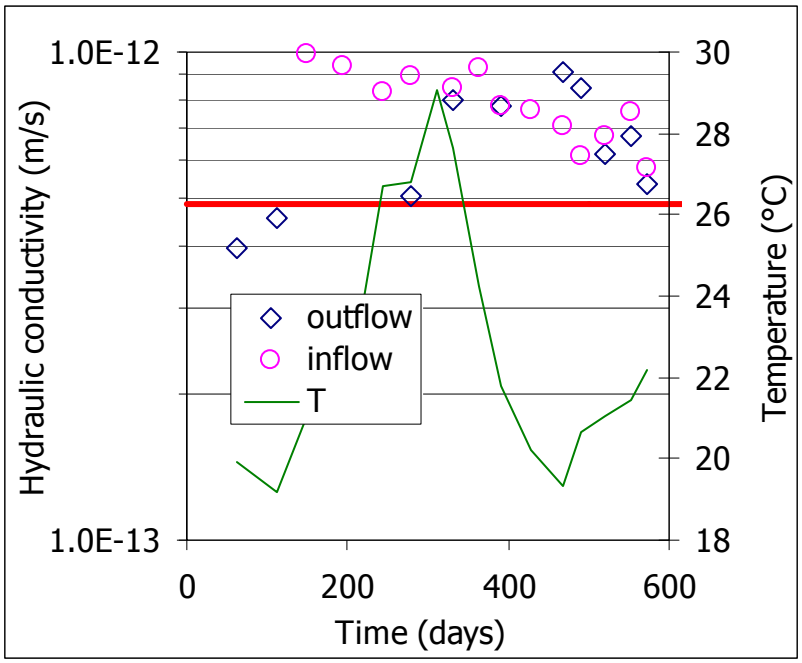

Figure 10: Evolution over time of hydraulic conductivity measured under different low hydraulic gradients of a specimen of FEBEX clay compacted at dry density 1.40 g/cm^3 as computed by using the water inflow or outflow (test Grad1.4_2). The horizontal line stands for the value obtained during FEBEX I with higher pressures

3.3.2 Dry density 1.5 g/cm^3

A uniaxial pressure of 9 MPa was applied to manufacture a sample of nominal dry density 1.50 g/cm^3 in a test done during FEBEX II (test Grad1.5). The actual dry density of the specimen was 1.49 g/cm^3 and the final water content was 33 percent, what gives a final degree of saturation of 111 percent. Test Grad1.5 went on for more than 400 days. The hydraulic gradients applied were between 200 and 600, with maximum injection pressures of 650 kPa. Six different combinations of injection and backpressures were applied, but outward flow was obtained only for an injection pressure of 550 kPa and a hydraulic gradient of 600. The hydraulic conductivity value obtained in this case was of $1.1 \cdot 10^{-13}$ m/s, which is in the order of the expected hydraulic conductivity value for the same dry density obtained with Equation 2, *i.e.* with higher hydraulic gradients. For lower injection pressures or hydraulic gradients no outflow occurred.

3.3.3 Dry density 1.55 g/cm^3

The results of a test that is being performed with a sample of nominal dry density 1.55 g/cm^3 (test Grad1.55) are shown in Figure 11. A uniaxial pressure of 5.5 MPa was applied to manufacture this sample.

The hydraulic gradients applied have been between 200 and 7200, with maximum injection pressures of 2400 kPa, and the average value of permeability found is $3.7 \cdot 10^{-14}$ m/s. The expected hydraulic conductivity value for the same dry density obtained with Equation 2, *i.e.* with higher hydraulic gradients, is $6.9 \cdot 10^{-14}$ m/s. The results in terms of flow and hydraulic conductivities obtained are plotted in Figure 11. It seems that the relation between hydraulic gradient and flow is different for hydraulic gradients above and below 3000. The results point

to an increase in hydraulic conductivity with hydraulic gradient. For backpressures of between 350 and 600 kPa it is necessary to apply an injection pressure of 900 to get outwards measurable flow, whereas for a backpressure of 300 kPa an injection pressure of 700 kPa is enough to measure outflow, and even lower if the backpressure is 250 kPa (Table VII).

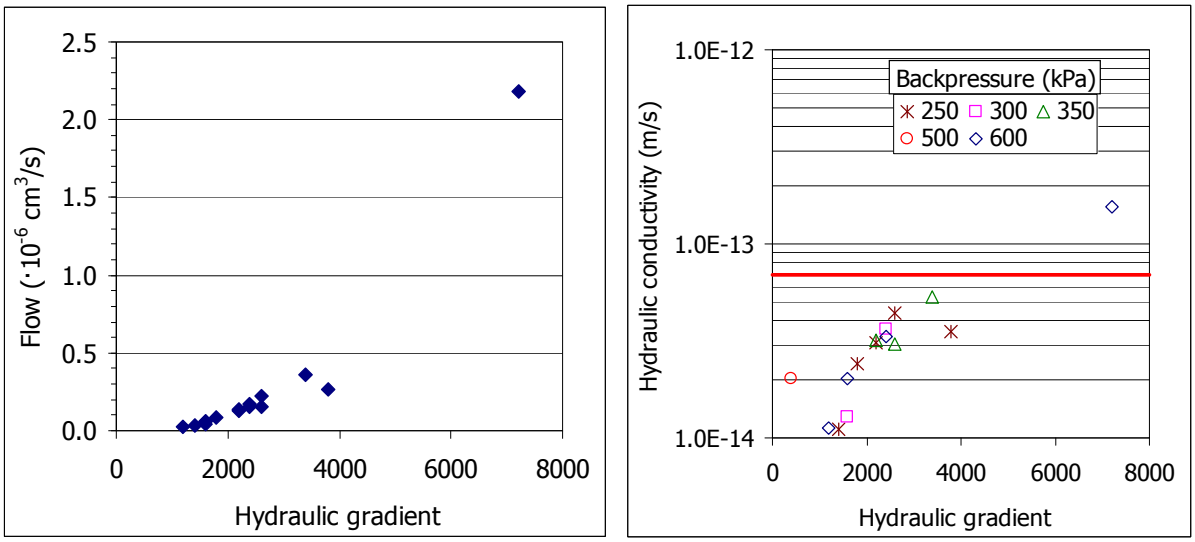

Figure 11: Flows and hydraulic conductivity obtained under low hydraulic gradients for a FEBEX sample compacted at nominal dry density 1.55 g/cm^3 (test Grad1.55). The horizontal line stands for the value obtained during FEBEX I with higher pressures

Table VII: Minimum injection pressures and hydraulic gradients applied to get measurable flow and permeabilities obtained in test Grad1.55 for different backpressures

Backpressure (kPa)	Minimum injection pressure (kPa)	Minimum hydraulic gradient	k_w (m/s)
250	<600	<1400	$2.9 \cdot 10^{-14}$
300	700	1600	$2.5 \cdot 10^{-14}$
350	900	2200	$3.9 \cdot 10^{-14}$
500	900	1602	$2.0 \cdot 10^{-14}$
600	900	1200	$5.4 \cdot 10^{-14}$

Test Grad1.55 has been going on for more than 1650 days, but no steady evolution of permeability over time has been found (Figure 12). The permeability coefficient has been calculated also using the water inflow instead of the outflow. The values obtained in both cases are plotted in the Figure. Those obtained from the outflow measurements are always lower, although the difference between both has decreased over time.

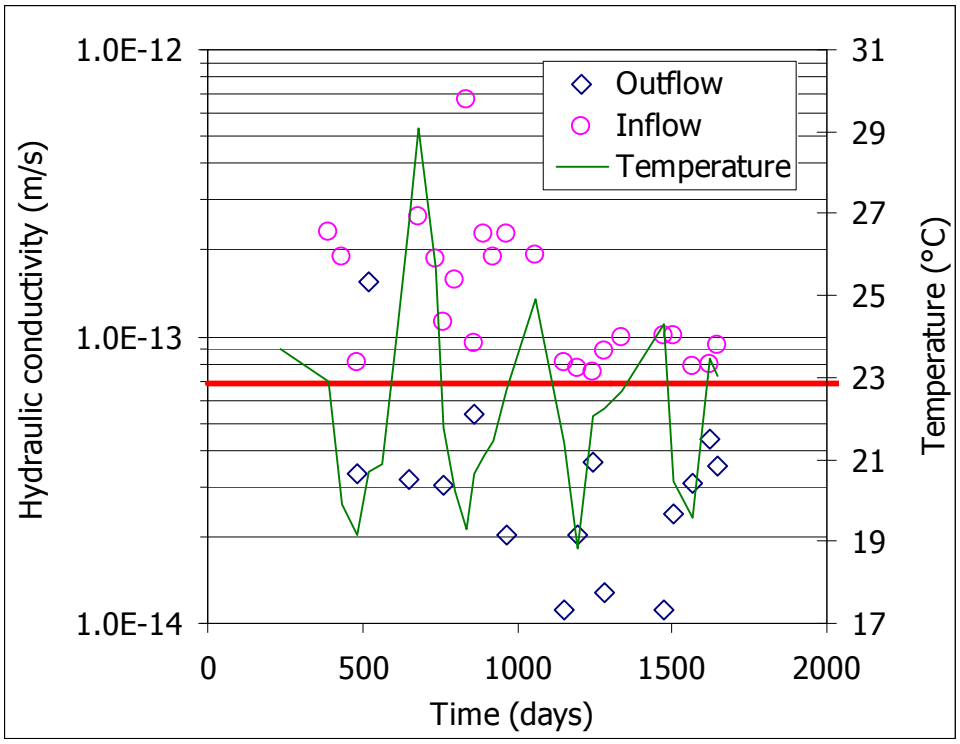

Figure 12: Evolution over time of the hydraulic conductivity measured under different low hydraulic gradients of a specimen of FEBEX clay compacted at nominal dry density 1.55 g/cm^3 as computed by using the water inflow or outflow (test Grad1.55). The horizontal line stands for the value obtained during FEBEX I with higher pressures

3.3.4 Dry density 1.65 g/cm^3

The results of a test that is being performed with a sample of nominal dry density 1.65 g/cm^3 (test Grad1.65) are shown in Figure 13. A uniaxial pressure of 21 MPa was applied to manufacture the specimen.

The hydraulic gradients applied have been between 400 and 7200, with maximum injection pressures of 2400 kPa, and the average value of permeability found is $2.8 \cdot 10^{-14}$ m/s. This is in the order of the expected hydraulic conductivity for the same dry density obtained with Equation 2, *i.e.* with higher hydraulic gradients, which is $3.5 \cdot 10^{-14}$ m/s. The flows measured do not show a clear linear relation with hydraulic gradient, and there is neither a relation between hydraulic gradient and permeability (Figure 13), although it seems that the permeability value obtained increases for high injection pressures. Table VIII shows the minimum injection pressures and hydraulic gradients that had to be applied in order to get measurable flows for each backpressure used, as well as the average of the hydraulic conductivities measured for each backpressure. No flow was recorded for hydraulic gradients smaller than 800-1000 if the injection pressure was lower than 500 kPa.

Test Grad1.65 has been going on for more than 1650 days, but no trend of permeability with time has been found, although the dispersion is of up to one order of magnitude (Figure 14). In addition, the permeability coefficient has also been calculated sometimes using both the water inflow and the outflow. The values obtained in both cases are plotted in the Figure. Those obtained from the outflow measurements are always higher, about one order of magnitude. In some cases no outflow has been recorded, but the inflow was high enough to compute a permeability value.

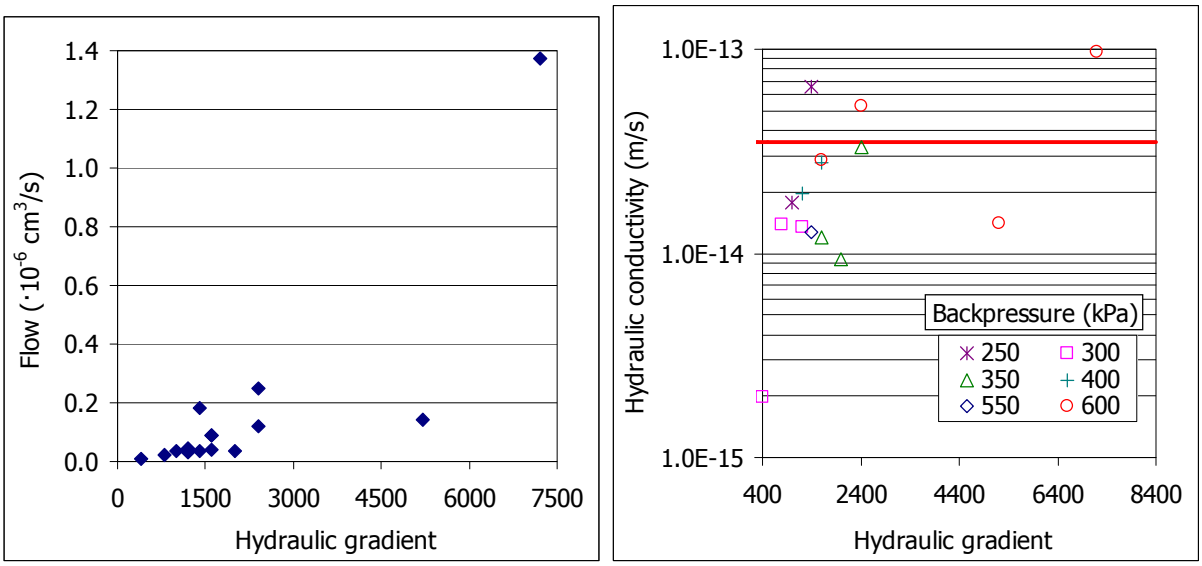

Figure 13: Flows and hydraulic conductivity obtained under low hydraulic gradients for a FEBEX sample compacted at nominal dry density 1.65 g/cm^3 (test Grad1.65). The horizontal line stands for the value obtained during FEBEX I with higher pressures

Table VIII: Minimum injection pressures and hydraulic gradients applied to get measurable flow and permeabilities obtained in test Grad1.65 for different backpressures

Backpressure (kPa)	Minimum injection pressure (kPa)	Minimum hydraulic gradient	k_w (m/s)
250	500	1000	$4.2 \cdot 10^{-14}$
300	500	800	$9.8 \cdot 10^{-15}$
350	750	1600	$1.8 \cdot 10^{-14}$
400	700	1200	$2.4 \cdot 10^{-14}$
550	900	1400	$1.3 \cdot 10^{-14}$
600	1000	1600	$4.8 \cdot 10^{-14}$

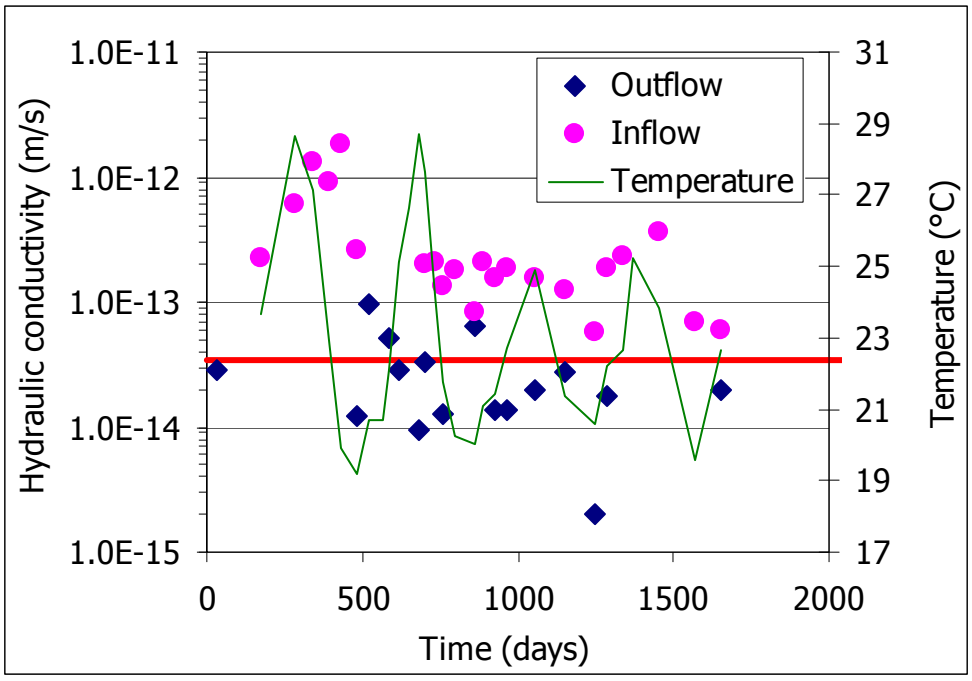

Figure 14: Evolution over time of the hydraulic conductivity measured under different low hydraulic gradients of a specimen of FEBEX clay compacted at nominal dry density 1.65 g/cm^3 as computed by using the water inflow or outflow (test Grad1.65). The horizontal line stands for the value obtained during FEBEX I with higher pressures

3.4 Summary and discussion

Up to now only three of the tests presented have been finished and disassembled, so the conclusions drawn must be taken as preliminary. From the results obtained, the following remarks can be made:

- Some of the tests have been going on for more than 1650 days, and no clear evolution of permeability with time has been observed in any of them.

- Since the tests have been carried out at laboratory temperature, which may vary between 18 and 29°C, the effect of temperature on the permeability coefficient has been sometimes noticeable for the lowest density tests (1.4 g/cm^3).

- The average hydraulic conductivity values obtained are in the order of those obtained for the same dry densities applying higher hydraulic gradients, *i.e.* obtained with Equations 1 and 2.

- In most of the tests, the permeability coefficient obtained is different if it is computed using the inflow or the outflow, being always lower in the last case. The difference between both values seems lower when the density of the bentonite is lower and decreases over time. This fact could be an indication of lack of full saturation, although the tests have been running for hundreds of days and the specimens are only 2.5 cm in height. The usual procedure followed to calculate permeability is to use the outflow measurement.

- All the permeability values obtained are plotted as a function of the hydraulic gradient in Figure 15. For the low density no trend becomes evident for the range of hydraulic gradients tested, although for the highest densities a slight trend to find higher hydraulic conductivities as the hydraulic gradient increases is observed.

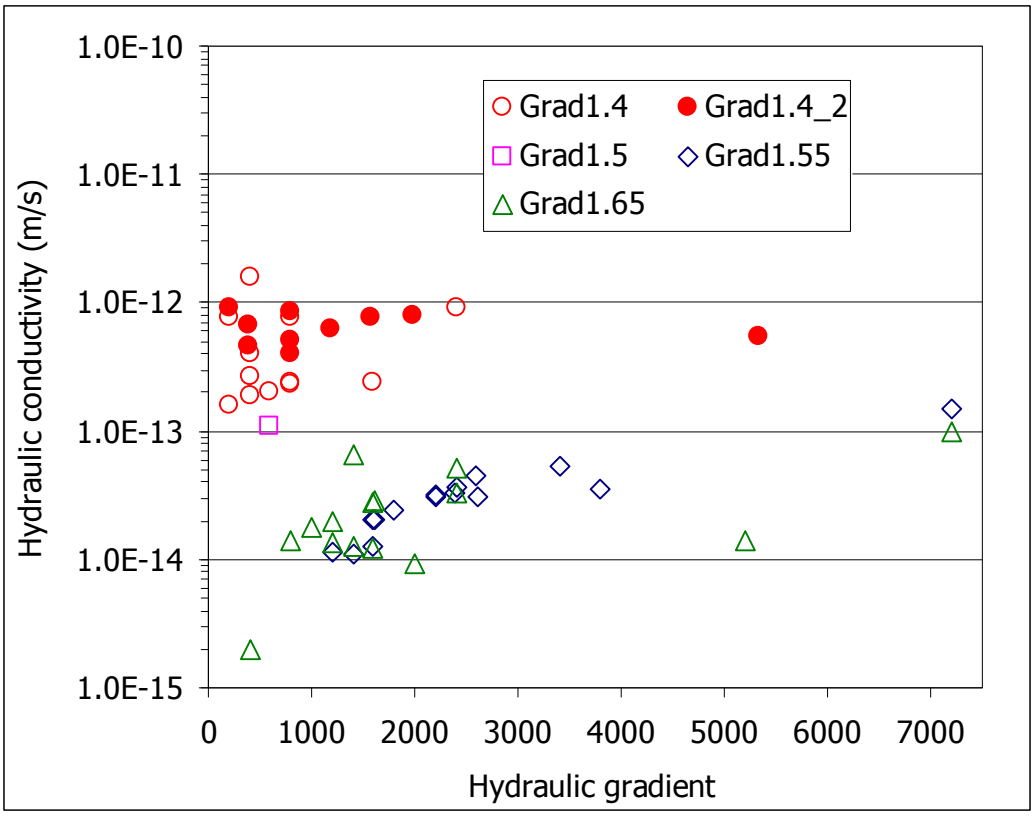

Figure 15: Hydraulic conductivity measured in compacted FEBEX bentonite (the test references in the legend include the densities, indicated in g/cm^3) as a function of the hydraulic gradients applied

- If the results obtained are plotted in terms of flow (cm^3/s) as a function of hydraulic gradient (Figure 16), the dispersion of data does not allow checking the proportionality between flow and hydraulic gradient that would prove the validity of Darcy's law, except for the lowest dry density (tests Grad1.4 and Grad1.4_2). Figure 17 shows again the same values along with those obtained during FEBEX under higher hydraulic gradients for samples of the same dry density, taken from Figure 4. The overall proportionality between flow and hydraulic gradient becomes clearer now. The dispersion found when hydraulic gradients lower than 2000 are applied could indicate that the critical gradient for this bentonite and this range of densities would be around this value. The critical gradient is the hydraulic gradient below which flow occurs but it is not Darcian.

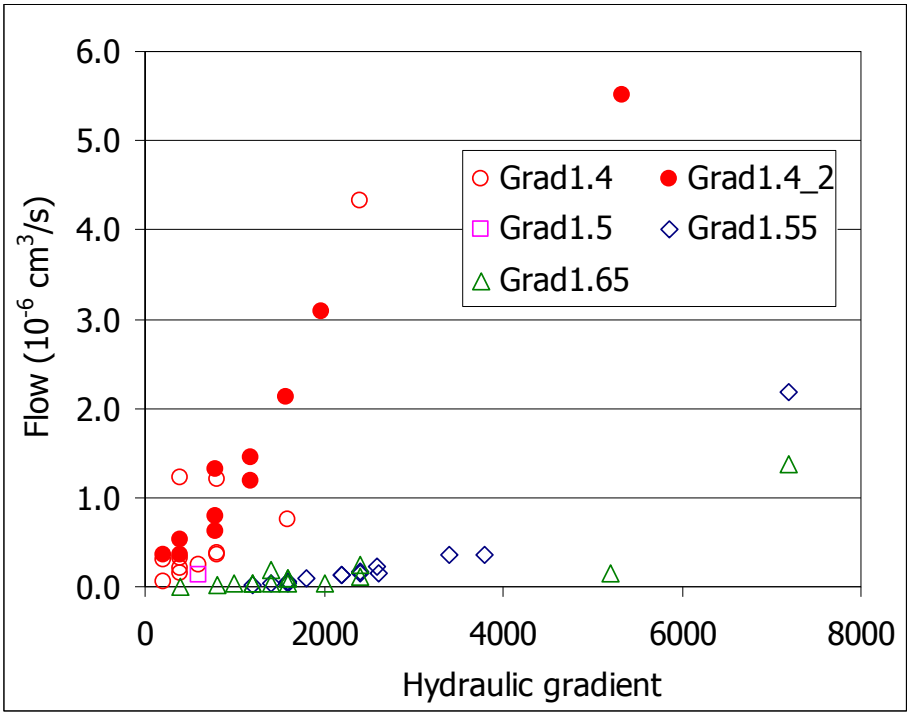

Figure 16: Flows measured during the permeability tests performed with compacted FEBEX bentonite (the test references in the legend include the densities indicated in g/cm^3)

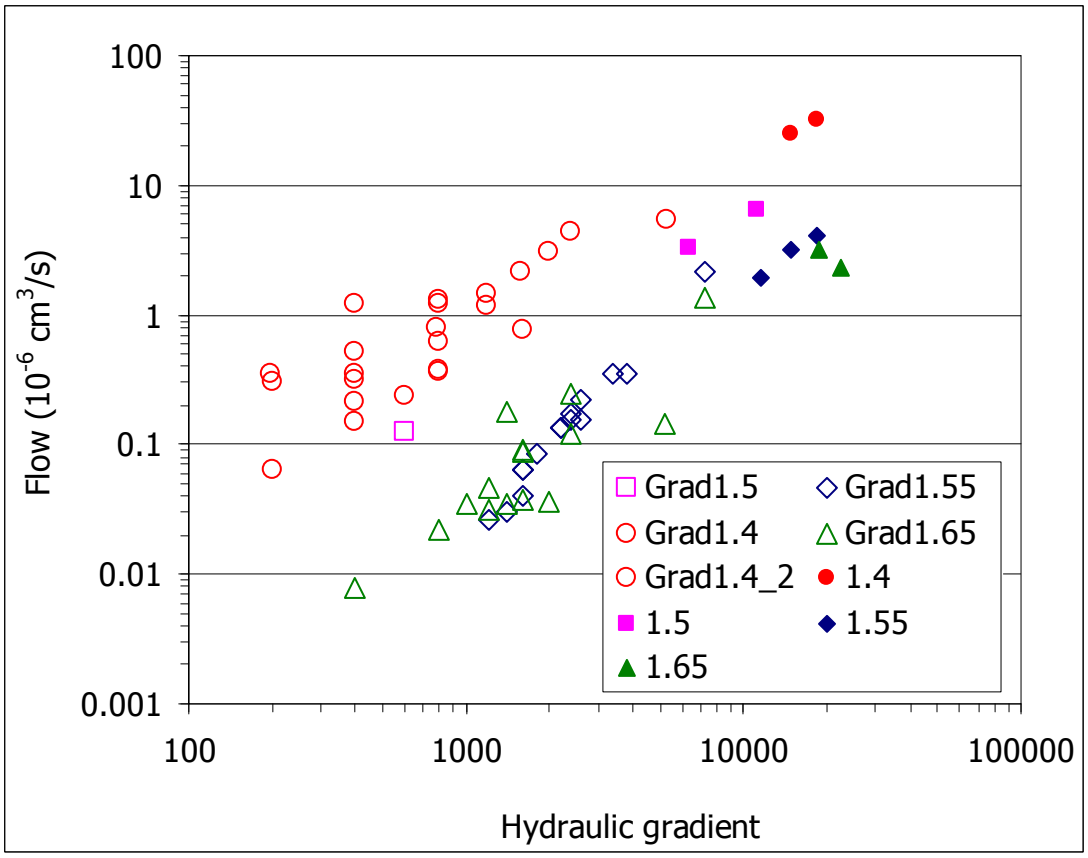

Figure 17: Flows measured during permeability tests performed on compacted FEBEX bentonite (the test references in the legend include the dry densities indicated in g/cm^3) applying low and high hydraulic gradients (the filled symbols correspond to the tests performed during FEBEX I)

- No measurable flows have been obtained when hydraulic gradients below 200 have been applied in a sample of dry density 1.4 g/cm^3. This value could be regarded as a threshold hydraulic gradient for dry density 1.4 g/cm^3, since no flow has been obtained below this gradient. For the dry density 1.65 g/cm^3 the threshold hydraulic gradient would be 800. However, there might be a dependency of these values also on the injection and backpressures applied (Figure 18).

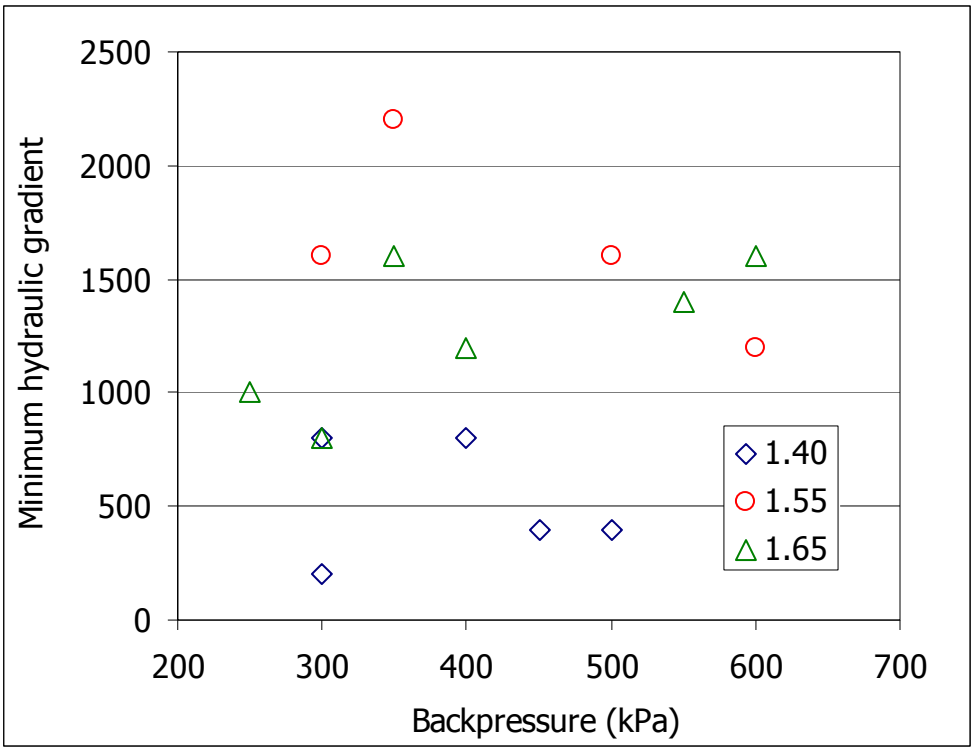

Figure 18: Minimum hydraulic gradients necessary to get measurable flow as a function of the backpressure applied and of the dry density of the bentonite (indicated in g/cm^3)

4 EVOLUTION OF HYDRATION OF BENTONITE WITH AND WITHOUT THERMAL GRADIENT

4.1 Introduction

It is expected that full saturation of the buffer be reached before the dissipation of the thermal gradient. However, it still remains unclear whether the high temperatures around the canister would hinder the full saturation of the inner part of the barrier or just delay it, but this seems to closely depend on the actual temperatures reached in the barrier and on its thickness. In most repository concepts it is expected that the temperature in the buffer be less than 100°C. In the 1-year test performed at Äspö for the Long Term Test of Buffer Material (LOT Project), the bentonite barrier –10-cm thick– had reached almost full saturation, the temperatures during the test being below 90°C (Karnland *et al*. 2000). On the contrary, at the Buffer Container Experiment performed at Lac du Bonnet (Canada), the areas of the buffer –whose thickness was 25 cm– adjacent to the heater had water contents below the initial one after 2.5 years of heating (Dixon *et al*. 2002). In the FEBEX *in situ* test, the bentonite closer

to the heater had water contents below the initial ones after five years of heating (the surface temperature of the heater was of 100°C), although they were recovering after the intense initial drying (Figure 19). On the contrary, in the same period of time, the sensors located at the same distance from the gallery wall, but in an area not affected by the thermal gradient, recorded much higher relative humidity. The thickness of the bentonite barrier in this case was of 65 cm (ENRESA 2000).

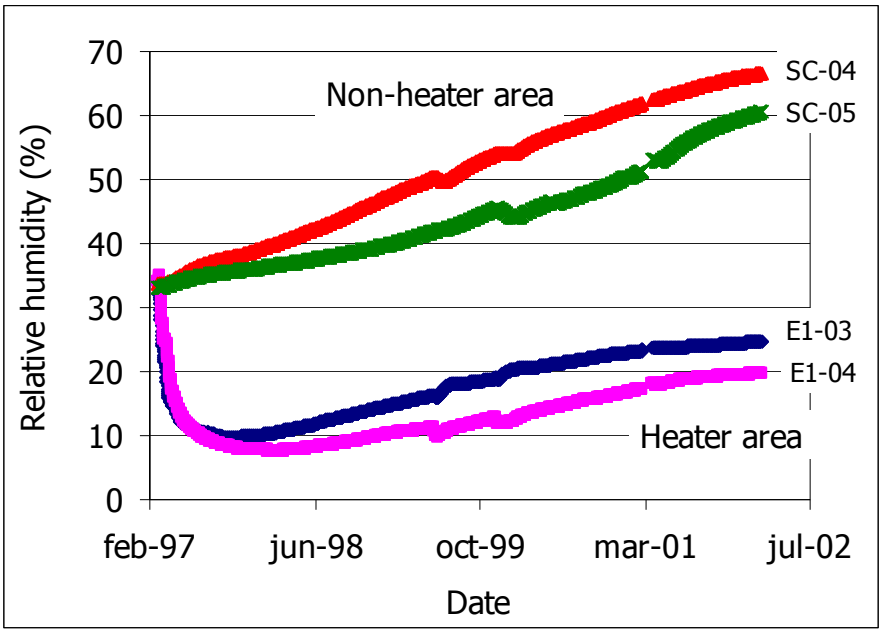

Figure 19: Evolution of the relative humidity of the bentonite recorded by two capacitive sensors located at 3.5 cm from the heater in section E1 and two sensors located at approximately the same distance from the gallery wall (54 cm) in section C (not affected by the heater) of the FEBEX *in situ* test (AITEMIN data base)

However, the performance of large-scale *in situ* tests as those mentioned above is complicated and time-consuming. Another drawback of *in situ* tests is that the boundary conditions are not always controlled and known. For this reason, laboratory tests of different scales are very useful to identify and quantify processes in shorter periods of time (Cuevas *et al*. 2002; Villar *et al*. 1996, 2005a). Among the laboratory tests started in the framework of the FEBEX Project (January 2002) and continued in the NF-PRO Project were those performed in cells in which the compacted bentonite is subjected simultaneously to heating and hydration, in opposite directions, in order to simulate the conditions of the clay barrier in the repository and better understand the hydration process. The results of two hydration tests performed under thermal gradient and at isothermal conditions are reported below.

4.2 Methodology

The hydration tests are being performed in cylindrical cells, already used during FEBEX I (Villar *et al*. 2005a), whose internal diameter is 7 cm and inner length 40 cm (Figure 20). They are made of Teflon to prevent as much as possible lateral heat conduction, and externally covered with steel semi-cylindrical pieces to avoid the deformation of the cell by bentonite swelling.

Five blocks of FEBEX clay compacted with its hygroscopic water content (around 14 percent) at an initial nominal dry density of 1.65 g/cm^3 were piled up inside each cell. Three of the blocks have a length of 10 cm, whereas the two placed at the ends of the cells have a length of 5 cm. An average compaction pressure of 30 MPa was applied to manufacture the blocks. A commercial granitic water of salinity 0.02 percent is injected through the upper lid of the cell at a pressure of 1.2 MPa. Its chemical composition is indicated in Table IX. This simulates the water that saturates the barrier in a repository excavated in granitic rock, and it is the same employed to saturate the mock-up test of the FEBEX Project (ENRESA 2000). The bottom part of the cell is a plane stainless steel heater. In one of the tests (GT40) the clay is being heated through the bottom surface at a temperature of 100ºC, which is the temperature expected on the surface of the waste container in the Spanish concept (ENRESA 1995). The other test (I40) is being carried out at isothermal conditions (laboratory temperature). Over the upper lid of the cells, there is a deposit in which water circulates at room temperature (20-30°C).

Table IX: Chemical composition of the water used in the tests (mmol/L)

Cl^-	SO_4^{2-}	HCO_3^-	Mg^{2+}	Ca^{2+}	Na^+	K^+	pH
0.37	0.15	2.36	0.39	1.12	0.48	0.026	8.3

The cells are instrumented with capacitive-type sensors placed inside the clay at three different levels separated 10 cm. The transmitters used are VAISALA HMP237, which include a humidity sensor (HUMICAP®) that changes its dielectrical characteristics with extremely small variations in humidity (capacitive-type relative humidity (*RH*) sensor). They include also a temperature sensing system (Pt 100). The accuracy of the humidity sensor is ±1 percent over the range 0-90 percent *RH* and ±2 percent over the range 90-100 percent *RH*. The water intake is being measured by electronic volume change measurement systems, with a resolution of 0.001 cm^3. The water intake and the relative humidity and temperature evolution at different levels inside the clay are being measured as a function of time. The two cells in operation are shown in Figure 21.

In addition to the tests described here, a test in a large-scale cell (60-cm height and 7-cm diameter) was set during FEBEX I and was running for 7.6 years. The cell and the experimental setup is analogous to the one described above. Six 10-cm height blocks of FEBEX clay compacted with its hygroscopic water content at an initial nominal dry density of 1.65 g/cm^3 were piled up inside the cell. Hydration with granitic water took place through the upper surface under an injection pressure of 1.2 MPa. The clay was heated through the bottom surface at a temperature of 100ºC. The water intake was measured as a function of time. No online measurements were carried out in this test, except for the water intake. The cell was disassembled in February 2006, and the study of the mineralogical, geochemical and physico-chemical modifications of the bentonite was undertaken. Similar cells running for 0.5, 1 and 2 years were dismantled and studied during FEBEX I (Villar *et al*. 2005a, Martín Barca 2002). The results acquired for these tests have been compared with the new ones to obtain the evolution over time. This task was performed in coordination with WP2.2 of the NF-PRO Project and the results obtained are collected in a specific report (Villar *et al*. 2008).

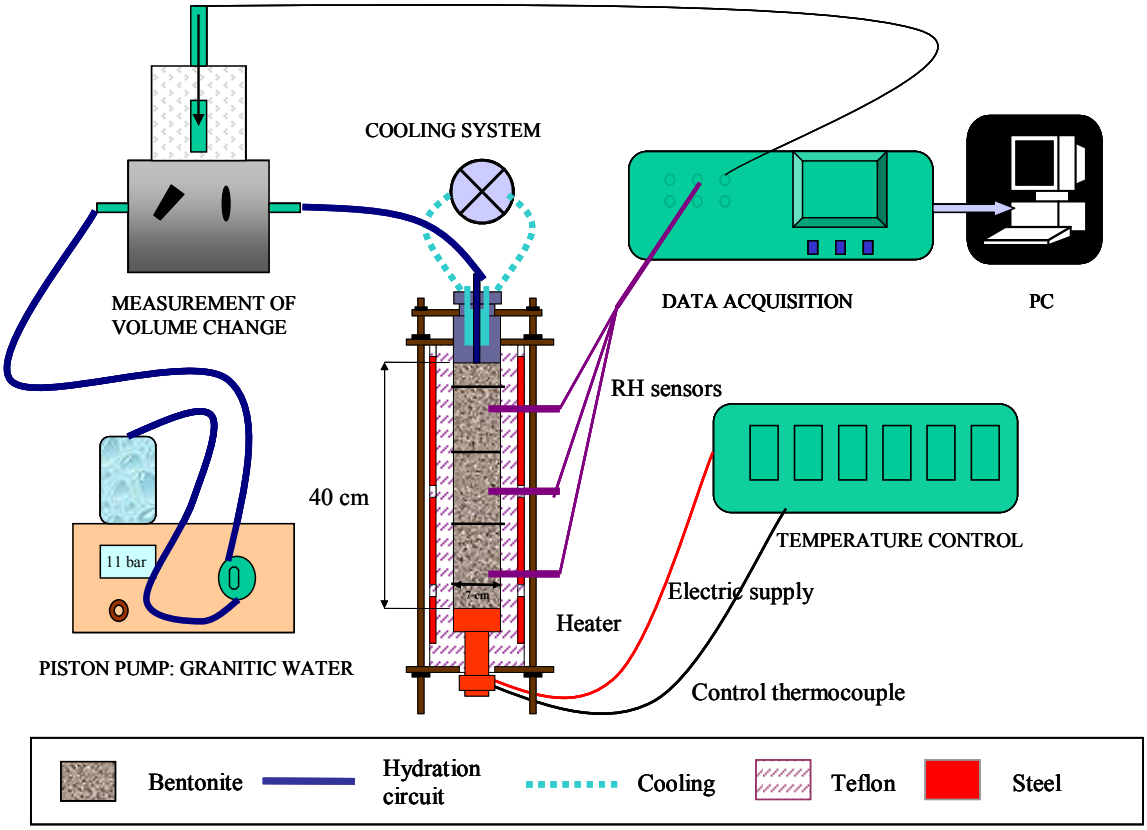

Figure 20: Experimental setup for the infiltration tests

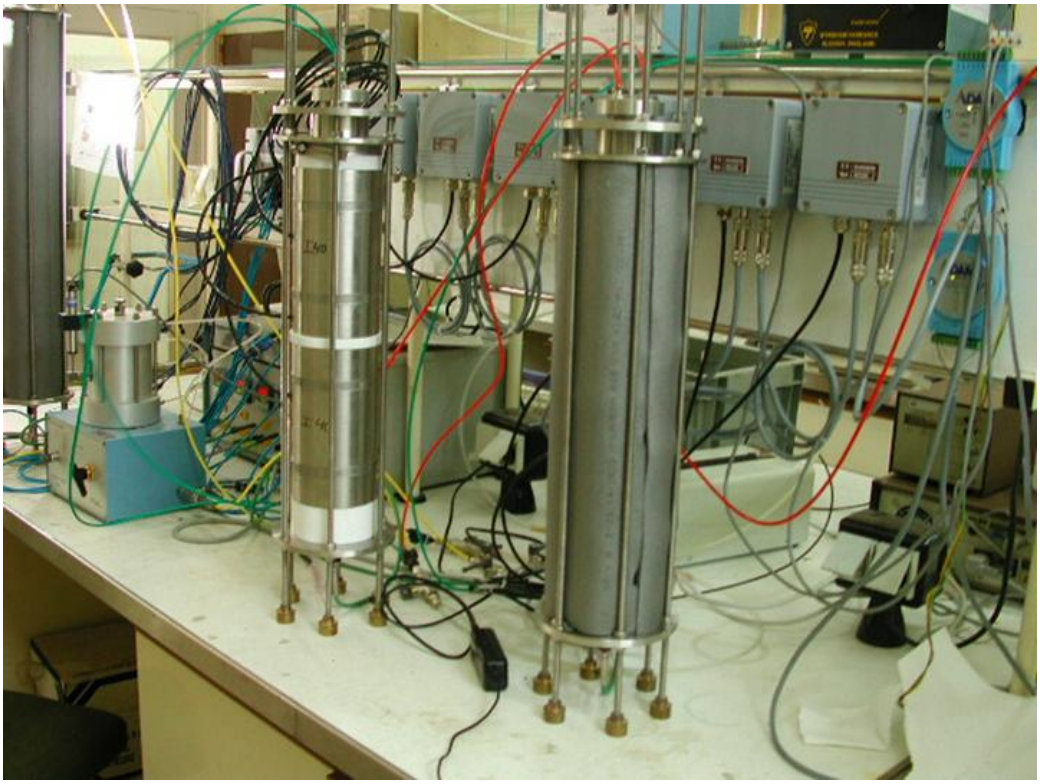

Figure 21: Infiltration cells in operation: isothermal (left) and with thermal gradient (right)

4.3 Results

In the case of the test performed under thermal gradient (GT40), firstly the temperature was set on top and bottom of the sample. The phase of temperature stabilisation in this test took three days (Figure 22). During this time, an increase in relative humidity was registered by the sensor placed at 10 cm from the bottom (RH3) and, to a lesser extent, by the sensors placed at 20 (RH2) and 30 cm (RH1) from the bottom, which revels the quick migration of water in the vapour phase from the bentonite near the heater towards cooler zones. However, the *RH* values of the two lower sensors had not stabilised after the temperature equalisation, what indicates that water vapour migration continued to take place.

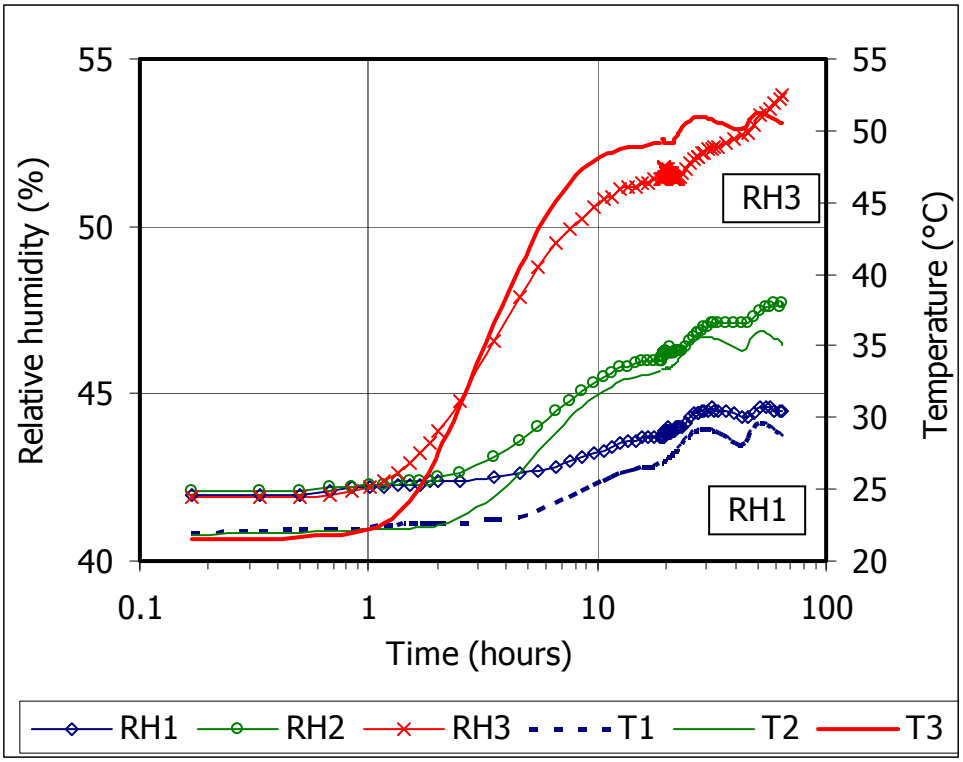

Figure 22: Initial stabilisation of temperature in test GT40 (sensor 1 placed at 30 cm from the bottom, sensor 2 at 20 cm and sensor 3 at 10 cm)

After this initial heating, hydration started. The evolution of relative humidity and temperature from the beginning of hydration in the test performed under thermal gradient (GT40) is shown in Figure 23 and Figure 24. The values plotted are those measured during infiltration, which begun after stabilisation of the temperature registered by the sensors, as explained above. For this reason, an initial difference in the relative humidity measured at different levels is observed in Figure 23. This trend is reversed when hydration starts, a clear increase in relative humidity being registered by the two upper sensors (RH1 and RH2), whereas desiccation starts to affect the zone in which sensor RH3 is placed: at least the 10 cm closest to the heater reduce its relative humidity after 300 hours of heating. This decrease in relative humidity goes down to values around 35 percent, which have increased only to values of 41 percent after 7 years of hydration. The relative humidity recorded by sensor RH2 has shown an increase of just from 76 to 78 percent from September 2006 to April 2009, what means that the rate of increase is very low. Sensor RH1 has been recording values around 93-94 percent since approximately July 2007. It occasionally shows signs of liquid water condensation inside (relative humidity values higher than 100 percent).

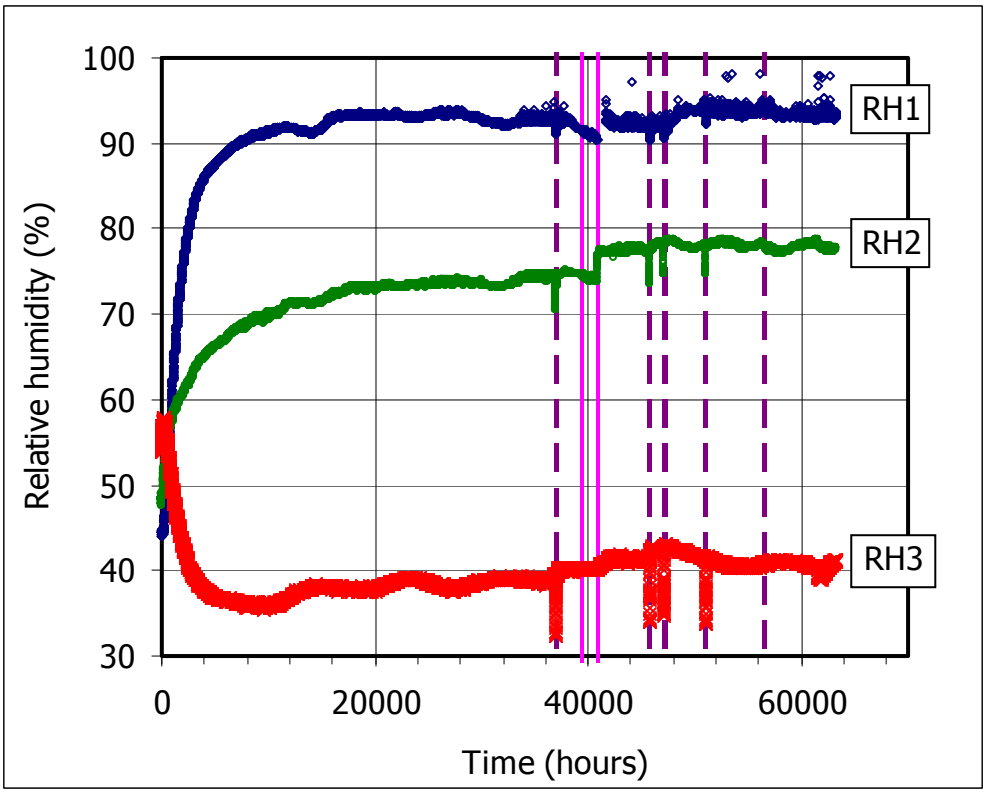

Figure 23: Evolution of relative humidity in the test performed under thermal gradient (GT40) during infiltration (sensor 1 placed at 30 cm from the bottom, sensor 2 at 20 cm and sensor 3 at 10 cm). The thicker vertical lines indicate periods of failure

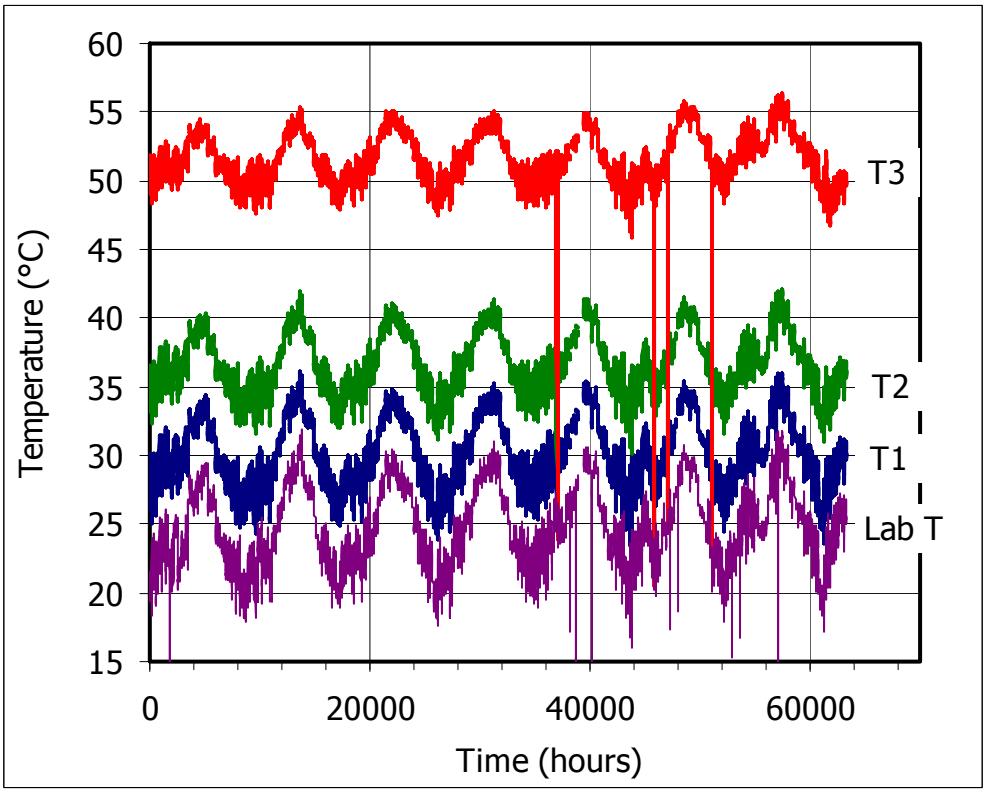

Figure 24: Evolution of temperature inside the bentonite and in the laboratory in the test performed under thermal gradient (GT40) during infiltration (sensor 1 placed at 30 cm from the bottom, sensor 2 at 20 cm and sensor 3 at 10 cm)

With respect to the temperatures inside the clay, they have remained constant since the beginning of the experiment, being just influenced by the distance to the heater and by the seasonal and daily changes in the laboratory temperature (Figure 24). Figure 25 shows the average temperatures measured by the three sensors over the test. The thermal gradient is not constant along the column, being steeper near the heater.

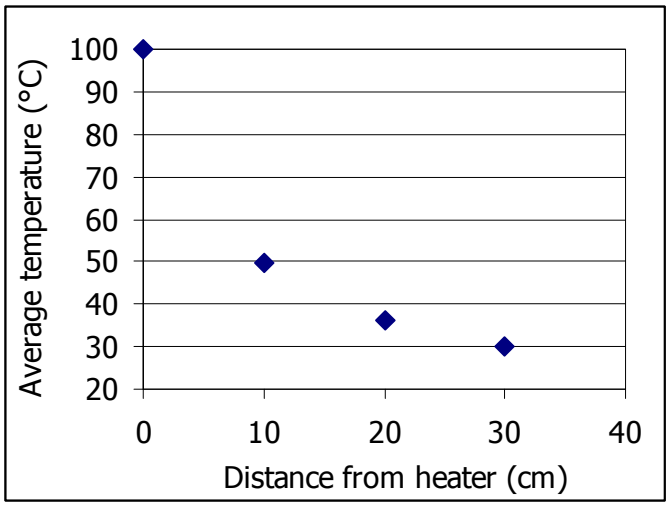

Figure 25: Average temperatures along test GT40 at different positions inside the clay

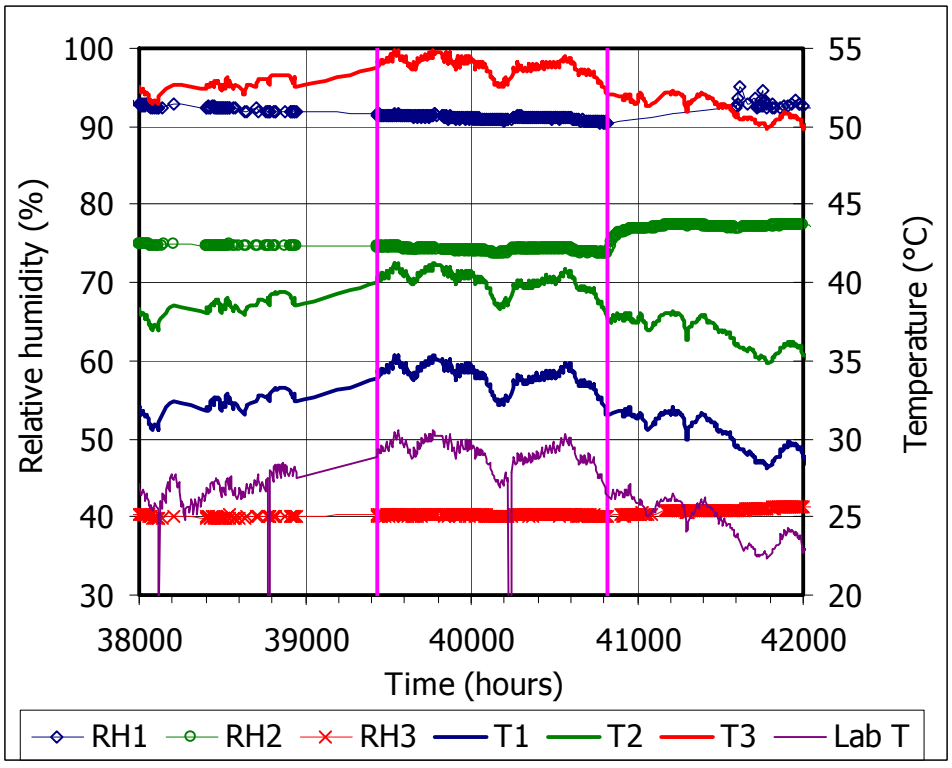

Figure 26: Relative humidity (RH) and temperature (T) recorded in test GT40 during the period of accidental no-hydration. The thicker vertical lines indicate the period of no-hydration (sensor 1 placed at 30 cm from the bottom, sensor 2 at 20 cm and sensor 3 at 10 cm)

From 39432 to 40825 hours (2 months) the water entry valve was accidentally closed. In the case of test I40 the water supply could have been stopped even before. This was reflected in a slight decrease in the relative humidity recorded by the two upper sensors (RH1 and RH2),

that showed a sudden recovery to values higher than the previous ones when hydration was restored (Figure 26). Also, when the water injection pressure was fixed again in 1.2 MPa, water came out by the RH1 sensor inlet, what could indicate that some bentonite shrinkage took place during the no-hydration period.

In addition to this, during the last years there have been failures in the system that have affected temporarily the measurements. Mostly they were blackouts that kept the system down for several hours. During this periods no heating, no hydration and no data recording took place. In all the cases, the bentonite quickly cooled, but the temperatures recovered as soon as the heater was switched on again. The changes recorded in relative humidity were those expected from the temperature change, and the values previous to the failure were recovered once the temperatures were set again. The periods during which the system was down are:

– From 36969 to 37055 hours (3.5 days).

– From 45778 to 45841 hours (2.5 days). The recordings of the sensors before and after this episode are shown in Figure 27.

– From 47057 to 47112 hours (2 days) and a few days later from 47286 to 47304 hours (1 day) (Figure 28).

– After 50991 hours the system was stopped for 17 hours.

– From 56468 to 56519 hours (2.3 days).

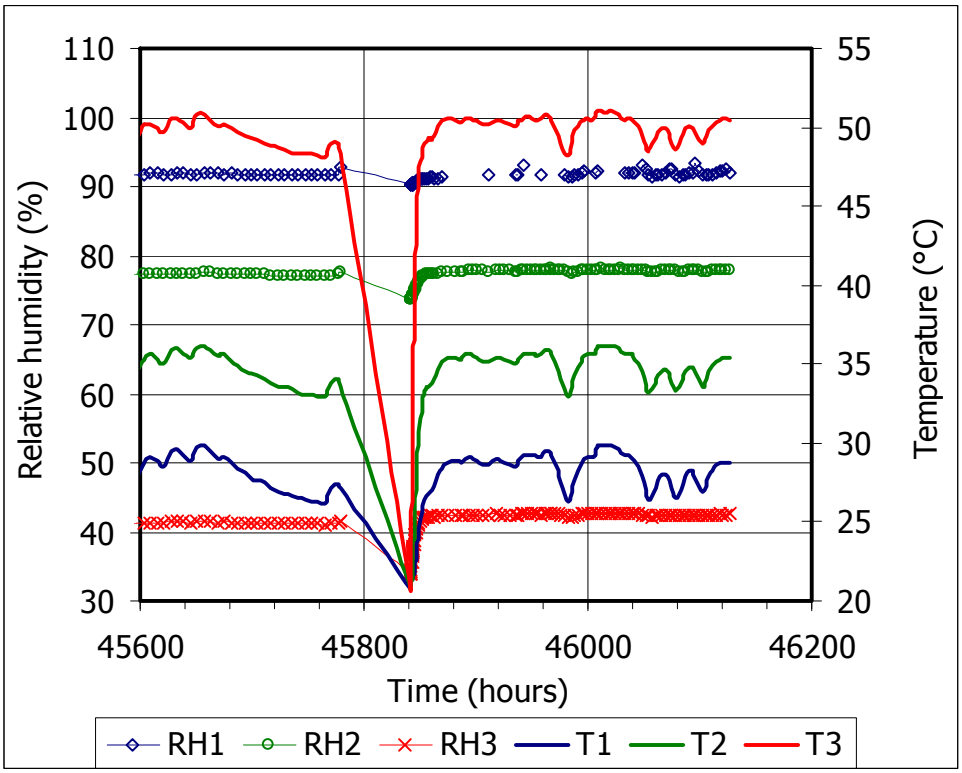

Figure 27: Relative humidity (RH) and temperature (T) recorded in test GT40 during a period of accidental cooling and no-hydration (sensor 1 placed at 30 cm from the bottom, sensor 2 at 20 cm and sensor 3 at 10 cm)

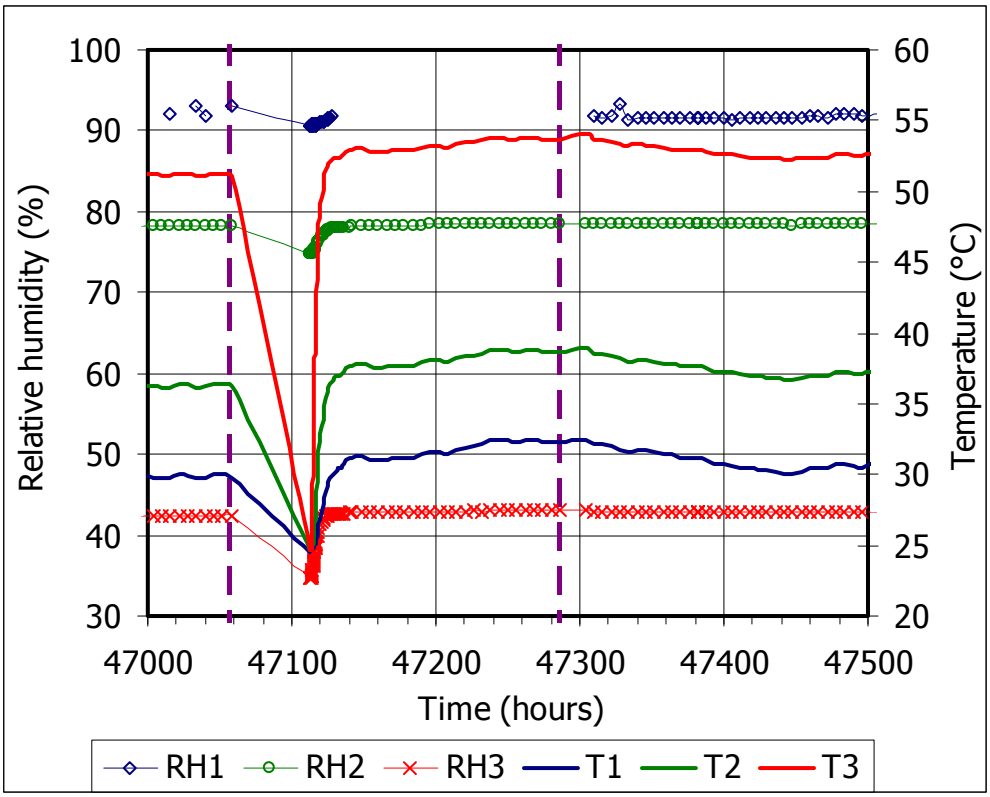

Figure 28: Relative humidity (RH) and temperature (T) recorded in test GT40 during two consecutive periods of accidental cooling and no-hydration (sensor 1 placed at 30 cm from the bottom, sensor 2 at 20 cm and sensor 3 at 10 cm)

In the case of the isothermal test (I40), the cooling system was set first and the data acquisition began. After 18 hours, the hydration system was connected. The evolution of relative humidity in the test performed under isothermal conditions is shown in Figure 29. The sensor placed at 10 cm from the hydration surface (RH1) shows a steady increase in relative humidity, which was noticeable after 250 hours of hydration. The sensor placed at 20 cm from the hydration surface (RH2) started to register an increase in relative humidity after 1200 hours of hydration, and the sensor placed towards the bottom (RH3), after 2500 hours of hydration. After 5000 hours of hydration, sensor RH3 records the sharpest increase, while relative humidity in the upper parts of the bentonite column (sensors RH1 and RH2) increases in a softer way, probably because the suction of the bentonite in these hydrated zones is lower. In turn, the high water content of the upper part of the bentonite provides enough water supply to the bottom. The relative humidity values recorded by the three sensors have remained quite constant in the last 4000 hours, after the last failure, although if we look at their evolution closely (Figure 30) the relative humidities recorded by sensors RH2 and RH3 have not stopped increasing.

The same failures described above for test GT40 affected test I40. During the accidental period of no hydration, the two upper relative humidity sensors (RH1 and RH2) recorded a decrease smaller than 1 percent that was recovered upon reinstatement of hydration (Figure 31). After the cooling and no-hydration periods, the relative humidity values recorded are similar to those before failure.

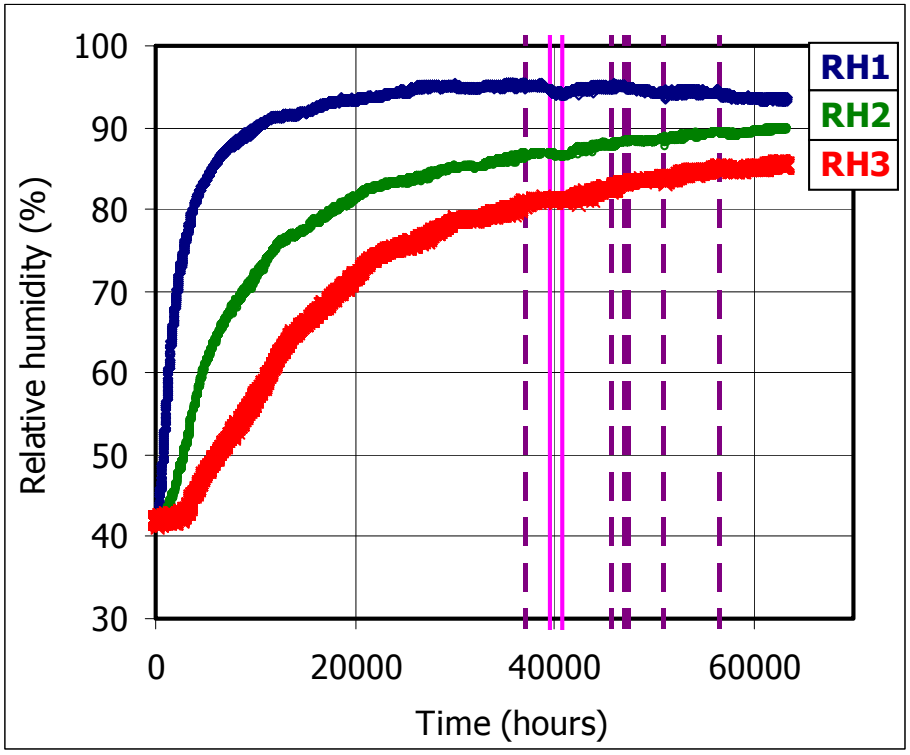

Figure 29: Evolution of relative humidity in the test performed under isothermal conditions (I40) during infiltration (sensor 1 placed at 30 cm from the bottom, sensor 2 at 20 cm and sensor 3 at 10 cm). The thicker vertical lines indicate periods of failure

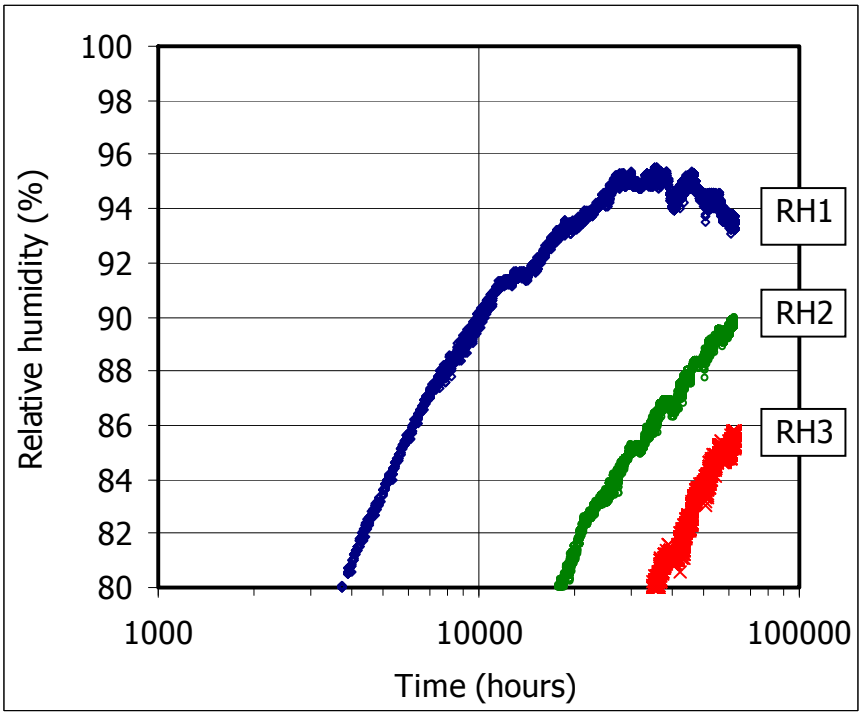

Figure 30: Enlargement of the upper part of Figure 29 (sensor 1 placed at 30 cm from the bottom, sensor 2 at 20 cm and sensor 3 at 10 cm)

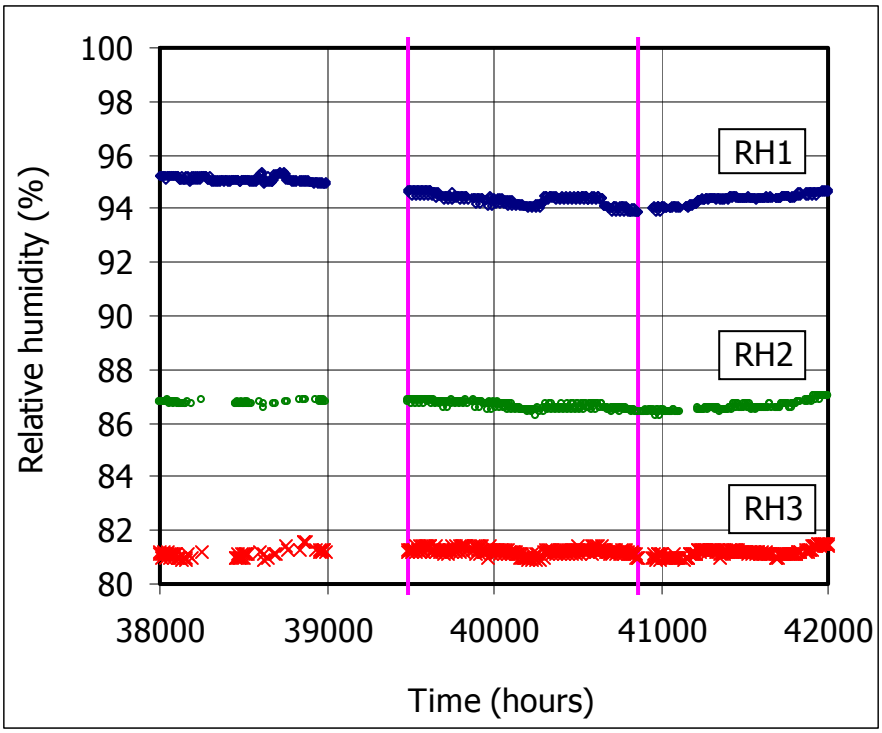

Figure 31: Relative humidity recorded in test I40 during the period of accidental no-hydration, indicated by thicker vertical lines (sensor 1 placed at 30 cm from the bottom, sensor 2 at 20 cm and sensor 3 at 10 cm)

The water intake measured by the volume change apparatuses for the two tests is shown in Figure 32. The total water intake is higher for the isothermal test. However, these curves must be taken as indicative, because there is a possibility of leakages that must be checked at the end of the tests, when the actual water intake will be determined as the difference between the final and initial sample weights. In fact, if we consider the actual volume of water intake measured up to now, the degrees of saturation would be much higher than 100 percent for both tests.

To overcome this drawback, both cells were placed on balances after four years of testing (35981 h for test I40 and 33566 h for test GT40), so that to check if the water intake recorded by the volume change apparatuses is reflected as an increase in weight. The water intake as measured by both methods since February 2006 is shown in Figure 33 for the two tests. In none of them the weight changes reflect the volume change measurements. For test I40, the balance has barely recorded any weight increase, whereas the volume change apparatus records a steady water intake, except in the no-hydration period. The volume change apparatus of test GT40 records also a steady water intake, whereas the balance recorded a weird weight increase up to the period of no-hydration, during which it did not displayed any weight change, and afterwards, periods of constant weight and slight increase have followed. From the last blackout on, this balance has recorded a slight but steady increase in weight. In any case, the measurements point to a very limited water intake, if any, in both cases. This seems to confirm that the volume change measurements are erroneous.

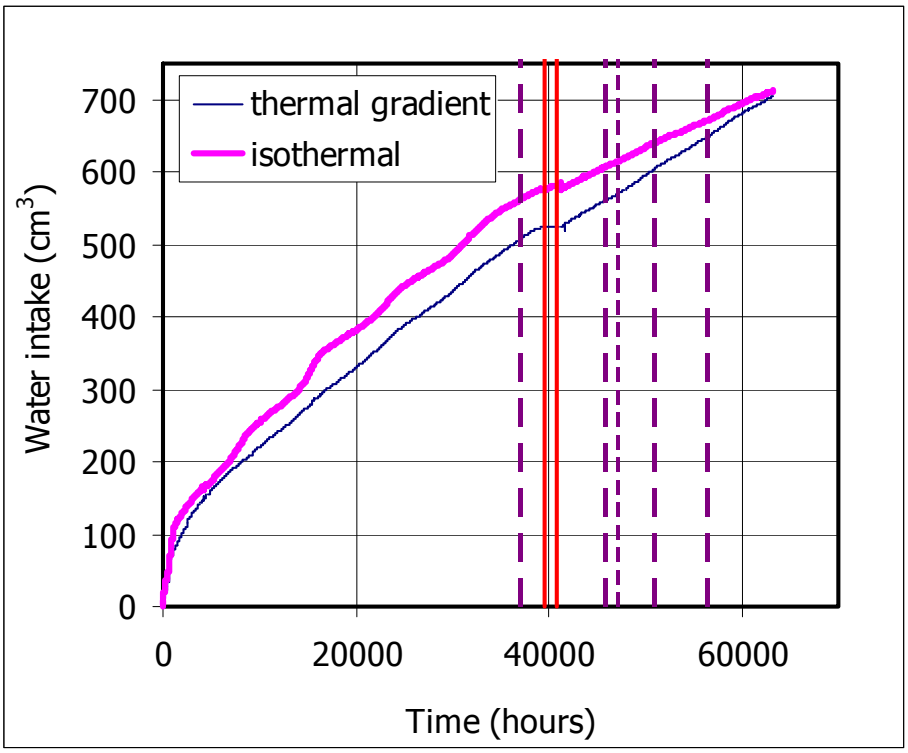

Figure 32: Water intake in the two infiltration tests (preliminary curves, to be adjusted at the end of the tests). The thick vertical lines indicate periods of failure

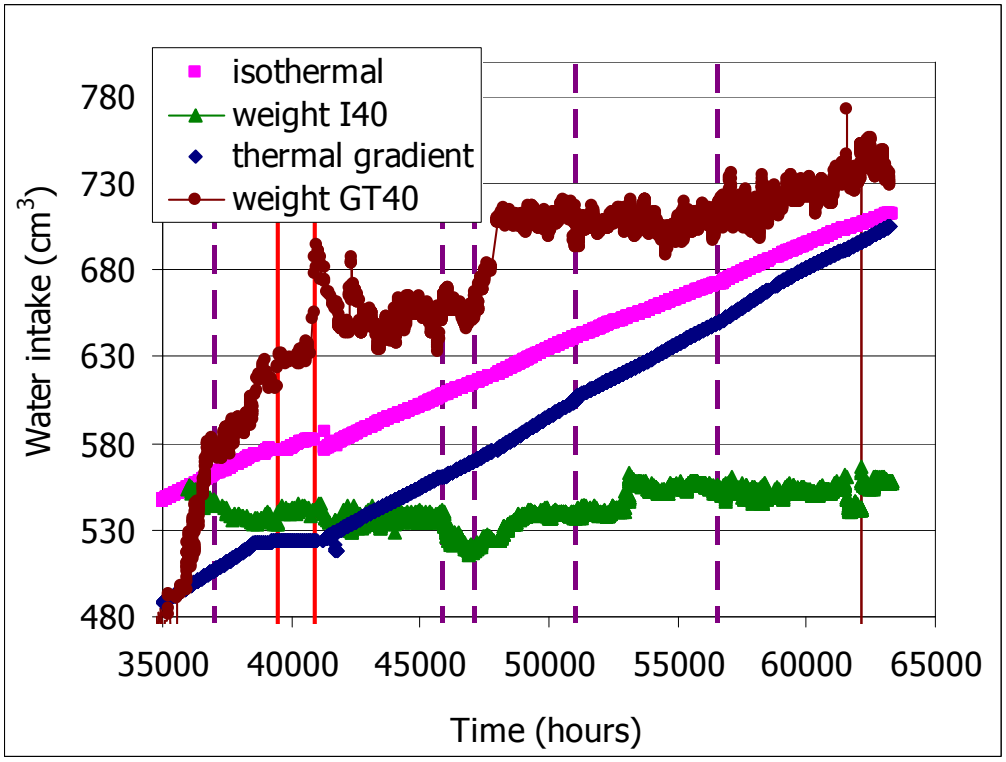

Figure 33: Water intake in the isothermal (I40) and thermal gradient (GT40) tests as measured by the volume change equipments and by the balances. The vertical lines indicate periods of failure

4.4 Summary and discussion

The infiltration test GT40 has shown that the permeability to water vapour of dry bentonite is very high, since a quick redistribution of water took place when the thermal gradient was established. The thermal gradient initially set has remained constant during the whole test, being influenced only by the seasonal and daily laboratory temperature variations. The initial hydration of compacted bentonite takes place quicker under thermal gradient (test GT40) than at laboratory temperature (test I40), as shown by the increase in humidity registered by the upper sensor (RH1), which is higher in test GT40 than in test I40, whereas the sensor placed in the middle (RH2) starts to perceive the humidity increase much earlier in the case of infiltration under thermal gradient than in the case of infiltration at laboratory temperature. In the case of test GT40, the humidity initially recorded by sensor RH2 could come in the form of water vapour from the lower part of the column. Otherwise, the increase in hydraulic conductivity with temperature would account for this initial quicker hydration of the test under thermal gradient.

However this behaviour is reversed as saturation proceeds and later on, the water intake is higher for the sample tested at room temperature, because the hot zones of the sample tested under thermal gradient remain desiccated for long time. For both cells, there was a reactivation of *RH* increase after the 2-month accidental no-hydration period that occurred between hours 39432 to 40825. After 63000 hours (7.2 years) of hydration, the average relative humidity recorded by the three sensors in test GT40 is 71 percent, and in test I40 is 90 percent. In test GT40 the average relative humidity has not increased in the last year.

The water intake measurements performed by the volume change apparatuses seem erroneous, as the weight changes recorded by the balances on which the cells are placed do not point to a measurable water intake. Since the behaviour of both tests is similar with respect to water intake, there is not a strong support to the hypothesis of evaporation taking place through some component of test GT40. In addition, the temperatures inside the bentonite are not too high. The process or artefact that causes the water intake to be so slow, must not be solely connected to the thermal gradient.

5 EFFECT OF TEMPERATURE ON HYDRO-MECHANICAL PROPERTIES

5.1 Introduction

Temperature changes affect important hydraulic characteristics of compacted clays such as water retention and water permeability, whose knowledge is crucial to predict the hydration rate of the barrier: any small variation can lead to very significant changes in saturation time. In addition, the mechanical response of the material, which has important implications on the design and performance of the repository, is also affected by temperature (swelling pressure, swelling and collapse, thermal dilatation and contraction, compressibility, yielding, effects on time-dependent behaviour). Laboratory tests may help to understand the processes that take place in the clay barrier under simple and controlled conditions and to develop the governing equations. The laboratory tests enable to isolate the different processes, making their interpretation easier, and provide fundamental data concerning the parameters to be used in the models.

The influence of temperature on different hydro-mechanical properties of the bentonite was tackled during FEBEX II, particularly with respect to its water retention and swelling capacity (Lloret *et al*. 2004). However, due to the difficulties in the laboratory experimentation under high temperatures, few results were available and the research carried out has shown that the effects of temperature may differ depending on the type of material and even on the type of cations in the exchange complex. This is why during the NF-PRO several tests, in which compacted specimens of FEBEX bentonite have been subjected to temperature and stress, have been performed and are presented below.

5.2 Methodology

5.2.1 Swelling pressure and hydraulic conductivity

The determination of the swelling pressure and hydraulic conductivity as a function of temperature has been performed in high-pressure oedometer equipments (Figure 34). Granulated clay is compacted uniaxially and statically at room temperature in the oedometer ring, which has an inner diameter of 5.0 cm, the length of the resulting specimen being 1.2 cm. Nominal dry densities of 1.50, 1.60 and 1.70 g/cm^3 have been reached by applying vertical stresses of 10.0±1.3, 16.0±1.5 and 29.1±1.0 MPa, respectively. The specimens thus obtained are confined between porous stainless steel sinters.

The oedometer assemblage is placed inside a silicone oil thermostatic bath that keeps the target temperature. Before increasing the temperature, a small vertical load of around 0.4 MPa was applied to the sample to assure a good contact with the load cell installed in the loading frame, and the deformation of the sample was hindered by means of setscrews. The stabilisation of temperature was reached in less than 24 hours. At the end of this period the equipment deformation gave place to vertical displacements of between -0.06 and 0.24 mm (corresponding to -0.5 and 2.0 percent of the specimen height, respectively) measured by two LVDTs placed in each oedometer assemblage. Also, the load cell recorded pressure increases due to the deformation of the metallic parts of the equipment during the temperature stabilisation period which ranged from 0.1 to 2.7 MPa for temperatures of between 30 and 80°C. These have been calibrated and deducted from the initial measurements. After the 24-hour period of temperature stabilisation, the sample was hydrated at constant volume through the bottom surface with deionised water injected at a pressure of either 0.6 MPa –for most of the samples of dry density 1.60 g/cm^3– or 0.01 MPa –for the samples of dry density 1.50 and 1.70 g/cm^3–, while the upper outlet remained open to atmosphere. At the same time, the load cell measured the swelling pressure exerted by the clay. The small vertical deformation of the specimen, due mainly to the load cell and frame deformability, was measured by LVDTs. An automatic volume change apparatus measured the water exchange of the specimen. The values of load, strain and water exchange were automatically recorded.

Once the sample is completely saturated (which is assumed by the stabilisation of swelling pressure development), the injection of water is stopped, and the pressure registered is considered the swelling pressure value for the dry density attained. The actual density may differ slightly from the nominal one due to the small displacement allowed by the equipment (about 0.1 mm when the vertical stress is 1 MPa and 0.4 mm when the vertical stress is of 7 MPa, *i.e*. between 1 and 3 percent of the sample height).

Afterwards, hydraulic conductivity is determined in the same equipment and on the same samples, which are kept at constant volume. In order to perform this determination, the water pressure at the bottom of the samples is increased, while a backpressure of 0.6 MPa is applied

on top, resulting in hydraulic gradients between 800 and 9600. At least two different hydraulic gradients have been applied in each sample. The water outflow is measured by a volume change apparatus and the hydraulic conductivity (k_w) is calculated applying Darcy's law (Equation 7). The intrinsic permeability (k) has been calculated from hydraulic conductivity through:

$$k = \frac{k_w \times \mu_w}{\rho_w \times g} \quad [8]$$

where μ_w is water dynamic viscosity (taken as $1.0 \cdot 10^{-3}$ Pa·s at 22°C), ρ_w is water density (taken as $1.0 \cdot 10^3$ kg/m^3 at 22°C) and g has been taken as 9.8 m/s^2.

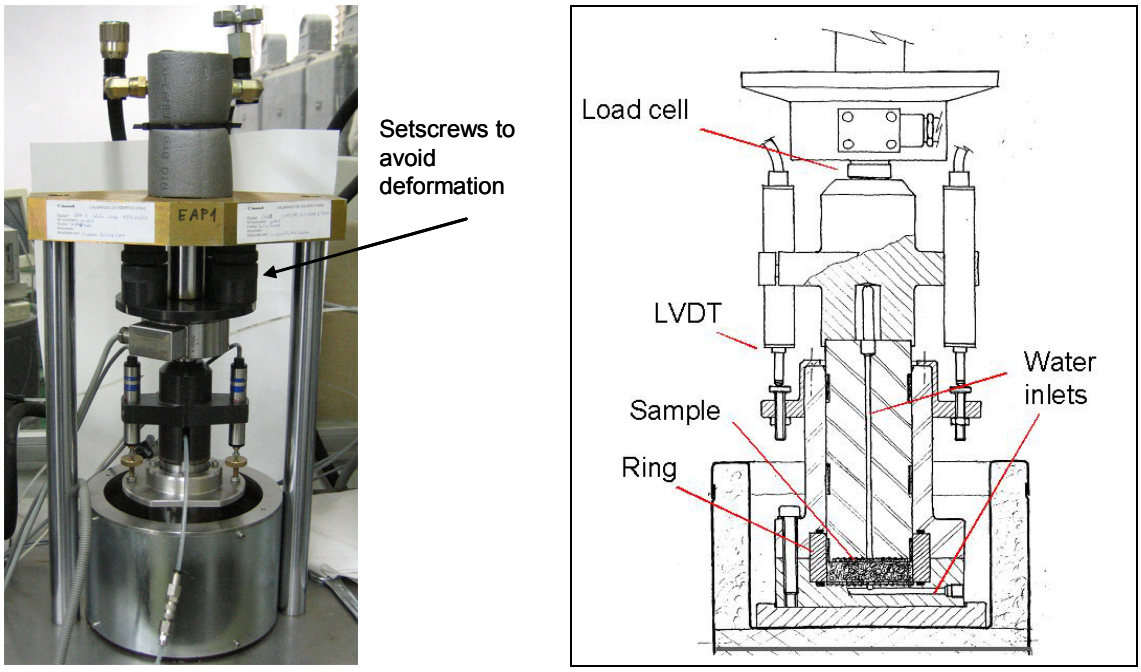

Figure 34: Schematic layout and appearance of the oedometric cell inside the thermostatic bath

5.2.2 Swelling capacity

The influence of temperature on the swelling capacity of clay has been checked by tests of swelling under vertical load. They are performed in oedometers whose cell is placed in a silicone oil thermostatic bath with controlled temperature (Figure 35). Granulated bentonite with its hygroscopic water content (about 14 percent) is compacted inside the cell ring, at room temperature, using static uniaxial compaction. To obtain specimens of 5.0 cm in diameter and 1.2 cm in height, vertical stresses of 10±1 MPa, 16±2 and 29±1 MPa were applied for the nominal dry densities of 1.50, 1.60 and 1.70 g/cm^3, respectively.

Once in the oedometer, the stabilisation of temperature is reached in less than 24 hours. After having reached the stabilisation of the target temperature in the oedometer, vertical pressures of 0.1, 0.5, 1.5 and 3.0 MPa are applied to the samples. Immediately afterwards, they are soaked with deionised water at atmospheric pressure from the bottom porous plate. The swelling strain experienced by the specimens upon saturation is recorded as a function of time until stabilisation. On completion of the tests, the water content of the specimens is determined and full saturation is verified. The tests have been performed at temperatures ranging from 30 to 90ºC, controlled by the silicone oil temperature in the bath.

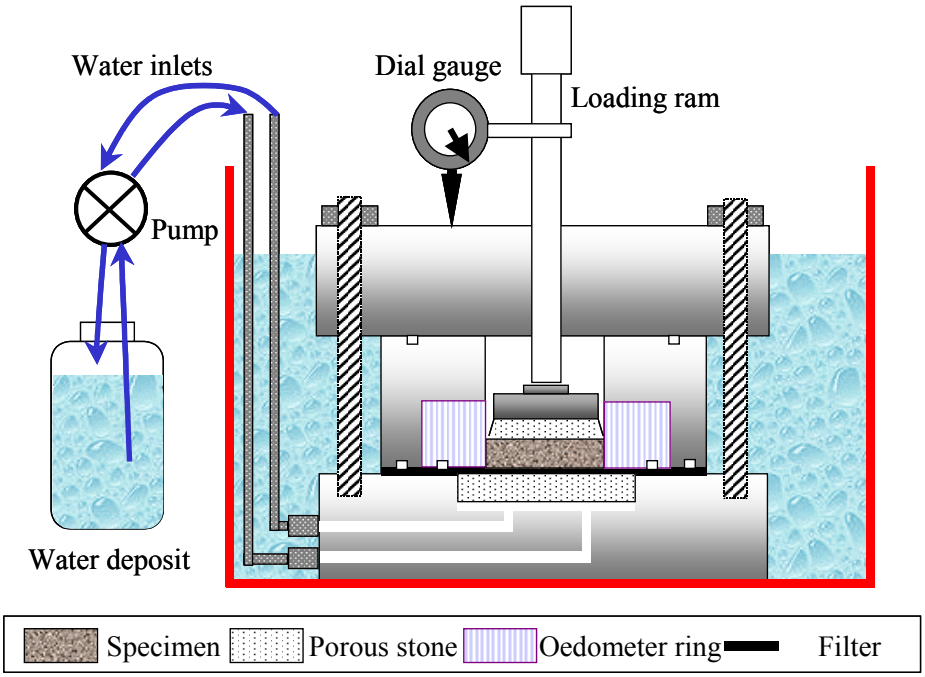

Figure 35: Schematic representation of the oedometer cell for tests at high temperature inside the thermostatic bath

5.2.3 Water retention capacity

To determine the water retention curve of the compacted bentonite at constant volume and at different temperatures, two methodologies were developed (Villar *et al*. 2005b). One of them is based on the imposition of a known relative humidity (*i.e*. total suction) to a specimen confined in a non-deformable cell and the measurement of its water content after equilibrium (cell method). The other method is based on the relative humidity measurement using capacitive sensors of specimens compacted at the same dry density with different water contents (sensor/cell method). Both have been adapted for the testing at high temperature. In the first case, the desiccators in which suction is imposed are placed inside ovens. In the second, the compacted blocks are placed in hermetic cells that can be externally heated.

The cell method is carried out in special cells designed to avoid the swelling of the clay in wetting paths (Villar 2002, Villar & Lloret 2004). The cells consist of a corrosion-resistant stainless steel cylindrical body with two perforated covers joined by bolts. Granulated clay is compacted inside the cell ring at room temperature using static uniaxial compaction. The length of the specimen is 1.20 cm and its cross section, 11.34 cm^2. Porous stones are placed between the specimen and the covers on top and bottom. The cells are placed in desiccators with a sulphuric acid solution or with a NaCl solution. There are temperature-dependent experimental relations between the concentration of the solution and its water activity (a_w). The calculation of suction on the basis of relative humidity ($RH = 100 \cdot a_w$) is accomplished through Kelvin's equation (Equation 9). In the cell method the suction is, therefore, imposed through the control of relative humidity. The perforated covers allow the exchange of water in the vapour phase between the clay and the atmosphere of the desiccators. Once the water content of the clay is stable (approximately 2 to 3 months, what is checked by periodic weighing), the solution in the desiccators is changed in order to apply a different suction. To determine the curve at different temperatures, the desiccators are placed inside ovens. At the end of the tests the final water content of the specimens is measured by oven drying.

Most of the results presented in this report were obtained with the sensor/cell method (Villar *et al*. 2006), which consists on the measurement of the relative humidity of compacted bentonite by means of a capacitive sensor (Figure 36). The bentonite block is kept inside a cylindrical hermetic cell made out of stainless steel. To reach the desired water content in the bentonite, the clay is mixed with the appropriated deionised water quantity to increase its hygroscopic water content, or it is slightly desiccated by softly heating the clay. The water content obtained has been between 7 and 22 percent. Then, the bentonite is uniaxially compacted to the desired dry density (1.50, 1.60 and 1.75 g/cm^3). The compacted block is put inside a cylindrical cell made out of stainless steel, the dimensions of the block being equal to the internal volume of the cell, 7 cm diameter and 10 cm height. A hole is drilled in the central upper part of the bentonite block to insert the sensor and the upper and lower lids of the cell are hermetically sealed to the body of the cell with thermo-resistant silicone. The upper lid of the cell has a central perforation, also sealed with silicone, to allow the passage of the sensor cable.

The transmitters used are VAISALA HMP237 or HMP233, which include a humidity sensor which changes its electrical characteristics with extremely small variations in humidity (capacitive type relative humidity sensor). They include also a temperature sensing system (Pt 100). The accuracy of the humidity sensor is ±1 percent over the range 0-90 percent *RH* and ±2 percent over the range 90-100 percent *RH*. To convert the values of relative humidity (*RH*, %) to suction values (*s*, MPa) the Kelvin's law has been used:

$$s = -10^{-6}\frac{R \times T}{V_w}\ln\left(\frac{RH}{100}\right) \qquad [9]$$

where R is the universal constant of gases (8.3143 J/mol·K), T the absolute temperature and V_w the molar volume of water ($1.80 \cdot 10^{-5}$ m^3/mol).

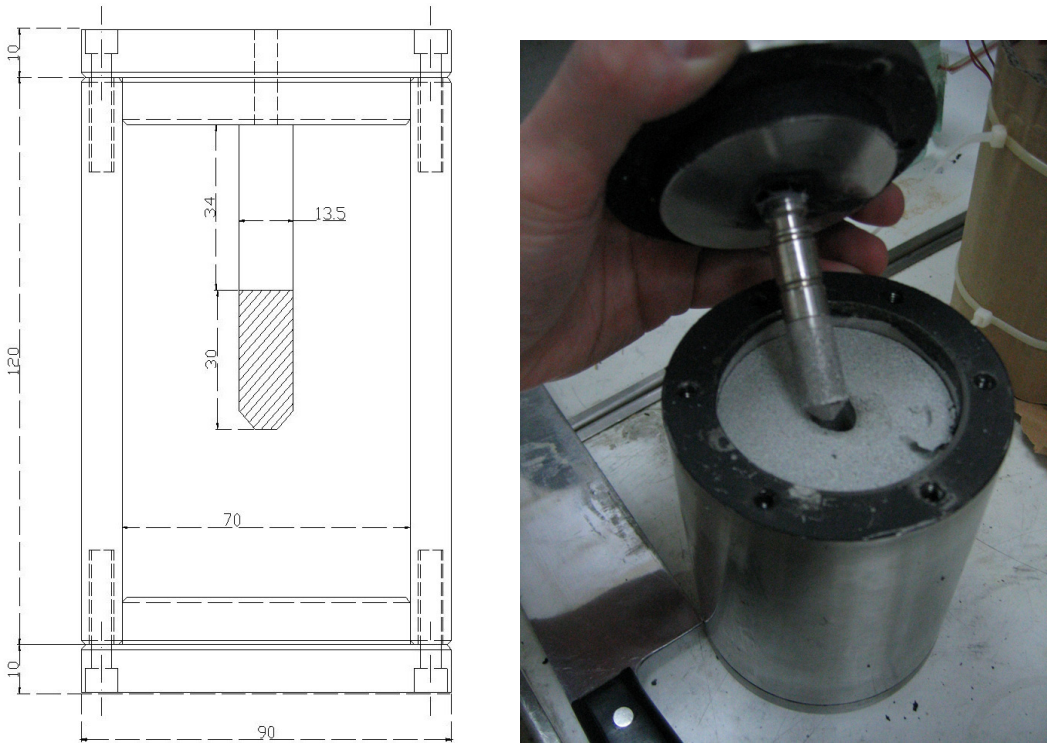

Figure 36: Layout of the cell for the measurement of suction at high temperature with the capacitive sensor inserted in it (dimensions in mm) and appearance of the cell with the compacted bentonite inside, drilled to allow the entrance of the sensor

The external wall of the cell is covered with a silicone-rubber laminated heater, which fixes the temperature all around the cell. The assembly is wrapped in isolating material. The suction is determined in a range of temperature between laboratory temperature and 120ºC. The thermal equilibrium is reached very quickly. After a time long enough to reach a stable measurement of relative humidity, the temperature is changed, what allows, in a single test, the determination of the change in suction with temperature for a given density and water content. The temperature was increased in steps of 10 or 20°C until reaching 120ºC. Afterwards, the temperature was decreased in steps until reaching the laboratory temperature. Each target temperature was kept for between 40 and 500 h. The temperature and relative humidity were recorded every 6 hours.

At the end of the test, the block is extracted, weighed and cut into four vertical sections, and each section is separated in external and internal. The water content and dry density of each section are measured.

5.3 Results

5.3.1 Swelling pressure

For the nominal dry density 1.50 g/cm^3, 13 tests were performed at temperatures between 27 and 80°C, for the nominal dry density 1.60 g/cm^3, 12 tests were performed at temperatures between 25 and 80°C and for the nominal dry density 1.70 g/cm^3, 15 tests were performed at temperatures from 30 to 80°C. The average values of dry density at the end of the process of saturation were in fact 1.48, 1.57 and 1.65 g/cm^3, due to the small displacement allowed by the equipment during saturation and to initial differences with respect to the nominal value caused during manufacturing of the specimens.

Swelling pressure starts to develop as soon as the water comes in contact with the clay, as can be observed in Figure 37, that shows the evolution of swelling pressure and water intake in test EAP2_22. Due to the fact that the upper outlet remained open to atmosphere during the tests, the water intake did not usually stabilise, since evaporation could continually take place from the upper part of the specimen. The evolution of swelling pressure in the tests performed with the bentonite compacted at nominal dry densities 1.5, 1.6 and 1.7 g/cm^3 is shown in Figure 38, Figure 39 and Figure 40, respectively. These figures show that swelling pressure does not develop in a uniform way. After a sharp initial increase, there is a period of time in which pressure increases more slowly or –in the case of densities 1.5 and 1.6 g/cm^3– even decreases. This behaviour is clearer in samples of lower dry density whose swelling pressure is lower.

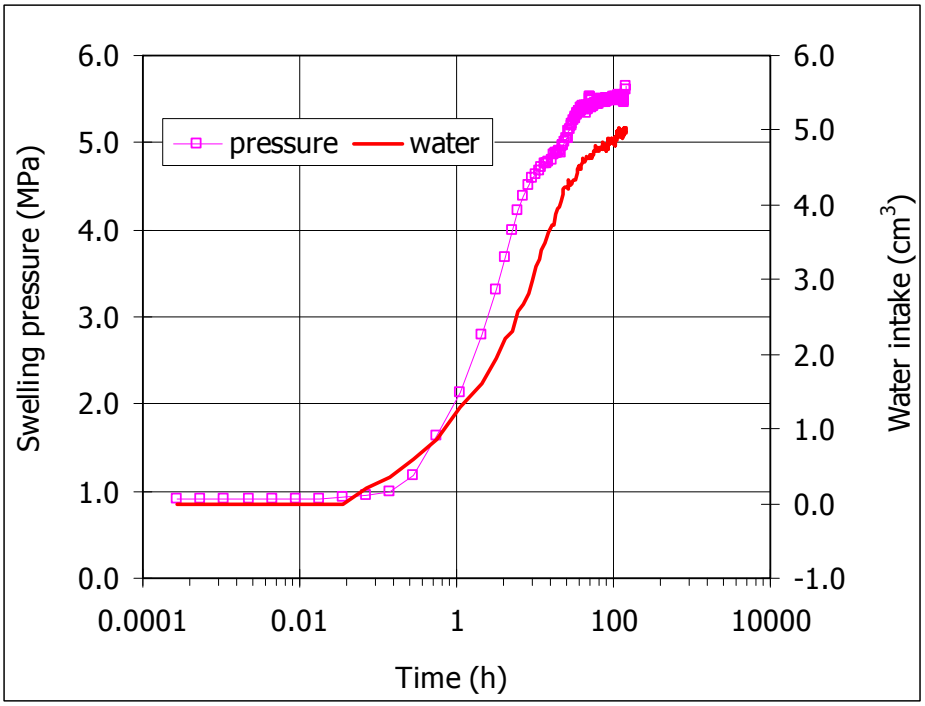

Figure 37: Evolution of swelling pressure and water intake in test EAP2_22 performed at 80°C with FEBEX bentonite compacted at nominal dry density 1.7 g/cm^3

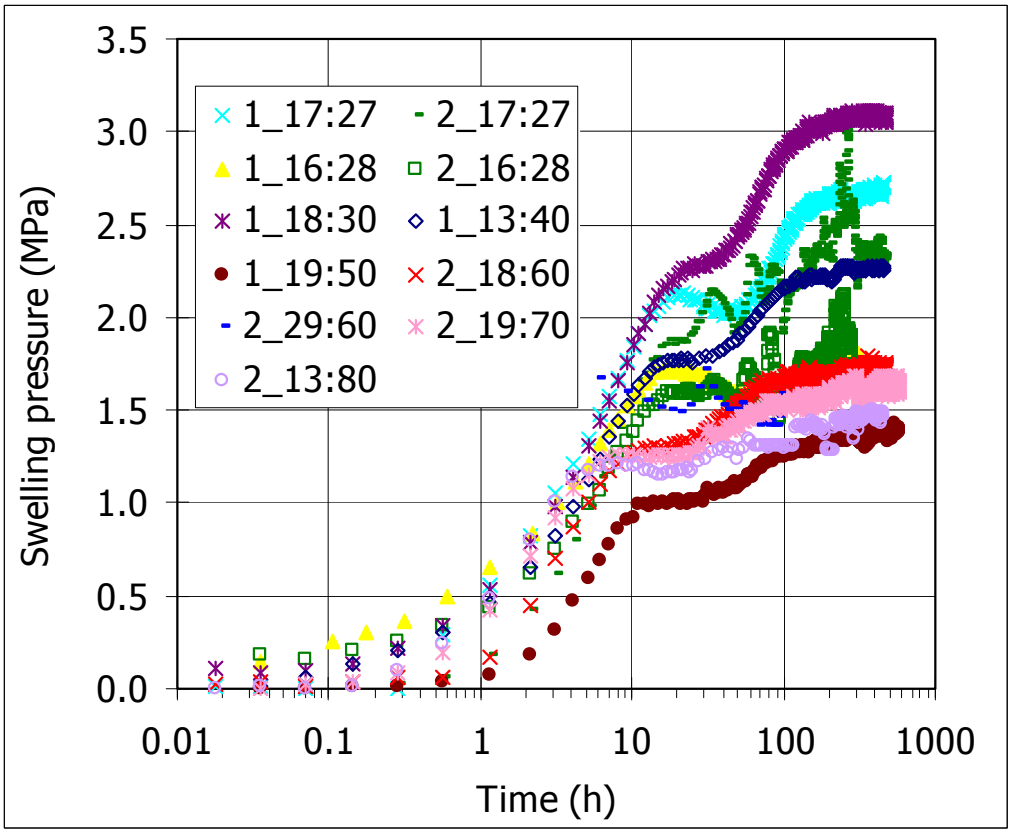

Figure 38: Evolution of swelling pressure in infiltration tests performed at different temperatures (indicated in °C after the test reference) in FEBEX samples compacted at nominal dry density 1.5 g/cm^3

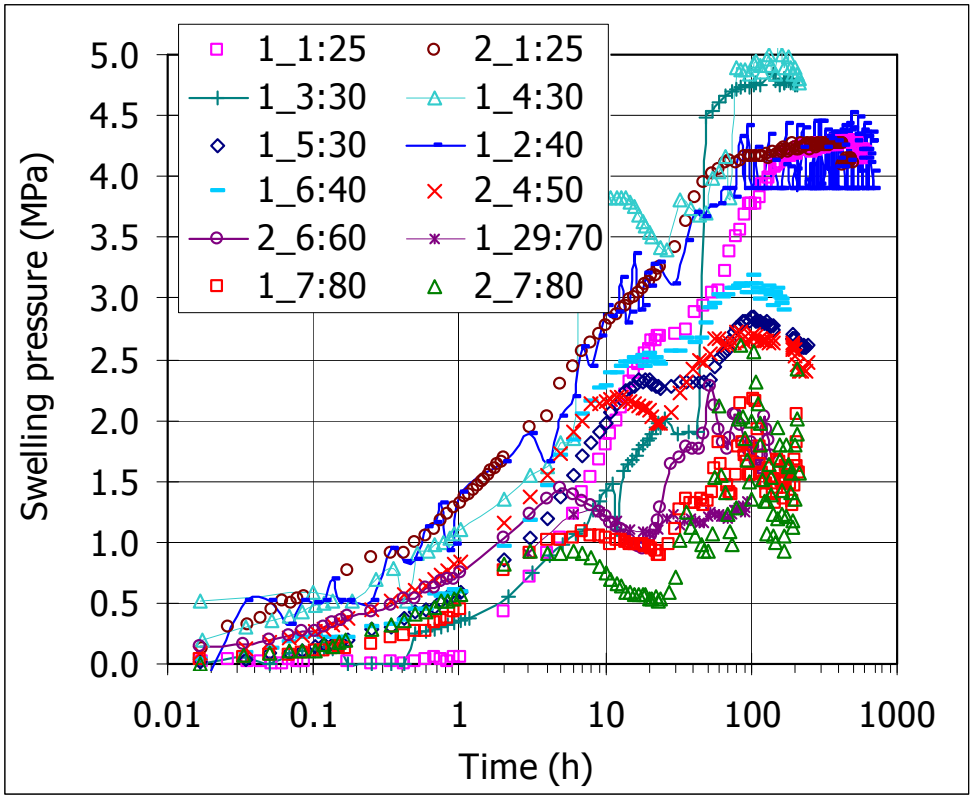

Figure 39: Evolution of swelling pressure in infiltration tests performed at different temperatures (indicated in °C after the test reference) in FEBEX samples compacted at nominal dry density 1.6 g/cm^3

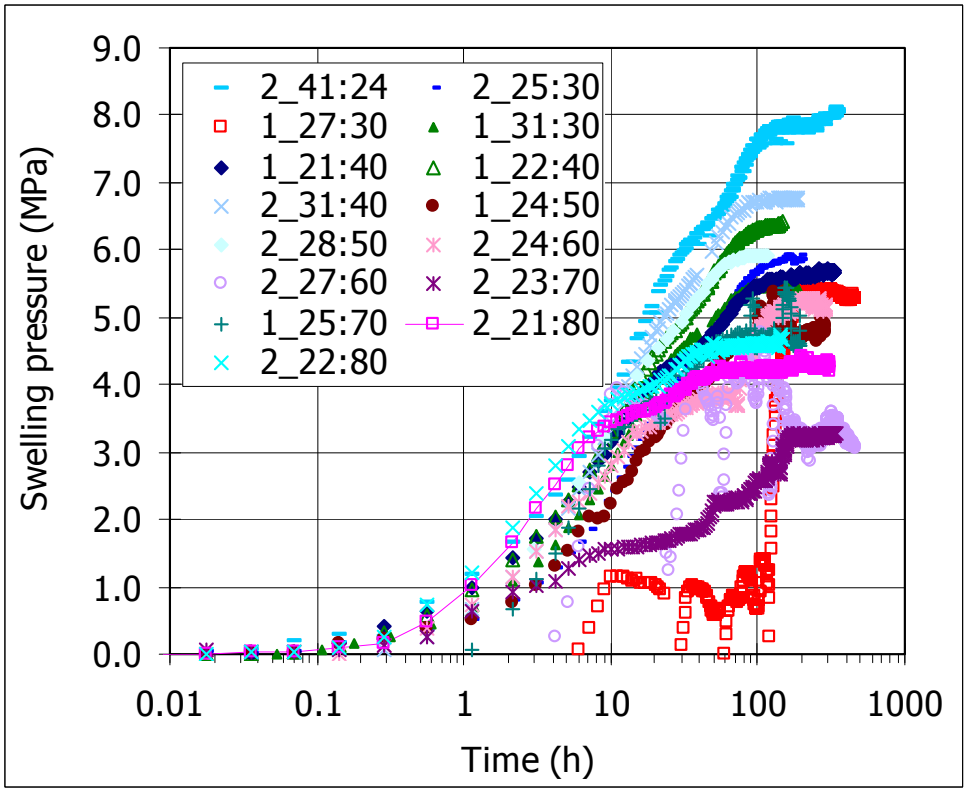

Figure 40: Evolution of swelling pressure in infiltration tests performed at different temperatures (indicated in °C after the test reference) in FEBEX samples compacted at nominal dry density 1.7 g/cm^3

The final swelling pressure values are plotted in Figure 41, where the dispersion of data can be mostly attributed to the variations in dry density, as the swelling pressure value is very sensitive to small density changes. The error bars shown in the figure were obtained from values measured in tests performed in standard oedometers at laboratory temperature to obtain Equation 3. A decrease in swelling pressure as a function of temperature is observed.

The results are plotted again in Figure 42 as swelling pressure as a function of dry density for different temperatures. Exponential trend lines have been fitted for every temperature between swelling pressure and dry density. The line resulting from Equation 3, corresponding to the values obtained at laboratory temperature (approximately 22°C), has also being plotted. Overall, all the swelling pressures measured in these tests are lower than those measured at laboratory temperature. The trend for the swelling pressure to decrease with temperature is only clear when the temperature is about 80°C. Also, the decrease in swelling pressure with temperature is higher as density increases.

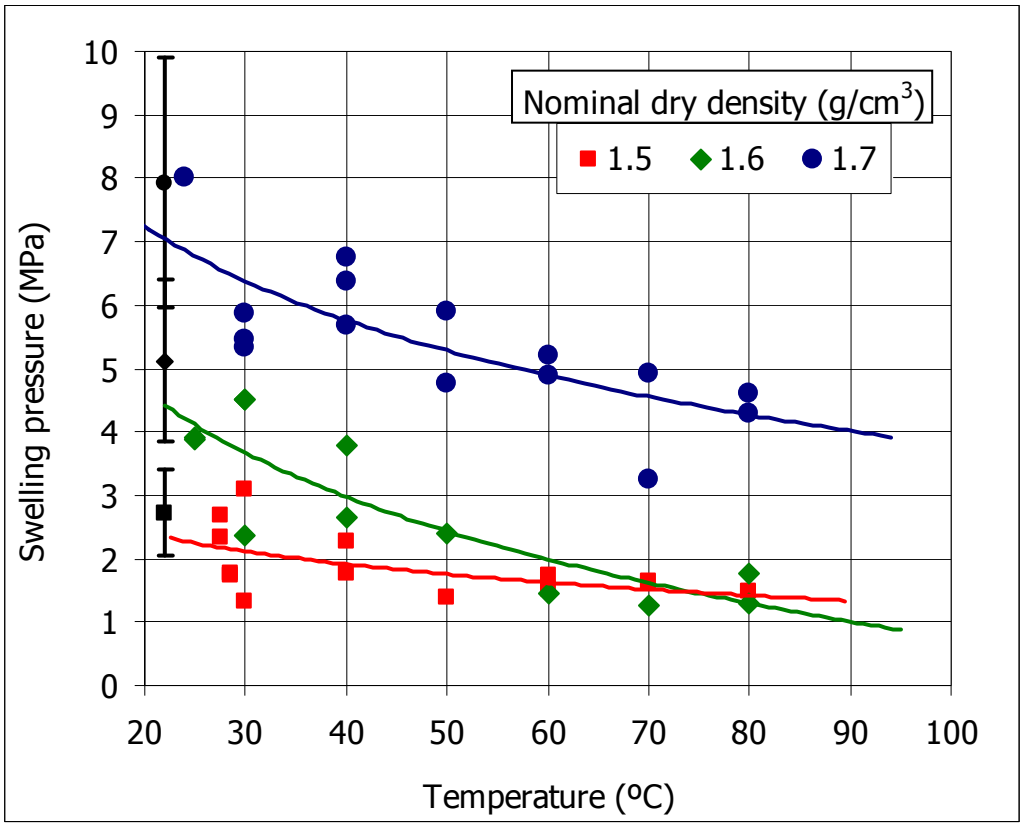

Figure 41: Swelling pressure as a function of temperature for saturated FEBEX clay compacted to different nominal dry densities (actual average dry densities were 1.48, 1.57 and 1.65 g/cm^3). The error bars have been obtained with Equation 3

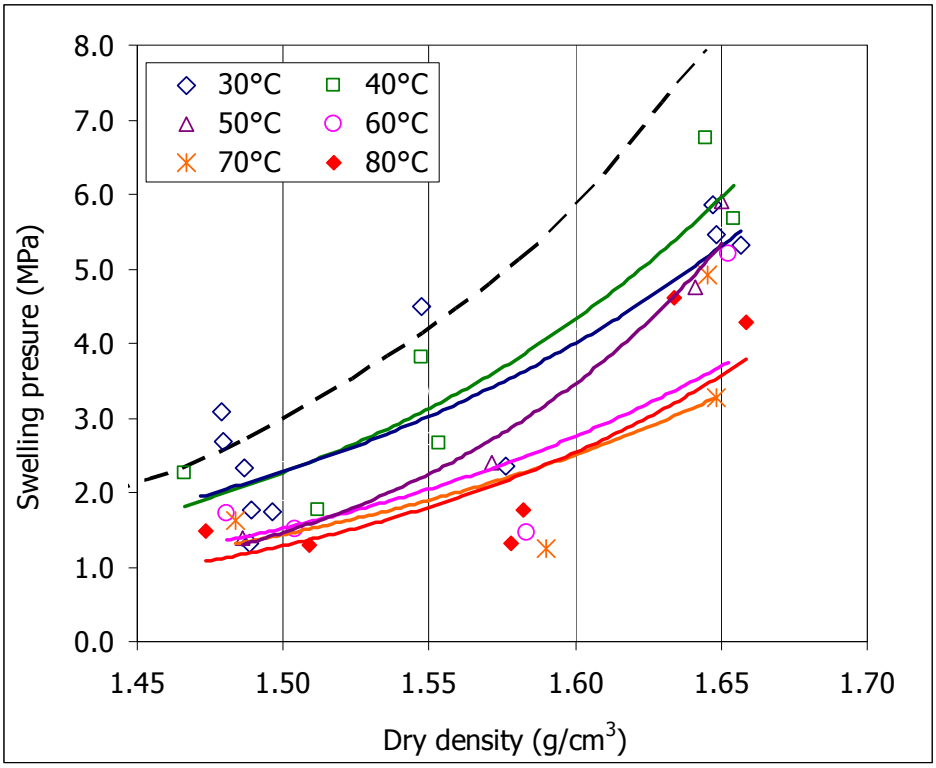

Figure 42: Swelling pressure as a function of dry density for different temperatures: experimental values and exponential fittings. The discontinuous line corresponds to the values obtained with Equation 3 (laboratory temperature)

5.3.2 Hydraulic conductivity

The hydraulic conductivity was measured in the samples described above, kept in the same equipments, once they were fully saturated. For that, various hydraulic gradients were applied between top and bottom of the specimens. For the nominal dry density 1.7 g/cm^3, the hydraulic gradients applied ranged from 5000 to 15000, for the nominal dry density of 1.6 g/cm^3 from 5600 to 20000, and for the nominal dry density of 1.5 g/cm^3 from 1700 to 15000. Lower hydraulic gradients were needed to obtain measurable flow as the temperature was higher. Below certain hydraulic gradients no flow was obtained, these threshold values depending on temperature and dry density of the bentonite. Although the issue has not been thoroughly analysed, in the case of nominal dry density 1.7 g/cm^3 the threshold hydraulic gradients have been from 3300 to 11700, with a trend to decrease with temperature; for the nominal dry density 1.6 g/cm^3 only in one test performed under hydraulic gradient 11700 and at temperature of 25°C no flow was observed; and for the nominal dry density 1.5 g/cm^3 a threshold gradient of 5000 has been found for temperatures of 40 and 80°C. Figure 43 shows two examples of the flows obtained in the permeability tests and the time required to get steady flows.

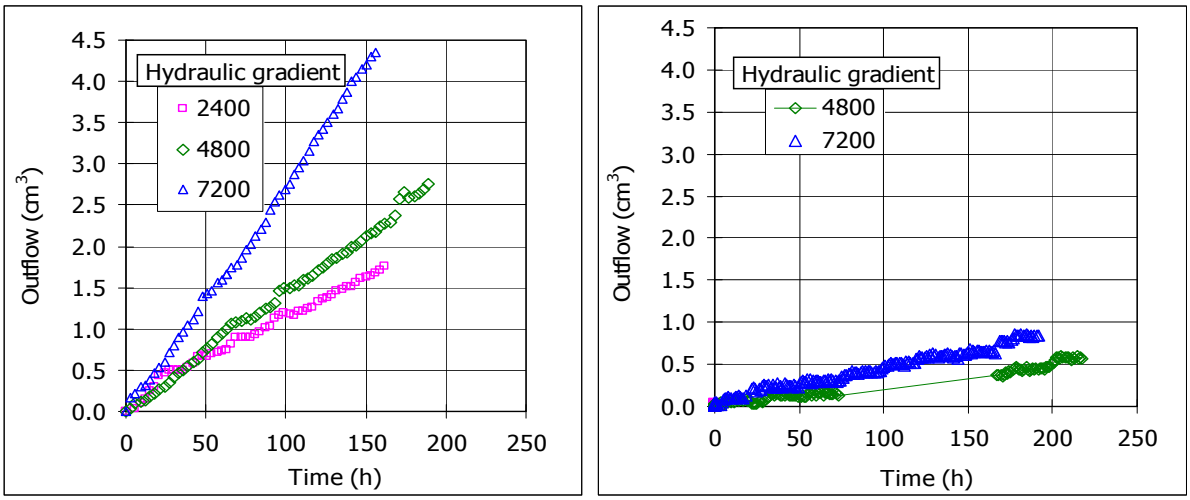

Figure 43: Water flow caused by the application of different hydraulic gradients in permeability tests performed at 40°C in samples of nominal dry density 1.5 g/cm^3 (left, test EAP2_30) and 1.7 g/cm^3 in which no flow occurred for a hydraulic gradient of 2400 (right, test EAP2_31)

Generally, during the permeability determination the density of the bentonite decreased slightly with respect to that at the end of saturation. This is due to the deformation of the equipment caused by the water injection pressures applied. Thus, the average density at the end of the permeability tests of the samples initially compacted at nominal dry density 1.7, 1.6 and 1.5 g/cm^3 was 1.64, 1.58 and 1.48 g/cm^3, respectively.

The permeability results are plotted in Figure 44. The error bars shown have been obtained from measurements at laboratory temperature (Equation 2). Despite the dispersion of data, it is clear that the permeability tends to increase with temperature, as expected from the decrease in water kinematic viscosity. Unexpected extremely low values have been measured for temperatures around 30°C in samples of nominal dry density 1.5 g/cm^3 and a very high value has been measured at 80°C for the nominal dry density 1.7 g/cm^3.

In the same figure the change in permeability expected as a consequence of the changes in water properties with temperature has been indicated with dotted lines, starting from the value obtained at laboratory temperature with Equation 2 for each dry density. For the nominal dry density 1.6 g/cm^3, the measured increase in permeability with temperature seems smaller than expected according to the changes in water permeability. However, for the other two densities, the behaviour is not so clear and, especially for the high temperatures, the permeabilities measured are higher than expected on the basis of changes in water properties.

Accordingly, Figure 45 shows the intrinsic permeability values corresponding to the hydraulic conductivities measured, computed taking into account the changes in water properties with temperature (kinematic viscosity and density) (Equation 8). For nominal dry density 1.6 g/cm^3, the increase in hydraulic conductivity is lower than predicted by the change in water viscosity, and for this reason the intrinsic permeability decreases with temperature, although the decrease is so small that it could be attributed to the experimental uncertainty and dispersion of the data. However, for nominal dry densities 1.5 and 1.7 g/cm^3, there is an increase in intrinsic permeability with temperature, what would mean that the hydraulic conductivity increase with temperature cannot be explained solely on the basis of the changes in water properties.

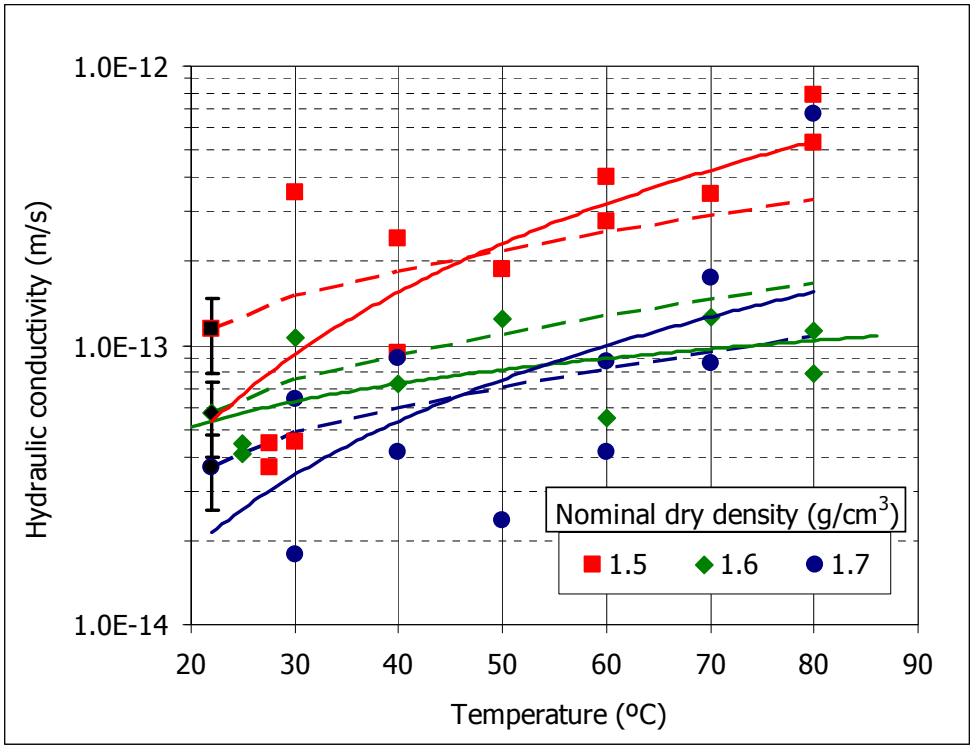

Figure 44: Hydraulic conductivity *vs.* temperature for saturated FEBEX clay compacted to different nominal dry densities (actual average dry densities are 1.48, 1.58 and 1.64 g/cm^3). Error bars obtained with Equation 2. The dotted lines indicate the change of permeability expected on the basis of water properties changes with temperature

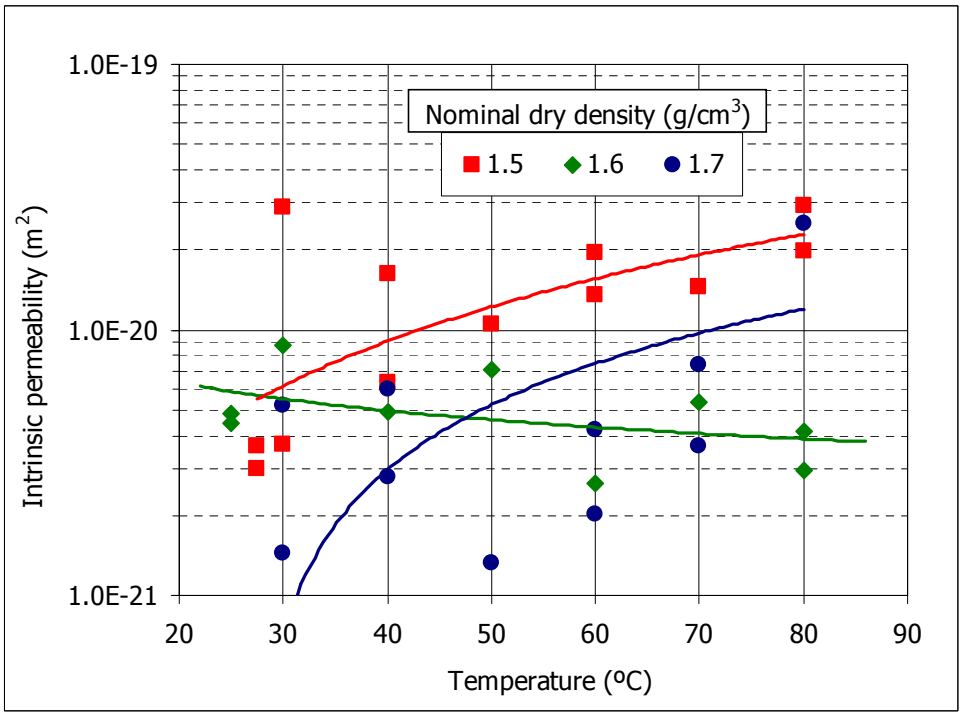

Figure 45: Variation of intrinsic permeability with temperature for FEBEX samples compacted at different nominal dry densities (actual average dry densities were 1.48, 1.58 and 1.64 g/cm^3)

5.3.3 Swelling capacity

Swelling under load tests have been performed with FEBEX bentonite compacted to nominal dry densities 1.50, 1.60 and 1.70 g/cm^3. Once in the oedometer, the samples were allowed to stabilise for 22 hours at the target temperature under no vertical load or hydration. This stabilisation period gave place to vertical strains of the samples around -0.1 percent in the case of samples of dry density 1.50 g/cm^3, -0.3 percent for samples of dry density 1.60 g/cm^3 and -0.2 percent for samples of dry density 1.70 g/cm^3, with a trend to be slightly higher for the higher temperatures, especially for the lower density. After having reached the stabilisation of the target temperature in the oedometer, vertical pressures of 0.1, 0.5, 1.5 and 3.0 MPa were applied to the samples, what implied a consolidation strain from 0 to 3 percent, depending on the dry density and the vertical load applied, the effect of temperature on this strain being difficult to asses. Immediately afterwards, the samples were saturated with deionised water.

The evolution of strain over time during saturation for the tests performed under different vertical loads on bentonite compacted to dry density 1.50, 1.60 (actual average 1.61 g/cm^3) and 1.7 g/cm^3 are plotted in Figure 46 to Figure 48, where the strain percentage is calculated as the increase in height with respect to the initial height of the sample, the negative values indicating swelling strains. It becomes clear the major influence of the pressure applied during hydration on the swelling behaviour. In the tests performed with bentonite compacted at dry density 1.50 g/cm^3 under high vertical load the samples are compressed when they are initially loaded, and in the case of the tests under 3 MPa, they barely swell during hydration. Even small collapses have been observed in the tests performed under this vertical load at high temperature. There is a first small collapse after 2 to 5 minutes of the beginning of hydration that is recovered after 1 or 2 hours. After 1 to 2 days there is a new collapse and a subsequent reactivation of swelling, which is never large. The second collapse seems more intense as the temperature is higher. For low temperatures there is just a temporary decrease in the swelling strain rate. These collapses were not observed for the other densities.

The final strains reached are plotted as a function of the temperature of the test in Figure 49 to Figure 51. As shown in the figures, the swelling capacity decreases with temperature and linear fittings can be drawn between swelling strain and pressure applied. It becomes clear that the influence of vertical load on swelling is much higher than the effect of temperature. Also, the effect of temperature seems more remarkable for the high densities and when the sample is tested under high vertical load. Although the fittings come from tests performed at temperatures ranging from 30 to 80°C, the extrapolation of lines towards higher temperatures seems to indicate that the swelling capacity would stand for temperatures around 100°C.

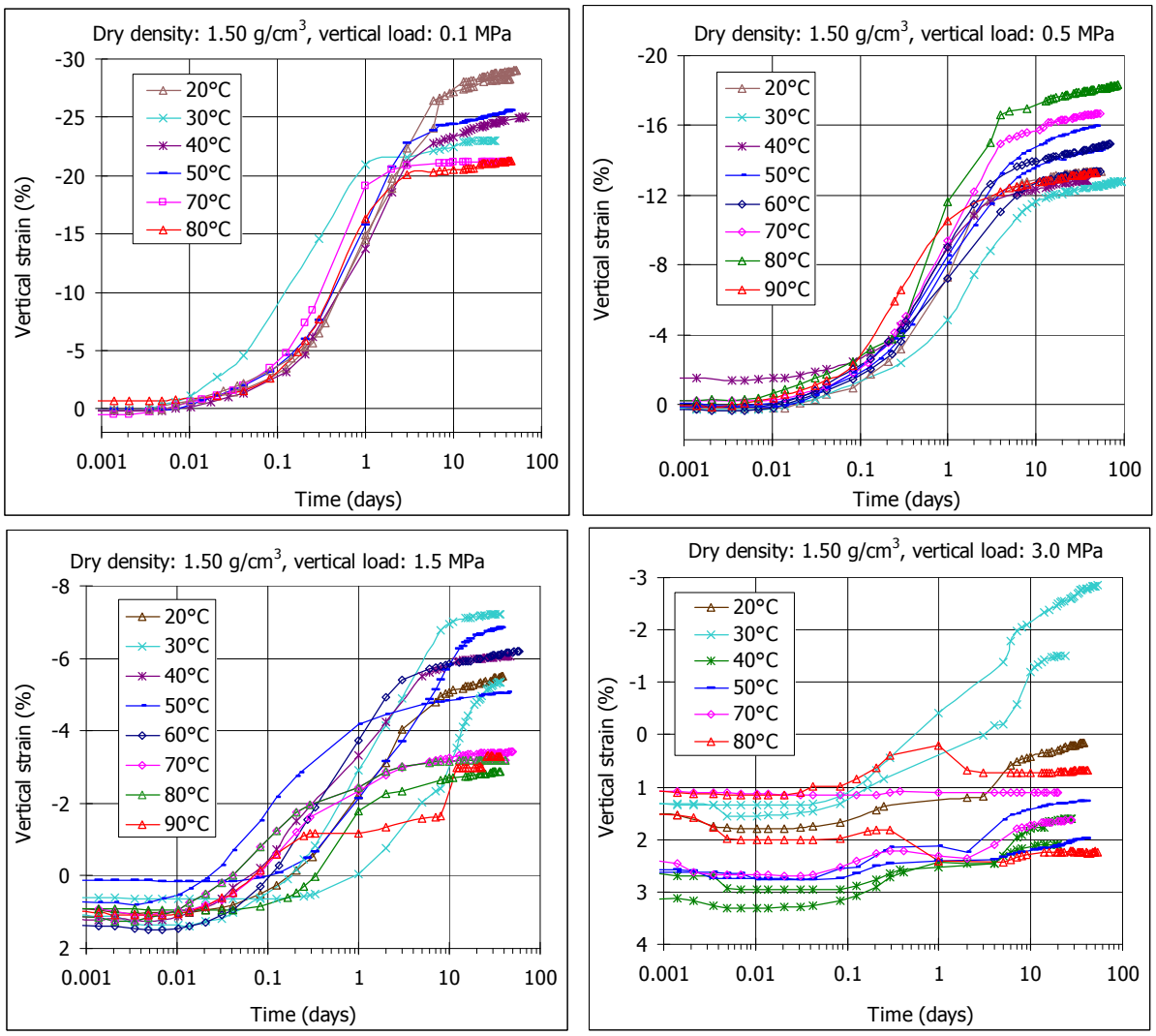

Figure 46: Evolution of strain of samples compacted to nominal dry density 1.50 g/cm^3 saturated with deionised water under different vertical pressures and temperatures

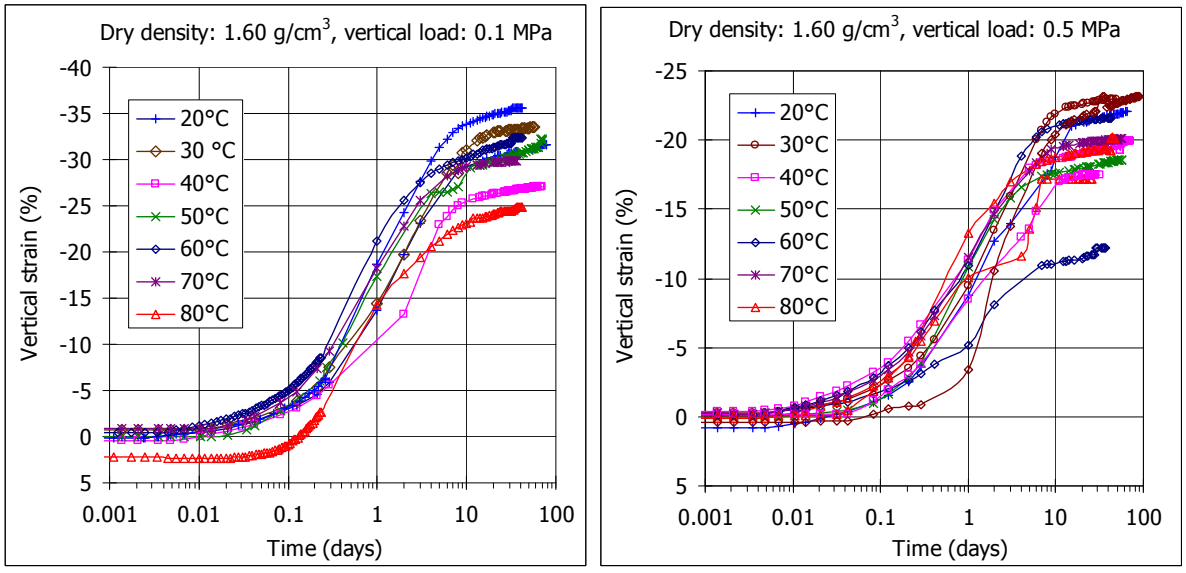

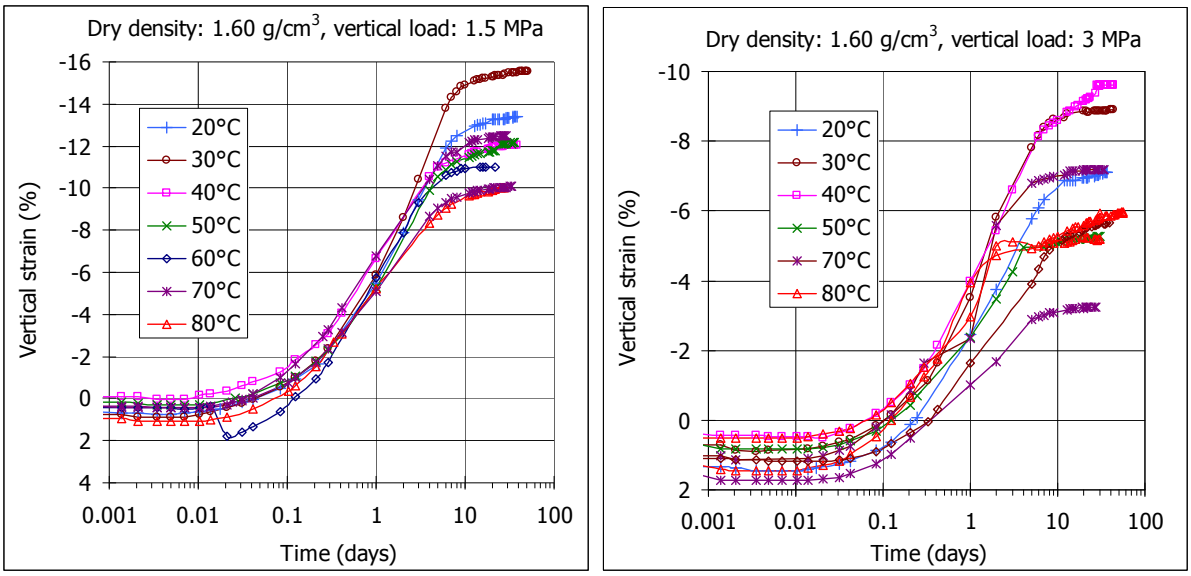

Figure 47: Evolution of vertical strain of samples compacted to nominal dry density 1.60 g/cm^3 saturated with deionised water under different vertical pressures and temperatures

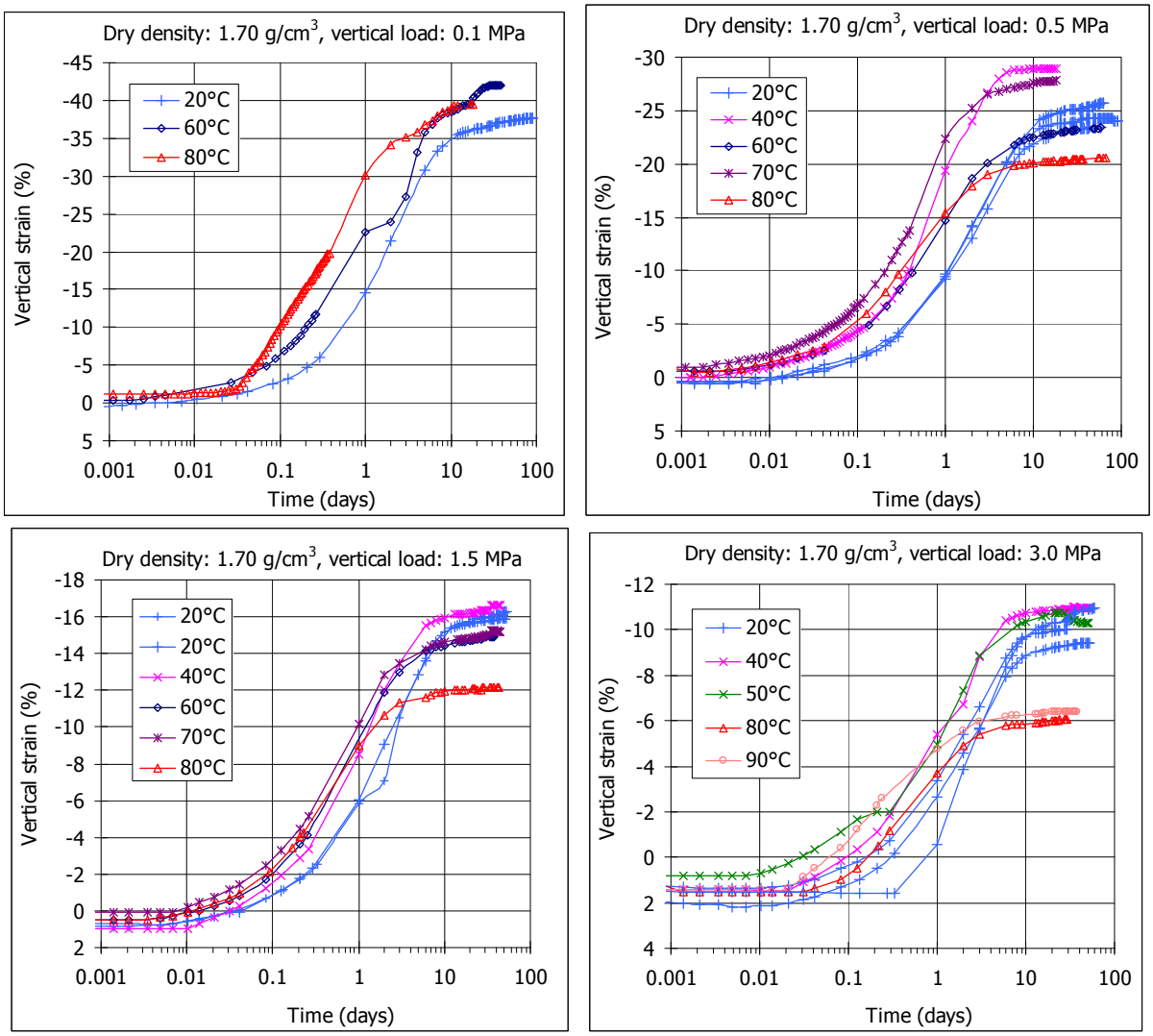

Figure 48: Evolution of vertical strain of samples compacted to nominal dry density 1.70 g/cm^3 saturated with deionised water under different vertical pressures and temperatures

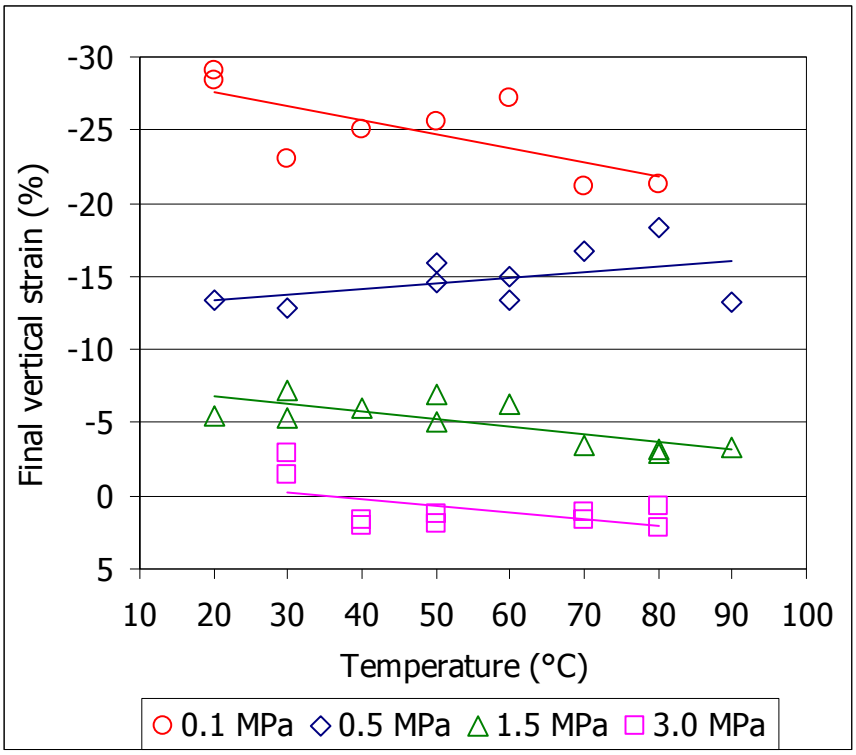

Figure 49: Final strain of samples compacted to nominal dry density 1.50 g/cm^3 saturated with deionised water under different vertical pressure and temperatures

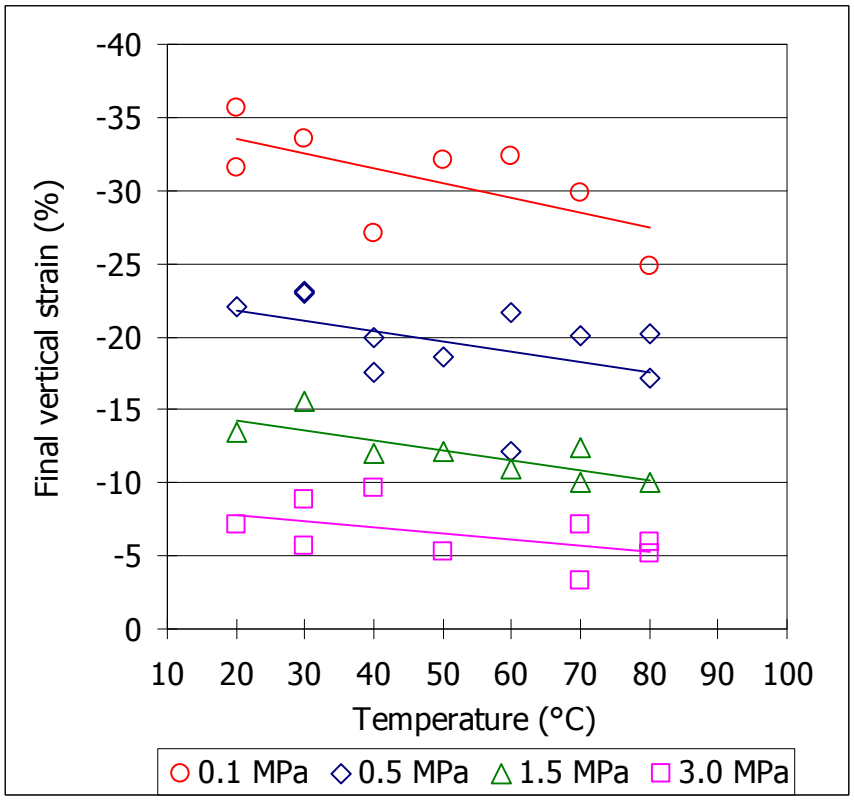

Figure 50: Final strain of samples compacted to nominal dry density 1.60 g/cm^3 saturated with deionised water under different vertical pressures and temperatures

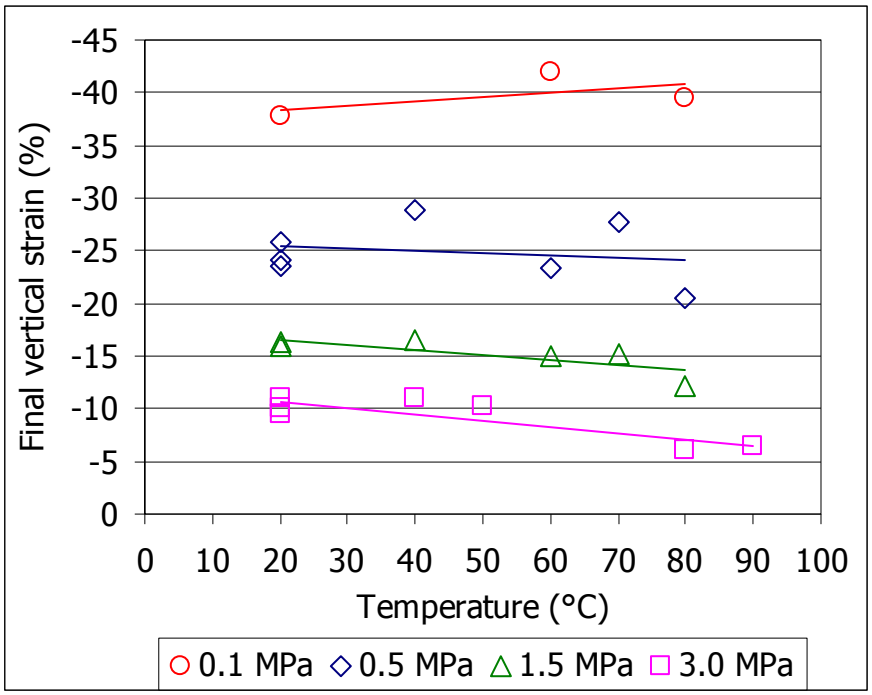

Figure 51: Final strain of samples compacted to nominal dry density 1.70 g/cm^3 saturated with deionised water under different vertical pressures and temperatures

5.3.4 Water retention capacity

Cell method

During the FEBEX project several tests were performed with the FEBEX bentonite compacted at nominal dry densities 1.60, 1.65 and 1.70 g/cm^3 at temperatures 20, 40, 60 and 80°C using the cell method (Figure 1, Lloret *et al*. 2004). During the NF-PRO project a wider range of densities has been tested, some of the tests being still underway (Table X).

Table X: Water retention tests in cells at different temperatures with FEBEX bentonite compacted to different dry densities performed during FEBEX (FBX), NF-PRO (NFP) or underway

	1.30 g/cm^3	1.40 g/cm^3	1.50 g/cm^3	1.60 g/cm^3	1.65 g/cm^3	1.70 g/cm^3	1.80 g/cm^3
20°C	NFP	NFP	NFP	FBX	FBX	FBX	
40°C					FBX	FBX	
60°C	NFP	underway	NFP	underway	FBX	underway	underway
70°C	NFP		NFP	underway		underway	underway
80°C				FBX		FBX	

The results obtained during FEBEX showed the decrease in the water retention capacity with temperature. However, for the lower densities tested afterwards (1.3 to 1.5 g/cm^3) no significant influence of temperature on the retention capacity has been observed. Figure 52 shows some of the results obtained plotted in the form of retention curves. Although some of them are preliminary because the tests have not been finished yet, it becomes clear that for the

low suctions the retention capacity is higher for the low-density samples, whereas for higher suctions there is not a significant influence of density on the retention capacity. This was also observed during the FEBEX project and for the MX-80 bentonite, *i.e.* that there is a suction threshold value above which, for a given water content, the suction of the higher density samples is higher, and below which the trend inverts. This threshold value is between 10 and 20 MPa for the range of temperatures studied (Villar 2007, Villar & Gómez-Espina 2008).

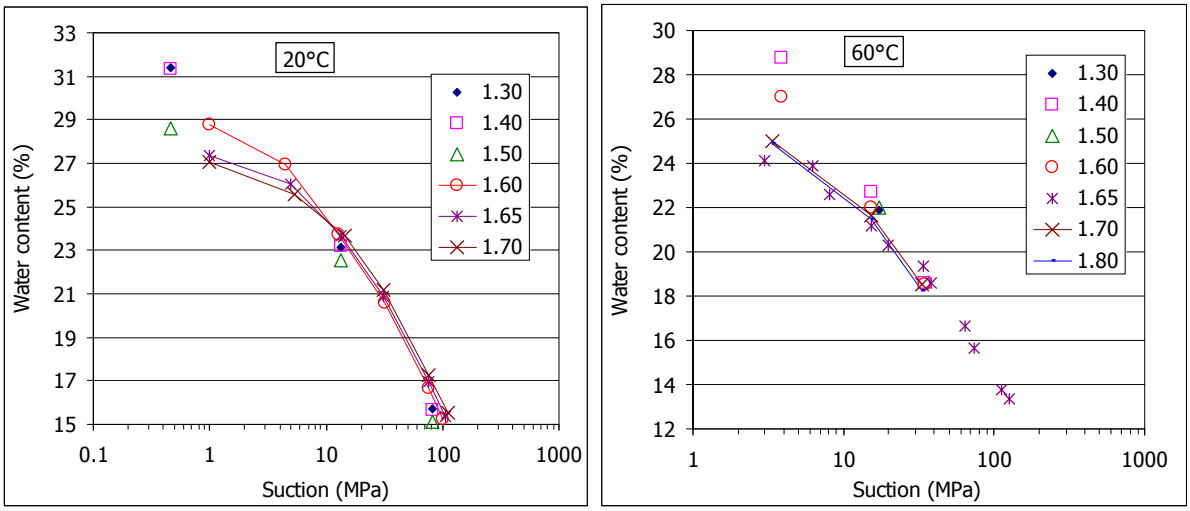

Figure 52: Water retention curves obtained in wetting paths for FEBEX bentonite compacted to different dry densities (in g/cm^3) at 20 and 60°C (some results are preliminary, check Table X)

Sensor/cell method

This method has been used to test FEBEX samples compacted to dry densities 1.50, 1.60 and 1.75 g/cm^3 in heating/cooling paths. The compacted samples had water contents between 7 and 22 percent. For each temperature the *RH* equilibrium was reached in a few hours (Figure 53)

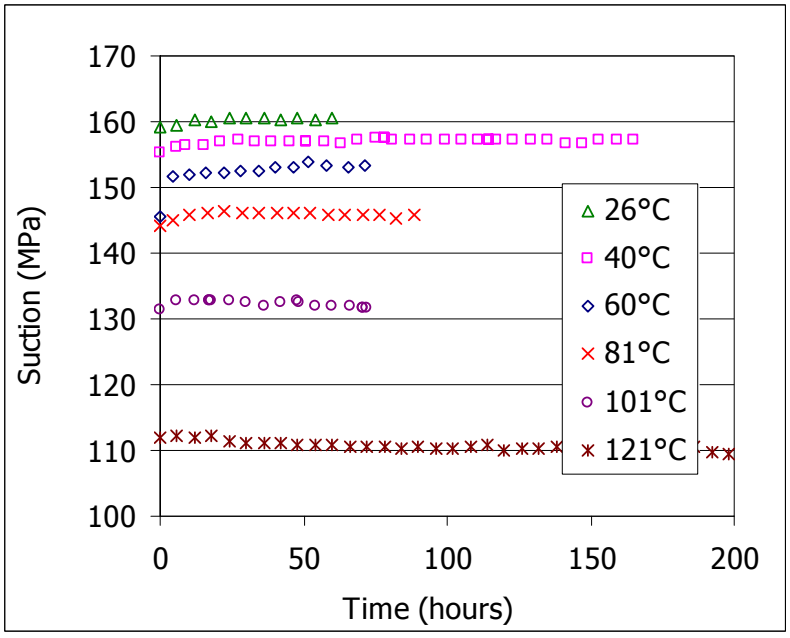

Figure 53: Evolution of suction in FEBEX bentonite compacted at dry density 1.50 g/cm^3 with water content 11 percent during the heating phase

The average equilibrium values of suction measured for each water content in samples compacted at dry density 1.50 g/cm^3 are plotted in Figure 54, which shows their evolution with temperature and how suction decreases with temperature, especially for temperatures above 60°C. There is barely any hysteresis during the heating-cooling phases. These values are plotted in Figure 55 for the heating paths and in Figure 56 for the cooling paths in the form of retention curves. They show a decrease in the retention capacity with temperature.

In some of the samples, there was a water loss during heating at the highest temperatures. In these cases there exists a difference between the initial and the final water contents (tests for w=14, 17 and 18%), and only the heating part of the test is valid. In tests with very high water content, during heating the *RH* reaches values very close to 100 percent and water condensates in the sensor, which stops working properly (test for w=21%). Also, the precision of the sensor decreases when *RH* is higher than 90 percent.

There were variations in the actual dry density of the samples between 1.45 and 1.54 g/cm^3, although the average value of the blocks was 1.50 g/cm^3. At the end of the tests, the water content in different positions inside the bentonite block was checked. The variation among the different samples tested in a block is less than 1.5 percent, with no clear trend along the height or the radius of the block.

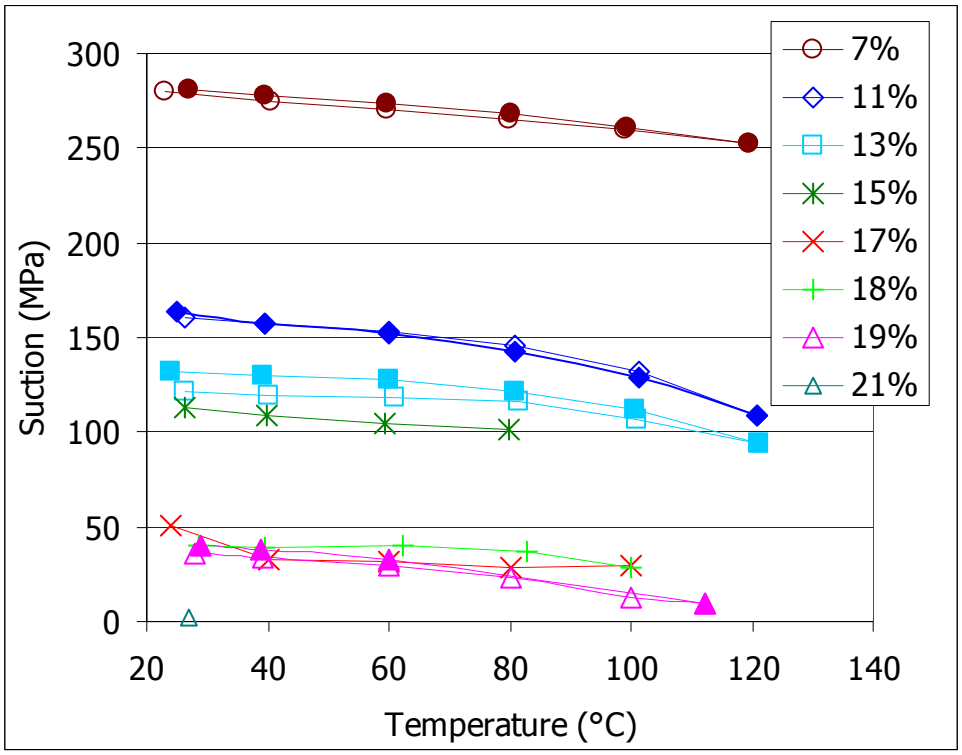

Figure 54: Equilibrium suction measured during heating/cooling in blocks of FEBEX bentonite compacted at 1.50 g/cm^3 with different water contents, indicated in the legend (filled symbols: cooling)

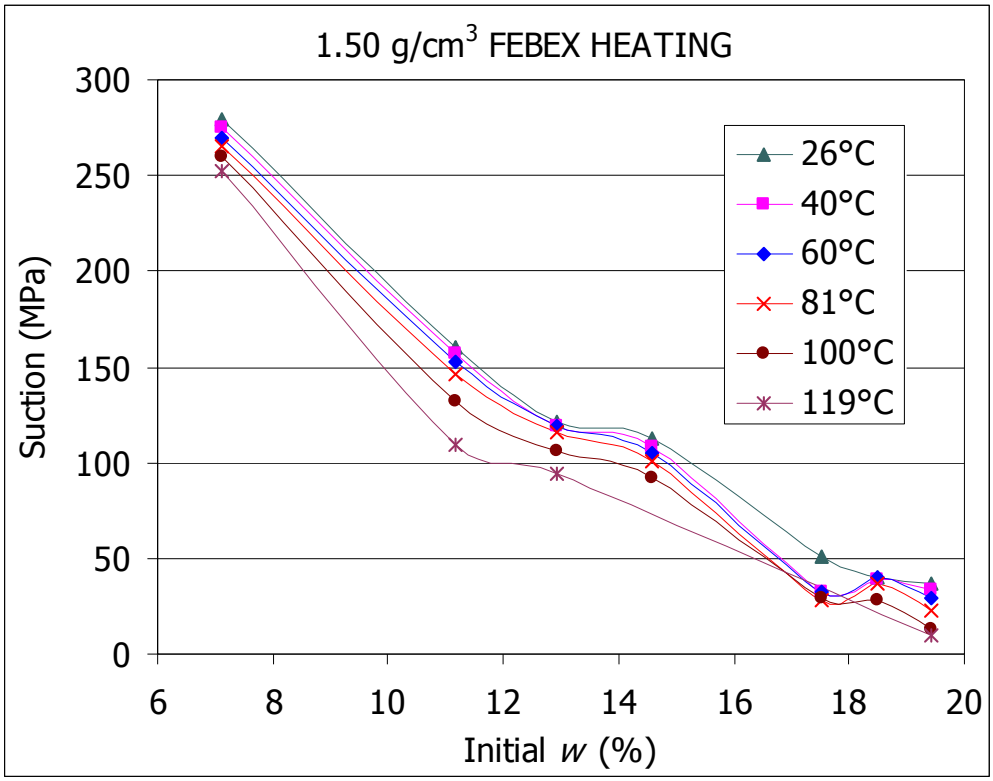

Figure 55: Retention curves obtained during heating with the sensor/cell method for the FEBEX bentonite compacted at 1.50 g/cm^3

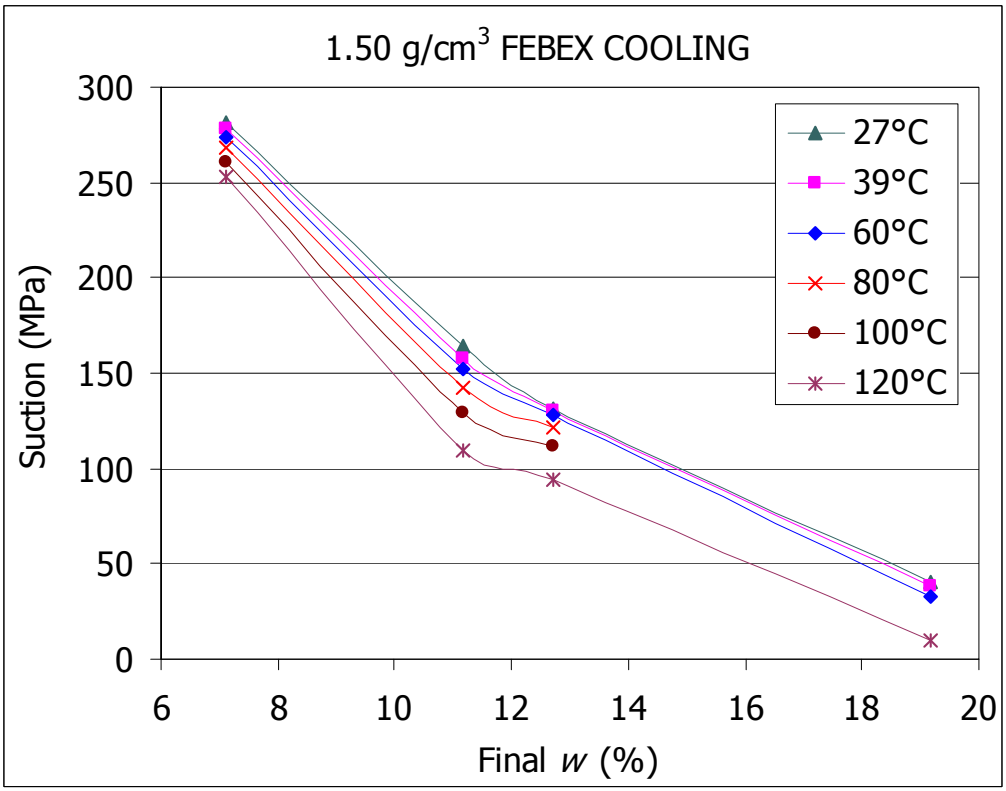

Figure 56: Retention curves obtained during cooling with the sensor/cell method for the FEBEX bentonite compacted at 1.50 g/cm^3

The average equilibrium values of suction measured in FEBEX bentonite compacted to nominal dry density 1.60 g/cm^3 for each water content are plotted in Figure 57, which shows the evolution with temperature. The decrease in suction with temperature is higher for the samples with low water content and for temperatures above 60°C. There are not hysteresis phenomena during the heating-cooling phases. These values are plotted in Figure 58 for the heating paths and in Figure 59 for the cooling paths in the form of retention curves. They show a decrease in the retention capacity with temperature.

In tests with very high water content, the *RH* reaches values close to 100 percent during heating and the sensor stops working (test for *w*=22%).

The average dry density of the compacted blocks is 1.61 g/cm^3. There are variations in the value obtained between 1.55 and 1.66 g/cm^3. At the end of the tests the water content in different positions inside the bentonite block was checked. The variation among the different samples tested in a block was less than 1 percent, with no clear trend along the height or the radius of the block.

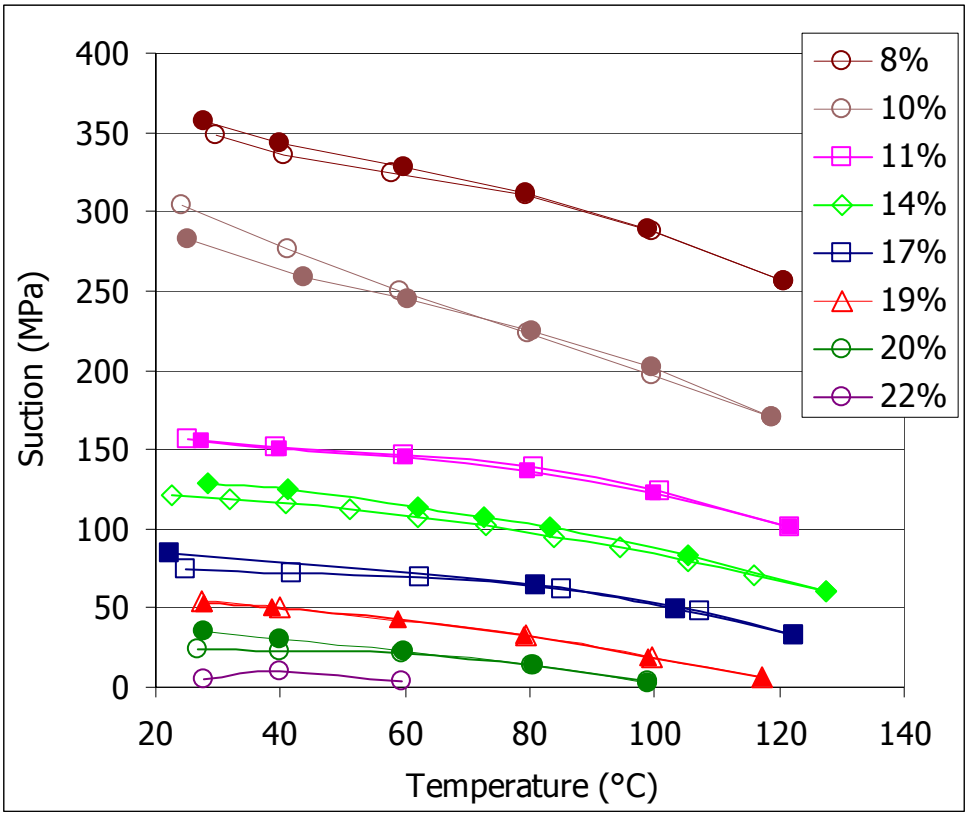

Figure 57: Equilibrium suction measured during heating/cooling in blocks of FEBEX bentonite compacted at 1.60 g/cm^3 with different water contents, indicated in the legend (filled symbols: cooling)

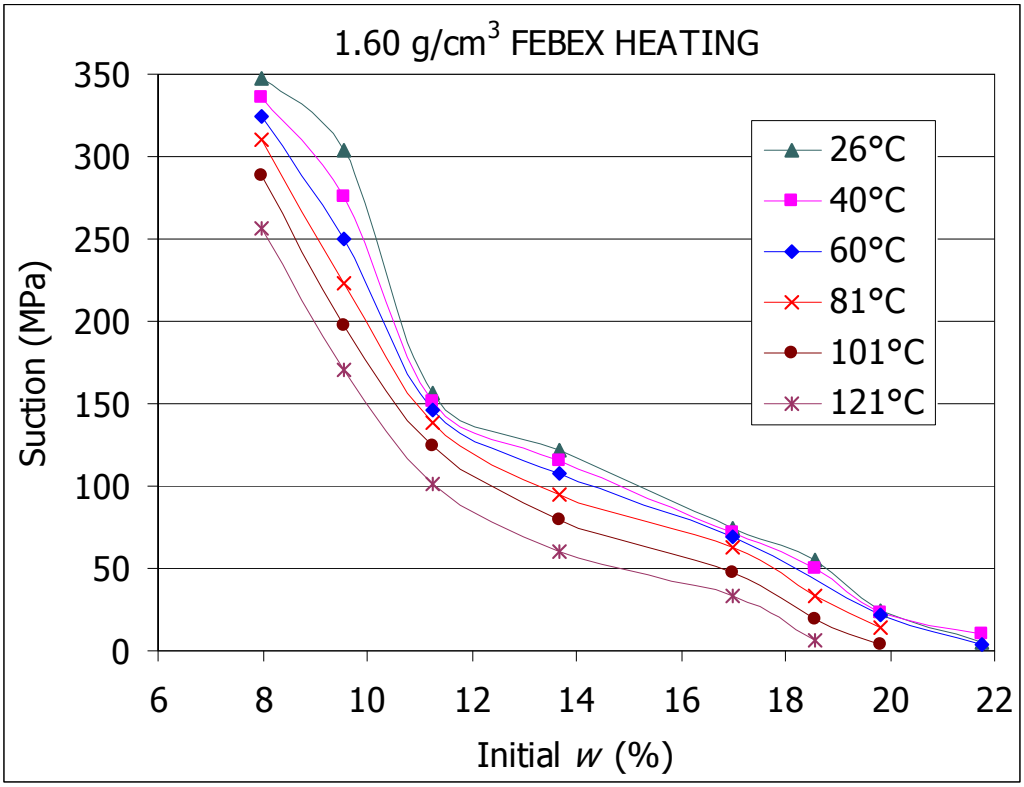

Figure 58: Retention curves obtained during heating with the sensor/cell method for the FEBEX bentonite compacted at 1.60 g/cm^3

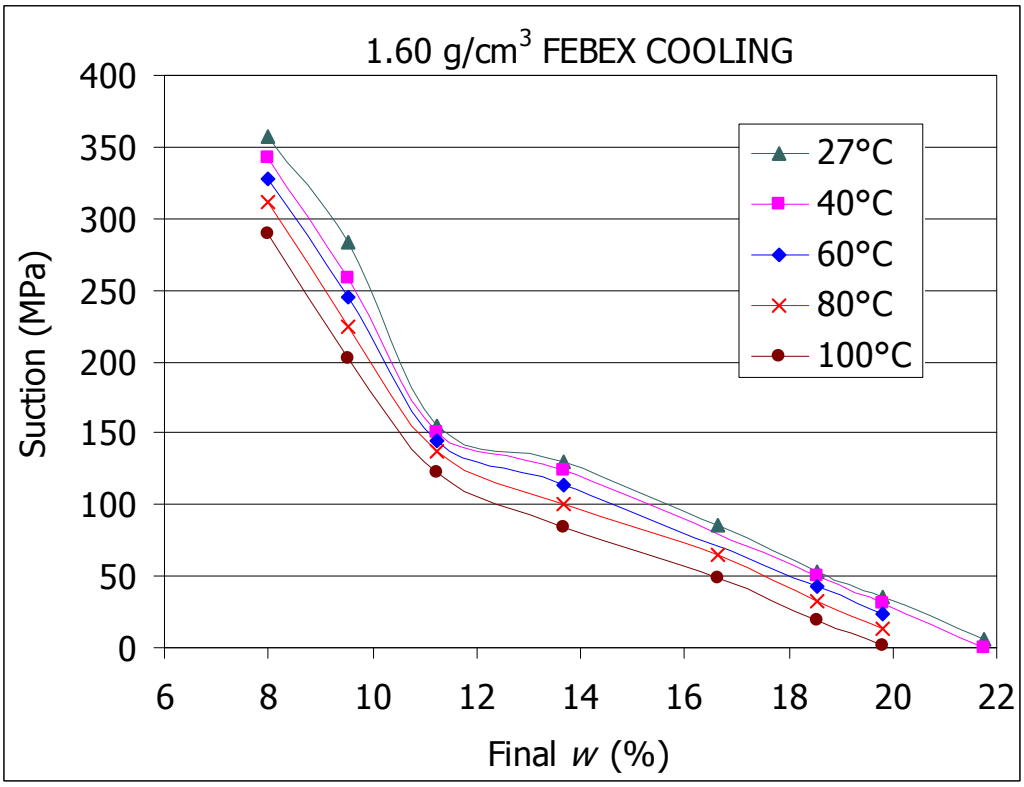

Figure 59: Retention curves obtained during cooling with the sensor/cell method for the FEBEX bentonite compacted at 1.60 g/cm^3

The average equilibrium values of suction measured in the FEBEX bentonite compacted to nominal dry density 1.75 g/cm^3 for each water content are plotted in Figure 60, which shows the evolution with temperature. Again, the decrease in suction with temperature is higher for the samples with water content below hygroscopic. For samples with high water content, the influence of temperature on suction is more significant for temperatures above 60-80°C. There are not hysteresis phenomena during the heating-cooling phases. These values are represented in Figure 61 for the heating paths and in Figure 62 for the cooling paths in the form of retention curves. They show a decrease in the retention capacity with temperature.

In some cases, there was a water loss during heating at the highest temperatures. In these cases there exists a difference between the initial and the final water contents (tests for w=12, 14, 18 and 19%).

The dry density of the blocks was sometimes lower than desired, the average value of all the tests being 1.71 g/cm^3. The variations in the value obtained are between 1.68 and 1.75 g/cm^3. At the end of the tests, the water content in different positions inside the bentonite block was checked. The variation among the different samples tested in a block is less than 1.5 percent, with no clear trend along the height or the radius of the block.

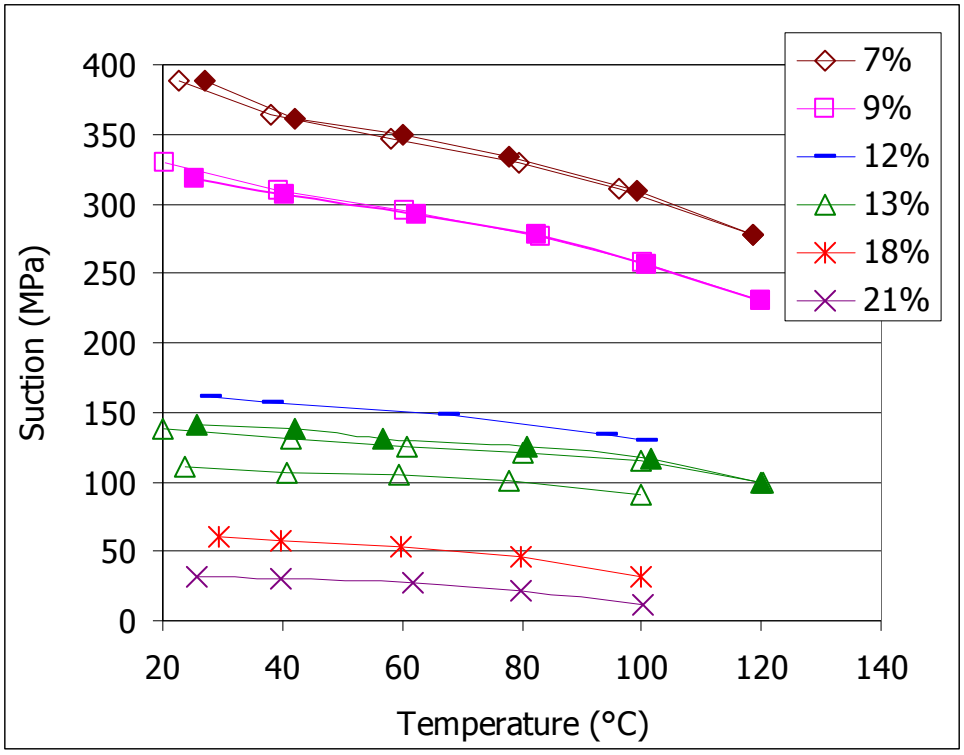

Figure 60: Equilibrium suction measured during heating/cooling in blocks of FEBEX bentonite compacted at 1.75 g/cm^3 with different water contents, indicated in the legend (filled symbols: cooling)

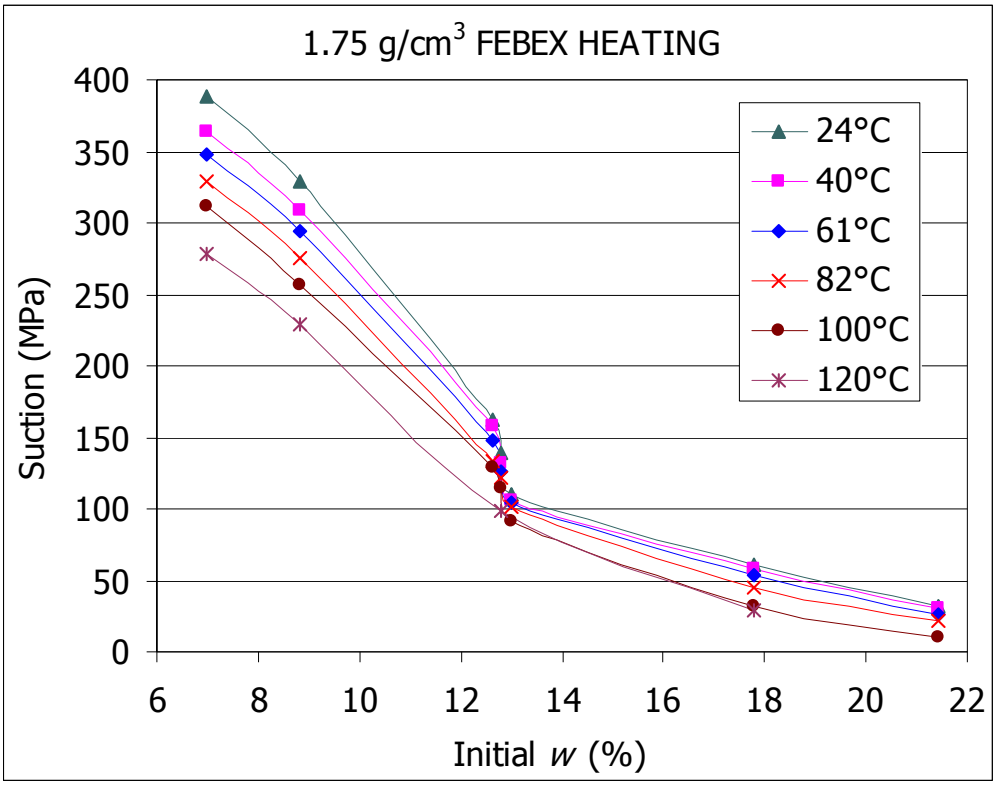

Figure 61: Retention curves obtained during heating with the sensor/cell method for the FEBEX bentonite compacted at 1.75 g/cm^3

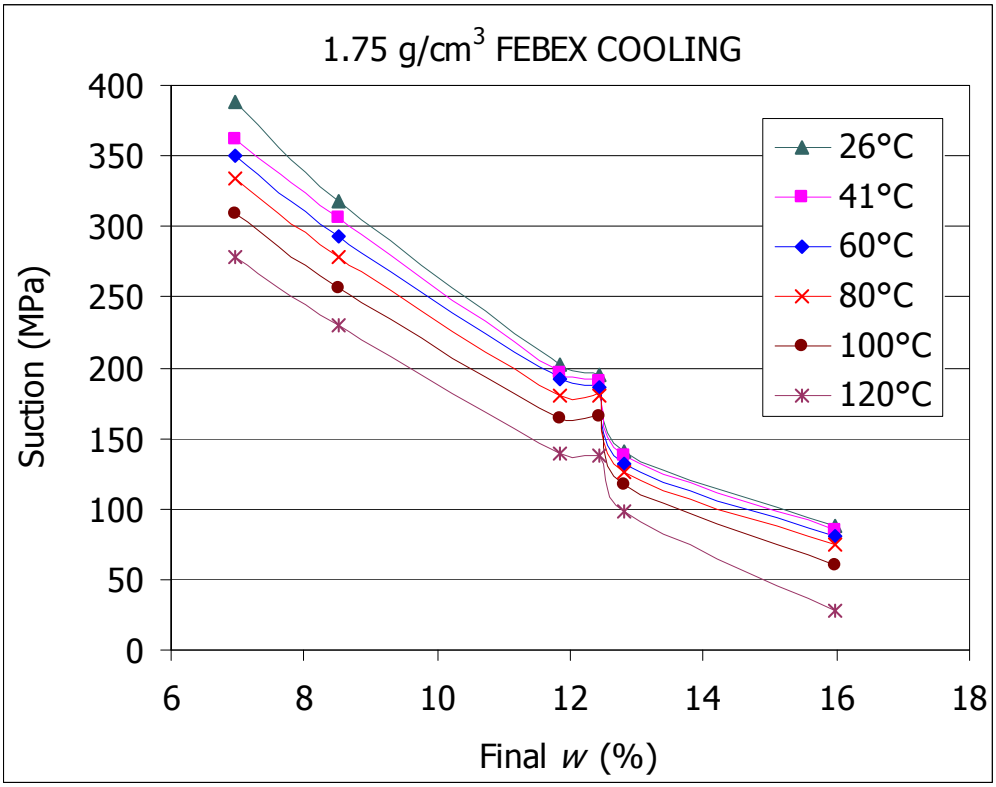

Figure 62: Retention curves obtained during cooling with the sensor/cell method for the FEBEX bentonite compacted at 1.75 g/cm^3

Analysis of results

The water retention capacity of the compacted bentonite at different temperatures has been tested using two methods. Figure 63 shows some of the results obtained with both methods, which are coherent. For the range of suctions considered, the retention capacity of the sample of dry density 1.7 g/cm^3 is higher than that of 1.5 g/cm^3. As it was explained above, this trend would invert for lower suctions. The results obtained with the sensor/cell method for two temperatures are shown in Figure 64. Although the retention capacity is higher for the higher densities, it can be observed that the difference becomes smaller as suction decreases, especially for suctions below 100 MPa.

Figure 63 and Figure 64 show that the samples tested at high temperature (80 or 100°C) have lower retention capacity than those tested at room temperature (Lloret *et al*. 2004, Lloret & Villar 2007). It can also be observed that the effect of temperature on the retention capacity is higher for the high dry density. This can be further checked in Figure 65, in which some results obtained with the sensor/cell method for dry densities 1.50 and 1.75 g/cm^3 are plotted. The decrease in suction with temperature is significant, especially for temperatures above 60°C and for the low water contents. There is barely any hysteresis between the initial heating and the subsequent cooling. The influence of temperature on the retention capacity seems to be higher than that of density, especially for the low suctions. Also, the smaller slope of the curves for the dry density 1.5 g/cm^3 would indicate a smaller effect of temperature on the retention capacity for the low-density samples.

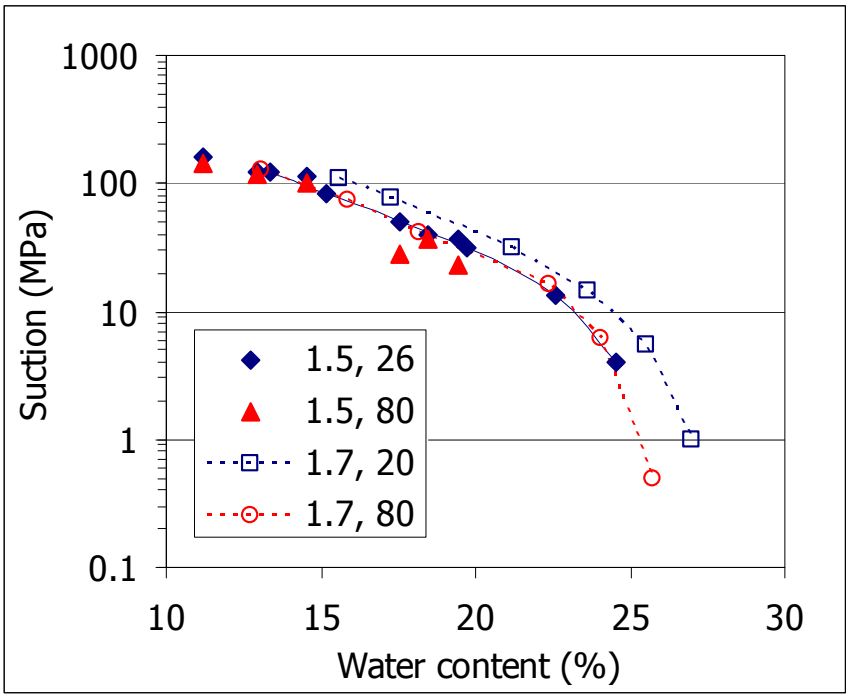

Figure 63: Retention curves obtained for the FEBEX bentonite compacted to different dry densities (indicated in g/cm^3) and temperatures (indicated in °C) (Villar & Gómez-Espina 2008)

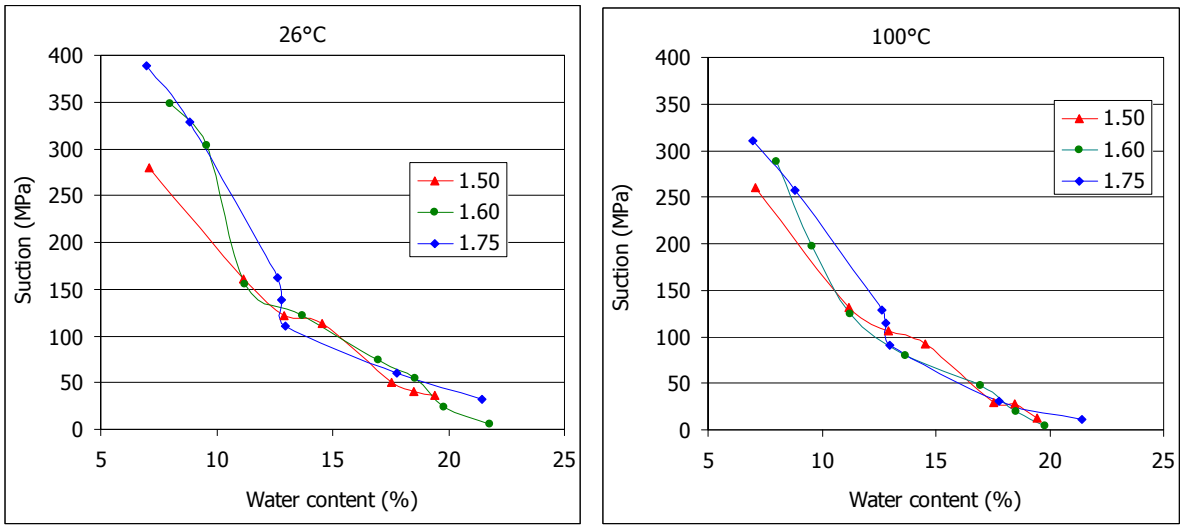

Figure 64: Retention curves at two temperatures obtained with the sensor/cell method for FEBEX bentonite compacted to different dry densities (indicated in g/cm^3)

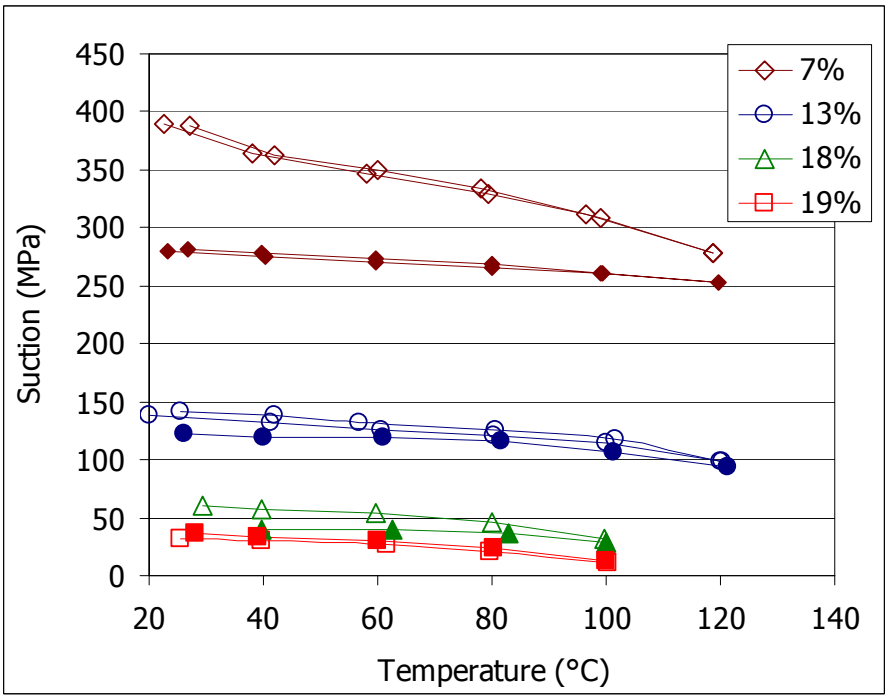

Figure 65: Evolution of suction with temperature (heating-cooling paths) for samples compacted with different water content (indicated in the legend) at dry density 1.75 g/cm^3 (open symbols) and 1.5 g/cm^3 (filled symbols)

Although it is generally acknowledged that suction in clayey soils is not exclusively a capillary process, the Laplace equation, which relates the capillary pressure and the pore size distribution, is a first approximation to explain the water retention processes in soils, if we assume that the soil suction, s, coincides with the capillary pressure, p_c, given by:

$$p_c = p_g - p_l = 2\sigma \cos\theta / r \qquad [10]$$

where p_g and p_l are gas and liquid pressure, respectively, σ is the interfacial tension between fluids, θ is the contact angle, and r is the effective mean radius of the capillary tubes. By mathematical derivation of Equation 10 it is possible to obtain the variation of suction with respect to temperature, for constant water content, as:

$$\left.\frac{\partial s}{\partial T}\right|_w = \frac{s}{\sigma}\frac{\partial \sigma}{\partial T} \qquad [11]$$

where the surface tension of water is a function of temperature, T, and w is the water content. In Figure 66, Figure 67 and Figure 68 the measured evolution of suction with temperature for some samples of nominal dry density 1.50, 1.60 and 1.75 g/cm^3 tested with the sensor/cell method has been plotted. The suction values computed with Equation 11 by taking into account the change in water surface tension when the temperature increases from 20 to 120°C have also been included. There is a discrepancy between measured and computed values – which is more significant for temperatures above 60°C– which is probably due to the fact that capillarity is not the main mechanism of water retention in bentonite (Jacinto *et al*. 2009). Instead, physico-chemical interactions between the clay particles and the water tightly attached to them are responsible for the soil retention capacity, especially in the high suction range. In this low water content region, changes in the interaction mechanisms between the clay and water are considered the main temperature effects on water retention capacity (Romero *et al*. 2001, Villar & Lloret 2004, Villar *et al*. 2005b).

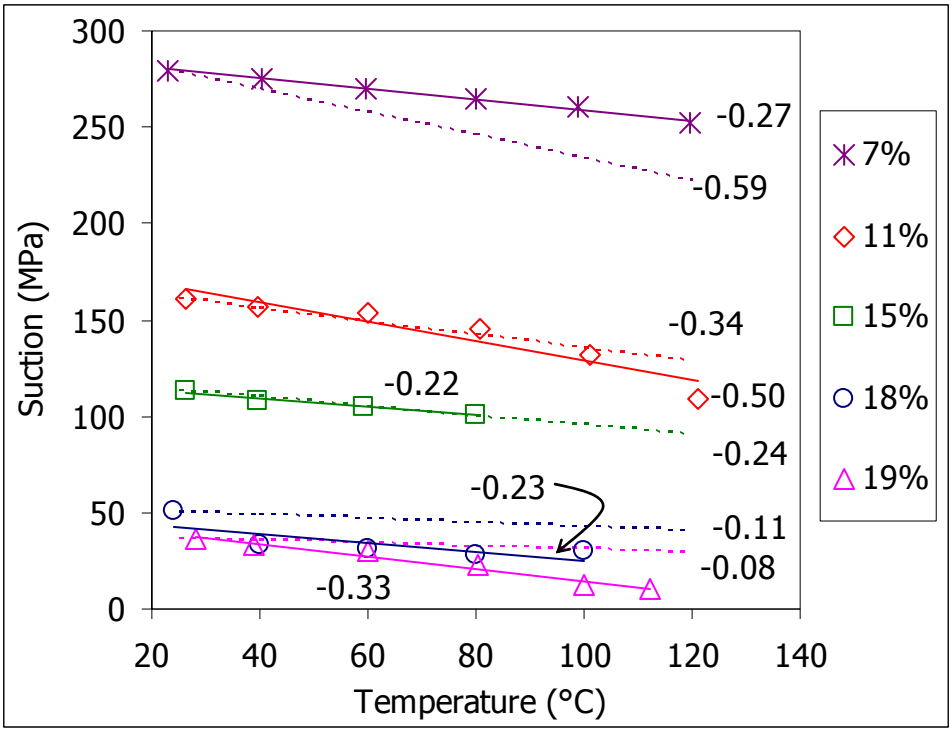

Figure 66: Change in suction with temperature for FEBEX bentonite compacted with different water contents (indicated in the legend) to dry density 1.50 g/cm^3 as measured with the sensor/cell method (continuous lines) and as computed by the change in water surface tension (dotted lines). The slope of the lines is indicated

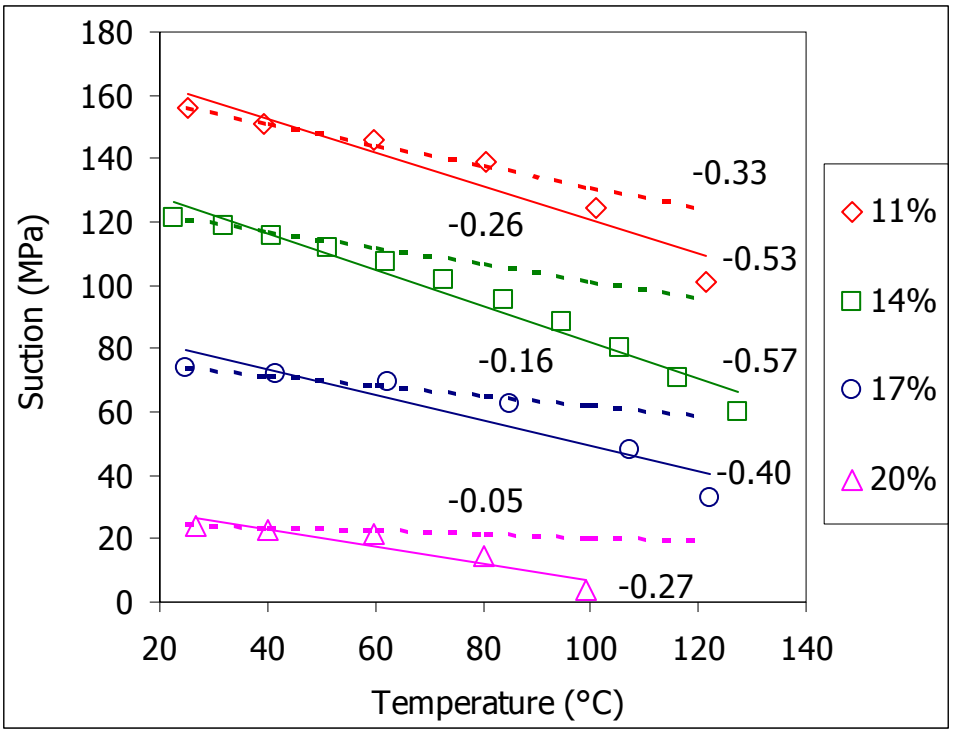

Figure 67: Change in suction with temperature for FEBEX bentonite compacted with different water contents (indicated in the legend) to dry density 1.60 g/cm^3 as measured with the sensor/cell method (continuous lines) and as computed by the change in water surface tension (dotted lines). The slope of the lines is indicated

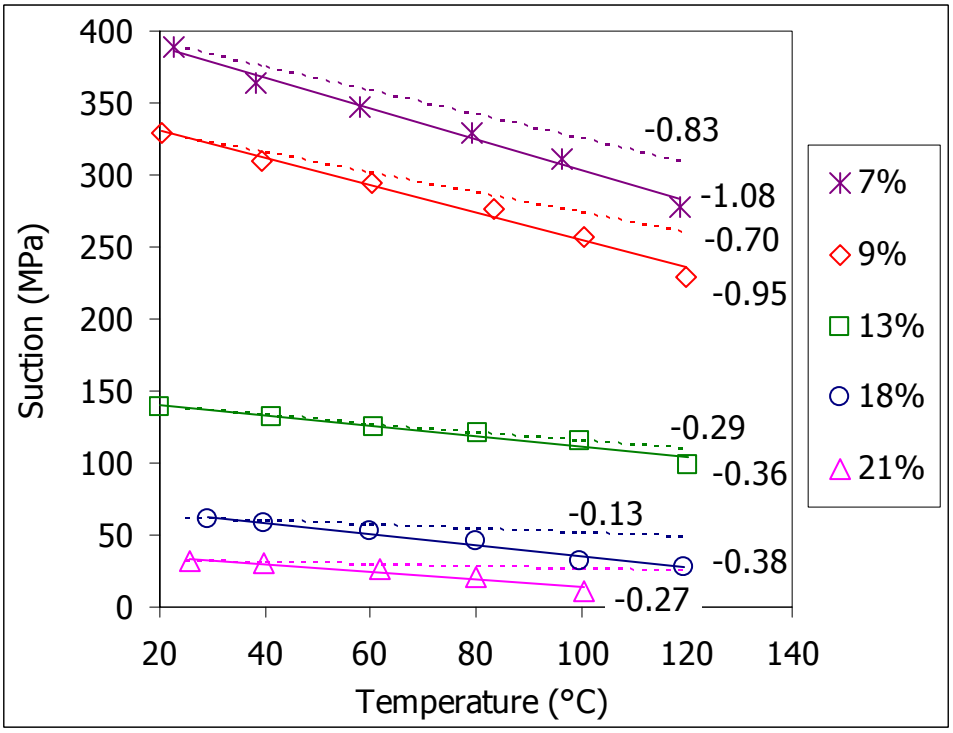

Figure 68: Change in suction with temperature for FEBEX bentonite compacted with different water contents (indicated in the legend) to dry density 1.75 g/cm^3 as measured with the sensor/cell method (continuous lines) and as computed by the change in water surface tension (dotted lines). The slope of the lines is indicated

5.4 Summary and discussion

The swelling under load tests have shown that the effect of temperature on the swelling capacity is smaller than the effect of the vertical load applied during hydration or the effect of initial dry density. The final strains obtained in all the tests have been plotted in Figure 69. For dry density 1.5 g/cm^3 the final vertical strain (ε, in %) can be related to vertical load (σ, in MPa) and temperature (T, in °C) through Equation 12, and the same type of relationship is given in Equation 13 for dry density 1.6 g/cm^3 and in Equation 14 for dry density 1.7 g/cm^3. The three equations can be merged in a single empirical equation that takes into account the effect of vertical load, temperature and initial dry density (ρ_d, g/cm^3) on the final vertical strain of the bentonite upon saturation with deionised water (Equation 15). The fittings obtained with this equation are also plotted in Figure 69. All these empirical relations are only valid for the ranges of density, vertical load and temperature tested.

$$\varepsilon = (-0.001\ \sigma + 0.04)\ T + (8.04\ \ln \sigma - 9.83) \quad [12]$$

$$\varepsilon = (-0.017\ \sigma + 0.09)\ T + (7.73\ \ln \sigma - 17.87) \quad [13]$$

$$\varepsilon = (0.029\ \sigma - 0.02)\ T + (7.50\ \ln \sigma - 20.40) \quad [14]$$

$$\varepsilon = 0.04\ T + 7.76\ \ln \sigma - 52.90\ \rho_d + 68.60 \quad [15]$$

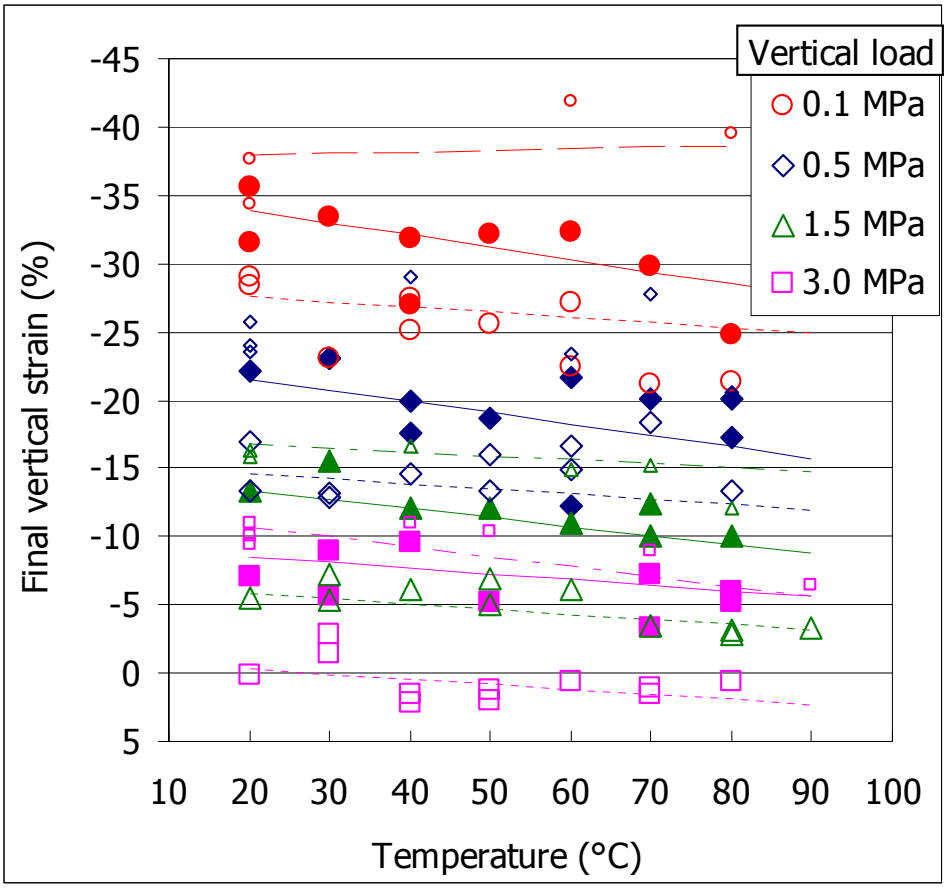

Figure 69: Final vertical strain of swelling under load tests performed with FEBEX bentonite compacted to nominal dry density 1.5 g/cm^3 (open symbols and dotted lines), 1.6 g/cm^3 (filled symbols and continuous lines) and 1.7 g/cm^3 (small symbols and discontinuous lines). The lines have been obtained with Equation 15

These results seem to indicate that the effect of temperature on the decrease in swelling capacity is rather independent of the density of the bentonite or of the vertical load applied, although the trends were less clear for the lowest dry density (1.5 g/cm^3, Figure 49). However, the results obtained in the swelling pressure tests (Figure 41) suggest that the effect of temperature is more important in high density samples.

Nevertheless, the extrapolation of the logarithmic correlation between swelling pressure and temperature (Figure 41) towards higher temperatures would indicate that swelling pressures higher than 1 MPa would develop even for temperatures of 100°C for the three densities tested. Lingnau *et al*. (1996) also observed a reduction in swelling pressure with temperature for a sand/bentonite mixture, although it did not show any loss in the self-healing capability of the material, even for temperatures of up to 100°C.

The decrease in swelling pressure and swelling capacity of the FEBEX bentonite with temperature has been explained as a consequence of the transfer of microstructural (interlayer) water to the macrostructure which is triggered by temperature (Ma & Hueckel 1992, 1993, Villar & Lloret 2004). Since the swelling in montmorillonites with predominance of divalent cations in the interlayer is mostly interlaminar and caused by the hydration of the exchangeable cations, the decrease in water in the interlayer would give place to a decrease in swelling. This process would be more significant in high-density samples, in which the interlayer water predominates initially over the "free" macroscopic water (Pusch *et al*. 1990).

With respect to the kinetics of swelling pressure development, the two-maximum path observed in the tests was also detected in infiltration tests performed in other clays and has been explained as a consequence of the collapse of the macropores caused by the decrease in suction due to the increase in water content, that is translated into a diminution of the initial swelling pressure. When the degree of saturation is higher, swelling affects all the material and predominates over the collapses, for what swelling pressure increases again and reaches a stable value (Imbert & Villar 2006).

No conclusive results have been obtained with respect to the influence of temperature on permeability. As expected, permeability increases with temperature, but it seems that this increase cannot be attributed solely to the water viscosity changes. The same processes responsible for the swelling decrease are probably involved in the additional increase in permeability.

The effect of density on the water retention capacity varies according to the suction range. For suctions below a threshold value –which is about 12-20 MPa– for a given water content and temperature the suction of the higher density samples is lower, and above this suction value the trend inverts. Anyway, the water retention capacity of the FEBEX bentonite decreases with temperature, especially when it is above 60°C and when the density of the bentonite is high, although the effect of dry density on the water retention capacity seems lower than that of temperature, at least for low suctions. This change cannot be explained on the basis of the changes of water surface tension with temperature. Instead, mechanisms related to the physico-chemical interactions that take place at microscopic level –in particular the transfer of interlayer water to the macropores triggered by temperature– seem to explain qualitatively the experimental observations. As it has been mentioned above, an increase in temperature produces a transfer of water from the interlayer region to the pores between the clay aggregates (macropores). Since the density of the interlayer, tightly-bound water in smectites is higher than one (Villar 2002, Marcial 2003, Jacinto *et al*. in press), the volume occupied by the interlayer water transferred to the macropores will be higher and the degree of saturation of the sample will increase –provoking a suction decrease– when the temperature is increased (Villar & Lloret 2004). The fact that the effect of temperature on the water retention capacity

is larger for high-density samples would be explained by the higher proportion of interlayer water in them.

Finally, taking into account all the results obtained with the sensor/cell method and the cell method, the following modified van Genuchten expression for the water retention curve has been fitted, and the parameters found for the Equation are shown in Table XI:

$$w = \left(b \cdot n^{c} \cdot e^{-\alpha(T-T_0)}\right)\left[1+\left(\frac{s}{P_0 \cdot e^{-\eta(n-n_0)} \cdot e^{-\alpha(T-T_0)}}\right)^{\frac{1}{1-\lambda}}\right]^{-\lambda} \qquad [16]$$

Table XI: Values of parameters in Equation 16

b	c	P_0 (MPa)	λ	η	n_0	α (1/ºC)	T_0 (ºC)
41.89	0.32	21.9	0.295	8.2	0.4	0.001	20

The difference between measured values and the values estimated using this Equation are smaller than 1.2 percent in terms of water content, with a trend to be lower for high density. Some of the experimental results and the fittings obtained with this equation are shown in Figure 70.

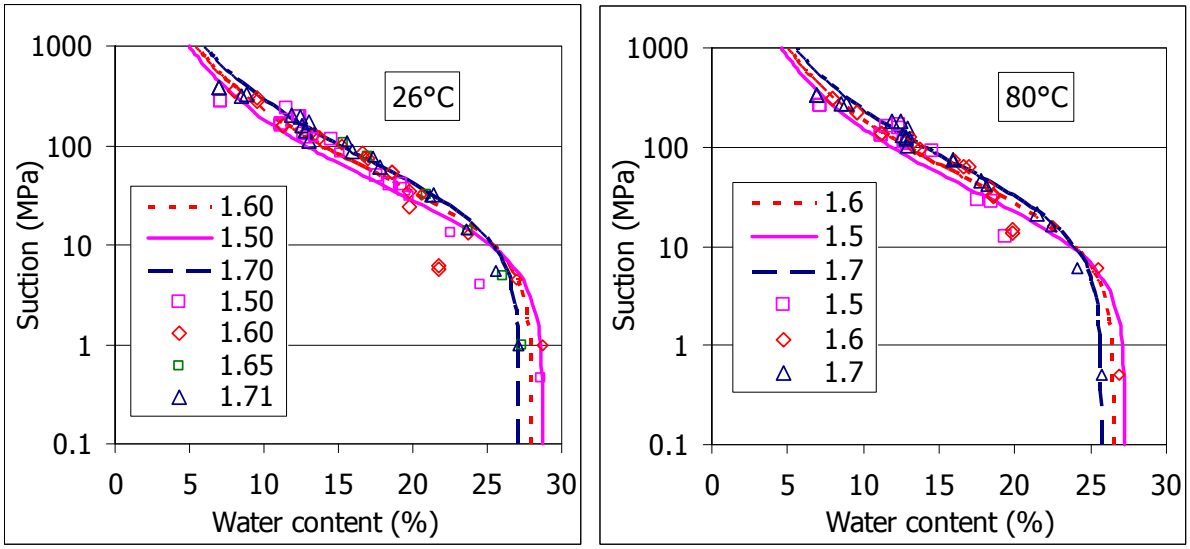

Figure 70: Water retention curves at different temperatures and for different bentonite densities (in g/cm^3) and fittings obtained with Equation 16 and parameters in Table XI

6 CONCLUSIONS

The results of the laboratory studies performed by CIEMAT in the context of WP3.2 of the NF-PRO Project and of the Agreement ENRESA-CIEMAT have been presented. They refer to the effect of the hydraulic gradient on the permeability of bentonite, the effect of the thermal gradient on the hydration of bentonite, and the repercussion of temperature on the hydro-mechanical properties of the bentonite. The information obtained improves the

knowledge on the behaviour of expansive clay and will help the development of constitutive models and the interpretation of the results obtained in the FEBEX mock-up and *in situ* tests.

The hydraulic conductivity of the FEBEX bentonite compacted at different dry densities between 1.4 and 1.65 g/cm^3 has been determined under low hydraulic gradients. No clear effect of the hydraulic gradient employed on the permeability value obtained has been detected. In addition, no evolution of the permeability with time (up to 1650 days) has been observed. The comparison of the new results with those obtained under higher hydraulic gradients during FEBEX I, points to the existence of a possible critical hydraulic gradient around 2000. The critical gradient is the hydraulic gradient below which flow occurs but it is not Darcian. The possible threshold hydraulic gradient would be around 200 or 1400, depending on the dry density. The dependence of the value of the threshold gradient on the density and injection pressure has been pointed out.

Infiltration tests with FEBEX bentonite compacted at dry density 1.65 g/cm^3 have been running for more than seven years. One of them is performed under thermal gradient, whereas another one is performed at isothermal conditions (laboratory temperature). The infiltration test performed under thermal gradient showed that the permeability to water vapour of the bentonite compacted with its hygroscopic water content (S_r~60%) is very high. The initial saturation of compacted bentonite takes place quicker under thermal gradient than at laboratory temperature. The increase in hydraulic conductivity with temperature would account for this. Afterwards, the water intake is higher for the sample tested under room temperature, as the hot zones of the sample tested under thermal gradient remain desiccated. In fact, both tests seem to have reached a steady state, since the relative humidity inside the bentonite barely changes, especially in test GT40, that reached a steady state much before. The weight changes of the cells have been also controlled, suggesting that the water intake is very low in both cases.

With respect to the effect of temperature on the hydro-mechanical properties of the clay, it has been measured the dependence of the swelling strains of bentonite compacted to dry densities of 1.7, 1.6 and 1.5 g/cm^3 on temperature in the interval from 20 to 90°C. At high temperatures the swelling capacity of the clay slightly decreases. On the other hand, a clear decrease in swelling pressure as a function of temperature was observed for the same dry densities. Nevertheless the deformation of bentonite is more dependent on the stress than on temperature. It has also been detected an increase with the temperature of the water saturated permeability of FEBEX bentonite compacted to these dry densities.

The effect of the temperature on the suction of bentonite has been determined for dry densities between 1.30 and 1.75 g/cm^3 and water contents between 7 and 22 percent in a range of temperature between 20 and 120ºC. For a given temperature and for suctions above 12-20 MPa, the suction measured in a sample is larger as the dry density is higher. This trend inverts for lower suctions. The water retention capacity of the bentonite decreases clearly with temperature, especially when it is above 60°C and when the density of the bentonite is high and the water content low. The decrease in retention capacity with temperature has been checked both on heating and on cooling, and there is not hysteresis between both processes. This decrease cannot be explained solely on the basis of the changes in water surface tension with temperature.

Overall, the observed effects of temperature on the hydro-mechanical properties can be qualitatively explained by considering the transfer of high-density interlayer water to the macropores that is triggered by the increase in temperature.

In spite of these observations, the FEBEX bentonite remains suitable as a sealing material in HLW repositories (from the hydro-mechanical point of view) for temperatures of up to 80°C, as it keeps its low permeability and self-healing ability. Not enough data are still available for higher temperatures, although the extrapolation of results points out to the preservation of properties for at least up to 100°C.

7 REFERENCES

Cuevas, J.; Villar, M.V.; Martín,M.; Cobeña, J.C. & Leguey, S. (2002): Thermo-hydraulic gradients on bentonite: distribution of soluble salts, microstructure and modification of the hydraulic and mechanical behaviour. *Applied Clay Science* 22 (1-2): 25-38.

Dixon, D.; Chandler, N.; Graham, J. & Gray M.N. (2002): Two large-scale sealing tests conducted at Atomic Energy of Canada's underground research laboratory: the buffer-container experiment and the isothermal test. *Can. Geotech. J.* 39: 503-518.

ENRESA (1995): Almacenamiento geológico profundo de residuos radiactivos de alta actividad (AGP). Diseños conceptuales genéricos. *Publicación Técnica ENRESA* 11/95. Madrid. 105 pp.

ENRESA (1998): FEBEX. Bentonite: origin, properties and fabrication of blocks. *Publicación Técnica ENRESA* 4/98. Madrid. 146 pp.

ENRESA (2000): FEBEX Project. Full-scale engineered barriers experiment for a deep geological repository for high level radioactive waste in crystalline host rock. Final Report. *Publicación Técnica ENRESA* 1/2000. Madrid. 354 pp.

ENRESA (2006): FEBEX Full-scale Engineered Barriers Experiment, Updated Final Report 1994-2004. *Publicación Técnica ENRESA* 05-0/2006. Madrid. 590 pp.

Fernández, A.M. (2003): Caracterización y modelización del agua intersticial en materiales arcillosos. Estudio de la bentonita de Cortijo de Archidona. *Ph.D. Thesis*. Universidad Autónoma de Madrid, 505 pp.

Imbert, Ch. & Villar, M.V. (2006): Hydro-mechanical response of a bentonite pellets/powder mixture upon infiltration. *Applied Clay Science* 32: 197-209.

Jacinto, A., Villar, M.V., Gómez-Espina, R. & Ledesma, A. (2009): Influence of temperature and density on the retention curve of compacted bentonite: modifications to the van Genuchten expression. *Applied Clay Science* 42: 575-582.

Jacinto, A., Villar, M.V., & Ledesma, A. in press. Influence of water density on the water retention curve of expansive clays. *Géotechnique*.

Karnland, O.; Sandén, T.; Johannesson, L.-E.; Eriksen, T.E.; Jansson, M.; Wold, S.; Pedersen, K.; Motamedi, M. & Rosborg, B. (2000): Long term test of buffer material. Final report on the pilot parcels. *SKB Technical Report* TR-00-22. Stockholm. 34 pp.

Lingnau, B.E.; Graham, J.; Yarechewski, D.; Tanaka, N. & Gray, M.N. (1996): Effects of temperature on strength and compressibility of sand-bentonite buffer. *Eng. Geol.* 41 (1-4): 103-115.

Lloret, A.; Villar M.V. & Pintado X. (2002): Ensayos THM: Informe de síntesis. Internal Report CIEMAT/DIAE/54520/1/02. *FEBEX Report* 70-UPC-M-0-04. Barcelona. 98 pp.

Lloret, A.; Romero, E. & Villar, M.V. (2004): FEBEX II Project Final report on thermo-hydro-mechanical laboratory tests. *Publicación Técnica ENRESA* 10/04. Madrid. 180 pp.

Ma, C. & Hueckel, T. (1992): Stress and pore pressure in saturated clay subjected to heat from radioactive waste: a numerical simulation. *Can. Geotech. J*. 29: 1087-1094.

Ma, C. & Hueckel, T. (1993): Thermomechanical effects on adsorbed water in clays around a heat source. *Int. J. Numer. Anal. Methods Geomech*. 17: 175-196.

Marcial, D. (2003): Comportement hydromécanique et microstructural des matériaux de barrière ouvragée. *Ph.D. Thesis*. École Nationale des Ponts et Chausées, Paris, 316 pp.

Martín Barca, M.(2002): Procesos geoquímicos y modificaciones texturales en bentonita FEBEX compactada sometida a un gradiente termohidráulico. *Ph.D. Thesis*. Universidad Autónoma de Madrid. 293 pp.

Missana T., Fernández, A.M., García-Gutiérrez, M., Mingarro, M., Rivas, P., Caballero, E., Huertas, F.J., García-Palma, S., Jiménez De Cisneros, C., Linares, J., Rozalén, M.L., Baeyens, B., Bradbury, M.H., Muurinen, A., Cormenzana, J.L. (2004): FEBEX II Project: THG Laboratory experiments. *Publicación Técnica ENRESA* 09/2004. Madrid. 137 pp.

Olsen, H.W. (1962): Hydraulic flow through saturated clays. 9th Nat. Conf. On Clays and Clay Minerals. *Pergamon*, Oxford. pp. 170-182.

Pintado X.; Ledesma, A. & Lloret, A. (2002): Backanalysis of thermohydraulic bentonite properties from laboratory tests. *Eng. Geol*. 64: 91-115.

Push R., Karnland O. & Hökmark H. 1990. GGM – A general microstructural model for qualitative and quantitative studies of smectite clays. *SKB Technical Report* 90-43.

Romero, E., Gens, A. & Lloret, A. (2001): Temperature effects on the hydraulic behaviour of an unsaturated clay. *Geotech. Geolog. Eng*. 19: 311-332.

Sánchez, M. (2004): Thermo-hydro-mechanical coupled analysis in low permeability media. *PhD Thesis*. Universitat Politècnica de Catalunya (UPC). Barcelona. 281 pp.

Villar, M.V. (2000): Caracterización termo-hidro-mecánica de una bentonita de Cabo de Gata. *Ph.D. Thesis*. Universidad Complutense de Madrid. Madrid. 396 pp.

Villar, M.V. (2002): Thermo-hydro-mechanical characterisation of a bentonite from Cabo de Gata. A study applied to the use of bentonite as sealing material in high level radioactive waste repositories. *Publicación Técnica* ENRESA 01/2002. Madrid. 258 pp.

Villar, M.V. (2007): Water retention of two natural compacted bentonites. *Clays and Clay Minerals* 55(3): 311-322.

Villar, M.V. & Lloret, A. (2004): Influence of temperature on the hydro-mechanical behaviour of a compacted bentonite. *Applied Clay Science* 26: 337-350.

Villar, M.V. & Gómez-Espina, R. (2008): Effect of temperature on the water retention capacity of FEBEX and MX-80 bentonites. In: Doll, D.G.; Augarde, C.E.; Gallipoli, D. & Wheeler, S.J. (eds.): Unsaturated soils: Advances in Geo-engineering. Proceedings of the first European Conference on unsaturated soils, E-UNSAT 2008. Durham, UK, July 2-4 2008. *CRC Press/Balkema*. Taylor & Francis Group, London. 257-262.

Villar, M.V.; Cuevas, J. & Martin, P.L. (1996): Effects of heat/water flow interaction on compacted bentonite. Preliminary results. *Eng. Geol*. 41: 257-267.

Villar, M.V., Martín, P.L. & Barcala, J.M. (2005a): Modification of physical, mechanical and hydraulic properties of bentonite by thermo-hydraulic gradients. *Eng. Geol*. 81: 284-297.

Villar, M.V., Martín, P.L. & Lloret, A. (2005b). Determination of water retention curves of two bentonites at high temperature. In Tarantino, A., Romero, E. & Cui, Y.J. (eds.),

Advanced experimental unsaturated soil mechanics. Experus 2005. *A.A. Balkema Publishers*, London. pp 77-82.

Villar, M.V., Gómez-Espina, R. & Martín, P.L. (2006): Behaviour of MX-80 bentonite at unsaturated conditions and under thermo-hydraulic gradient. *Informes Técnicos CIEMAT* 1081. Julio 2006. Madrid. 45 pp.

Villar, M.V.; Fernández, A.M.; Martín, P.L., Barcala, J.M., Gómez-Espina, R. & Rivas, P. (2008): Effect of heating/hydration on compacted bentonite: tests in 60-cm long cells. *Colección Documentos CIEMAT*. Madrid, 72 pp.

Yong, R.N.; Boonsinsuk, P. & Wong, G. (1986): Formulation of backfill material for a nuclear fuel waste disposal vault. *Can. Geotech. J.* 23: 216-228.

ANNEX TO REPORT ON THERMO-HYDRO-MECHANICAL LABORATORY TESTS PERFORMED BY CIEMAT ON FEBEX BENTONITE

2004-2008

TABLES OF DATA

Table A- I: Characteristics of the hydraulic conductivity measurements performed in test Grad1.4 (nominal ρ_d 1.40 g/cm^3)

Injection pressure (kPa)	Backpressure (kPa)	Hydraulic gradient	k_w (m/s)	Temperature (ºC)	Time (days)
499	400	399	$4.0 \cdot 10^{-13}$	20	112
450	400	200	$1.6 \cdot 10^{-13}$	21	143
399	300	399	$2.7 \cdot 10^{-13}$	21	182
350	300	200	$7.8 \cdot 10^{-13}$	21	201
350	299	201	No flow	27	260
399	300	399	$1.6 \cdot 10^{-12}$	28	290
499	299	801	$7.7 \cdot 10^{-13}$	28	304
499	299	800	$2.4 \cdot 10^{-13}$	25	367
549	399	600	$2.0 \cdot 10^{-13}$	20	462
449	350	400	$1.9 \cdot 10^{-13}$	19	487
549	349	800	$2.3 \cdot 10^{-13}$	21	502
1200	600	2400	$9.2 \cdot 10^{-13}$	23	544
1000	600	1600	$2.4 \cdot 10^{-13}$	22	564

Table A- II: Characteristics of the hydraulic conductivity measurements performed in test Grad1.40_2 (nominal ρd 1.40 g/cm^3)

Injection pressure (kPa)	Backpressure (kPa)	Hydraulic gradient	Outflow k_w (m/s)	Inflow k_w (m/s)	Temperature (ºC)	Time (days)
600	400	802	$3.9 \cdot 10^{-13}$		20	63
600	499	402	$4.5 \cdot 10^{-13}$		19	112
599	549	200	No flow	$9.8 \cdot 10^{-13}$	21	150
499	449	200	No flow	$9.3 \cdot 10^{-13}$	21	195
499	399	400	No flow	$8.2 \cdot 10^{-13}$	27	245
499	300	799	$5.0 \cdot 10^{-13}$	$8.9 \cdot 10^{-13}$	27	280
799	300	1999	$7.9 \cdot 10^{-13}$	$8.3 \cdot 10^{-13}$	28	332
399	299	400	No flow	$9.2 \cdot 10^{-13}$	24	364
699	300	1599	$7.6 \cdot 10^{-13}$	$7.6 \cdot 10^{-13}$	22	390
549	397	609	No flow	$7.5 \cdot 10^{-13}$	20	429
549	499	201	$9.0 \cdot 10^{-13}$	$7.0 \cdot 10^{-13}$	19	468
700	500	800	$8.3 \cdot 10^{-13}$	$6.0 \cdot 10^{-13}$	21	491

Injection pressure (kPa)	Backpressure (kPa)	Hydraulic gradient	Outflow k_w (m/s)	Inflow k_w (m/s)	Temperature (ºC)	Time (days)
699	400	1200	$6.1 \cdot 10^{-13}$	$6.7 \cdot 10^{-13}$	21	520
549	449	400	$6.7 \cdot 10^{-13}$	$7.5 \cdot 10^{-13}$	21	553

Table A- III: Characteristics of the hydraulic conductivity measurements performed in test Grad1.5 (nominal ρ_d 1.50 g/cm^3)

Injection pressure (kPa)	Backpressure (kPa)	Hydraulic gradient	k_w (m/s)	Temperature (ºC)	Time (days)
500	450	200	No flow	20	199
650	600	200	No flow	27	363
450	400	200	No flow	29	377
450	400	200	No flow	31	384
550	400	600	$1.1 \cdot 10^{-13}$	27	413

Table A- IV: Characteristics of the hydraulic conductivity measurements performed in test Grad1.55 (nominal ρ_d 1.55 g/cm^3)

Injection pressure (kPa)	Backpressure (kPa)	Hydraulic gradient	Outflow k_w (m/s)	Inflow k_w (m/s)	Temperature (ºC)	Time (days)
549	350	800	No flow	$2.3 \cdot 10^{-11}$	24	237
799	600	798	No flow	$1.5 \cdot 10^{-11}$	23	393
699	600	398	No flow	$1.9 \cdot 10^{-11}$	20	433
1199	600	2398	$3.3 \cdot 10^{-14}$	$8.1 \cdot 10^{-12}$	19	482
2400	600	7201	$1.5 \cdot 10^{-11}$		21	520
450	350	402	No flow		21	565
400	349	202	No flow		24	615
900	350	2202	$3.2 \cdot 10^{-12}$		27	650
700	350	1402	No flow	$2.6 \cdot 10^{-13}$	29	681
800	349	1802	No flow	$2.1 \cdot 10^{-13}$	26	734
1000	349	2602	$3.1 \cdot 10^{-14}$	$1.1 \cdot 10^{-13}$	22	760
600	350	1002	No flow	$1.6 \cdot 10^{-13}$	20	799
650	599	202	No flow	$6.7 \cdot 10^{-13}$	19	838
1200	350	3402	$5.4 \cdot 10^{-14}$	$9.4 \cdot 10^{-14}$	21	861
700	499	802	No flow	$2.3 \cdot 10^{-13}$	21	891
800	500	1202	No flow	$1.9 \cdot 10^{-13}$	21	923

Injection pressure (kPa)	Backpressure (kPa)	Hydraulic gradient	Outflow k_w (m/s)	Inflow k_w (m/s)	Temperature (ºC)	Time (days)
900	499	1602	$2.0 \cdot 10^{-14}$	$2.3 \cdot 10^{-13}$	23	967
700	600	400	No flow	$1.9 \cdot 10^{-13}$	25	1057
899	599	1200	$1.1 \cdot 10^{-14}$	$8.1 \cdot 10^{-14}$	21	1153
999	600	1600	$2.0 \cdot 10^{-14}$	$7.7 \cdot 10^{-14}$	19	1195
899	300	2400	$3.6 \cdot 10^{-14}$	$7.5 \cdot 10^{-14}$	22	1247
699	300	1600	$1.3 \cdot 10^{-14}$	$8.8 \cdot 10^{-14}$	22	1283
599	299	1200	No flow	$9.9 \cdot 10^{-14}$	23	1335
600	250	1400	$1.1 \cdot 10^{-14}$	$1.0 \cdot 10^{-13}$	24	1471
699	250	1799	$2.4 \cdot 10^{-14}$	$1.0 \cdot 10^{-13}$	20	1505
799	250	2199	$3.1 \cdot 10^{-14}$	$7.9 \cdot 10^{-14}$	20	1566
899	249	2600	$4.4 \cdot 10^{-14}$	$7.9 \cdot 10^{-14}$	23	1622
1199	250	3799	$3.5 \cdot 10^{-14}$	$9.3 \cdot 10^{-14}$	23	1650

Table A- V: Characteristics of the hydraulic conductivity measurements performed in test Grad1.65 (nominal ρ_d 1.65 g/cm^3)

Injection pressure (kPa)	Backpressure (kPa)	Hydraulic gradient	Outflow k_w (m/s)	Inflow k_w (m/s)	Temperature (ºC)	Time (days)
548	350	795	No flow	$2.3 \cdot 10^{-13}$	24	175
649	350	1200	No flow	$6.1 \cdot 10^{-13}$	29	285
449	349	400	No flow	$1.3 \cdot 10^{-12}$	27	342
749	550	799	No flow	$9.2 \cdot 10^{-13}$	23	393
649	549	400	No flow	$1.9 \cdot 10^{-12}$	20	433
749	349	1599	$1.2 \cdot 10^{-14}$	$2.6 \cdot 10^{-13}$	19	482
2400	600	7201	$9.7 \cdot 10^{-14}$		21	520
750	599	602	No flow		21	565
1200	599	2402	$5.2 \cdot 10^{-14}$		22	588
1000	600	1602	$2.9 \cdot 10^{-14}$		25	615
800	599	802	No flow		27	650
850	350	2002	9.3·10-15		29	681
950	349	2402	$3.3 \cdot 10^{-14}$	$2.0 \cdot 10^{-13}$	28	702
900	599	1202	No flow	$2.1 \cdot 10^{-13}$	24	734
900	550	1402	$1.3 \cdot 10^{-14}$	$1.4 \cdot 10^{-13}$	22	760

Injection pressure (kPa)	Backpressure (kPa)	Hydraulic gradient	Outflow k_w (m/s)	Inflow k_w (m/s)	Temperature (ºC)	Time (days)
800	550	1002	No flow	$1.8 \cdot 10^{-13}$	20	799
600	249	1402	$6.5 \cdot 10^{-14}$	$8.4 \cdot 10^{-14}$	20	861
600	399	804	No flow	$2.1 \cdot 10^{-13}$	21	890
600	300	1202	$1.4 \cdot 10^{-14}$	$1.6 \cdot 10^{-13}$	21	923
499	300	800	$1.4 \cdot 10^{-14}$	$1.9 \cdot 10^{-13}$	23	967
700	400	1200	$2.0 \cdot 10^{-14}$	$1.5 \cdot 10^{-13}$	25	1057
800	400	1600	$2.8 \cdot 10^{-14}$	$1.3 \cdot 10^{-13}$	21	1153
400	300	400	$2.0 \cdot 10^{-15}$	$5.7 \cdot 10^{-14}$	21	1247
500	249	1002	$1.8 \cdot 10^{-14}$	$1.9 \cdot 10^{-13}$	22	1283
400	250	602	No flow	$2.4 \cdot 10^{-13}$	23	1335
500	400	402	No flow	$3.6 \cdot 10^{-13}$	24	1456
1200	599	2402	No flow	$6.8 \cdot 10^{-14}$	20	1566
1899	599	5200	$1.4 \cdot 10^{-14}$	$6.2 \cdot 10^{-14}$	23	1650

Table A- VI: Results of the swelling pressure (P_s) tests at different temperatures for nominal dry density 1.40 g/cm^3 (actual 1.39 g/cm^3)

Test	Temperature (°C)	ρ_d (g/cm^3)	Duration (days)	P_s (MPa)	Final w (%)
EAP1_32	30	1.38	8	2.0	33.3
EAP2_32	80	1.39	8	0.7	28.5

Table A- VII: Results of the hydraulic conductivity (k_w) tests at different temperatures for nominal dry density 1.40 g/cm^3 (actual 1.38 g/cm^3)

Test	Temperature (°C)	ρ_d (g/cm^3)	Threshold hydraulic gradient	Hydraulic gradient	k_w (m/s)
EAP1_32	30	1.38	5000	10000-15000	$1.5 \cdot 10^{-13}$
EAP2_32	80	1.39		5000-15000	$4.7 \cdot 10^{-13}$

Table A- VIII: Results of the swelling pressure (P_s) tests at different temperatures for nominal dry density 1.50 g/cm^3 (actual 1.48 g/cm^3)

Test	Temperature (°C)	ρ_d (g/cm^3)	Duration (days)	P_s (MPa)	Final w (%)
EAP1_17	27	1.48	19	2.7	35.6
EAP2_17	27	1.49	19	2.3	34.0
EAP1_16	28	1.49	13	1.8	35.9
EAP2_16	28	1.50	13	1.7	34.6
EAP1_18	30	1.51	21	3.1	30.0
EAP1_30	30	1.49	33	1.3	38.3
EAP1_13	40	1.46	20	2.3	35.9
EAP2_30	40	1.51	33	1.8	33.6
EAP1_19	50	1.51	25	1.4	36.5
EAP2_18	60	1.48	21	1.7	33.5
EAP2_29	60	1.50	5	1.5	32.6
EAP2_19	70	1.49	25	1.6	33.1
EAP2_13	80	1.49	20	1.5	36.4
EAP1_28	80	1.51	8	1.3	29.0

Table A- IX: Results of the hydraulic conductivity (k_w) tests at different temperatures for nominal dry density 1.50 g/cm^3 (actual 1.48 g/cm^3)

Test	Temperature (°C)	ρ_d (g/cm^3)	Threshold hydraulic gradient	Hydraulic head gradient	k_w (m/s)
EAP1_17	28	1.48		5000-8333	$4.5\cdot10^{-14}$
EAP2_17	28	1.48		8333	$3.7\cdot10^{-14}$
EAP1_18	30	1.47		3333-5000	$4.5\cdot10^{-14}$
EAP1_30	30	1.47		15000	$3.5\cdot10^{-13}$
EAP1_13	40	1.46	5000	10000	$9.4\cdot10^{-14}$
EAP2_30	40	1.50		5000-15000	$2.4\cdot10^{-13}$
EAP1_19	50	1.48		1667-3333	$1.9\cdot10^{-13}$
EAP2_18	60	1.48		3333-5000	$2.8\cdot10^{-13}$
EAP2_29	60	1.50		5000	$4.0\cdot10^{-13}$
EAP2_19	70	1.48		1667-5000	$3.5\cdot10^{-13}$
EAP2_13	80	1.47	5000	10000	$5.3\cdot10^{-13}$
EAP1_28	80	1.45		5000-15000	$7.9\cdot10^{-13}$

Table A- X: Results of the swelling pressure (P_s) tests at different temperatures for nominal dry density 1.60 g/cm^3 (actual 1.57 g/cm^3)

Test	Temperature (°C)	ρ_d (g/cm^3)	Duration (days)	P_s (MPa)	Final w (%)
EAP1_1	25	1.56	26	3.9	39.5
EAP2_1	25	1.55	21	3.9	33.0
EAP1_3	30	1.55	9	4.5	31.5
EAP1_4	30	1.59	10	4.5	26.4
EAP1_5	30	1.58	10	2.4	29.9
EAP1_2	40	1.55	29	3.8	31.7
EAP1_6	40	1.55	7	2.7	32.5
EAP2_4	50	1.57	10	2.4	33.1
EAP2_6	60	1.58	6	1.5	25.5
EAP1_29	70	1.59	5	1.3	28.1
EAP1_7	80	1.58	25	1.3	29.0
EAP2_7	80	1.58	25	1.8	34.8

Table A- XI: Results of the hydraulic conductivity (k_w) tests at different temperatures for nominal dry density 1.60 g/cm^3 (actual 1.58 g/cm^3)

Test	Temperature (°C)	ρ_d (g/cm^3)	Threshold hydraulic gradient	Hydraulic gradient	k_w (m/s)
EAP1_1	25	1.56		11667-20000	$4.4\cdot10^{-14}$
EAP2_1	25	1.55	11667	16667-20000	$4.1\cdot10^{-14}$
EAP1_5	30	1.57		11667-16667	$1.1\cdot10^{-13}$
EAP1_6	40	1.61		11667-15000	$7.3\cdot10^{-14}$
EAP2_4	50	1.56		11667-16667	$1.2\cdot10^{-13}$
EAP2_6	60	1.62		11667-15000	$5.5\cdot10^{-14}$
EAP1_29	70	1.58		5000	$1.3\cdot10^{-13}$
EAP1_7	80	1.57		11667-15000	$1.1\cdot10^{-13}$
EAP2_7	80	1.58		11667-15000	$7.9\cdot10^{-14}$

Table A- XII: Results of the swelling pressure (P_s) tests at different temperatures for nominal dry density 1.70 g/cm^3 (actual 1.65 g/cm^3)

Test	Temperature (°C)	ρ_d (g/cm^3)	Duration (days)	P_s (MPa)	Final w (%)
EAP2_41	24	1.63	14	8.0	26.5
EAP2_25	30	1.65	9	5.9	27.5
EAP1_27	30	1.66	20	5.3	31.6
EAP1_31	30	1.65	12	5.5	27.8
EAP1_21	40	1.66	16	5.7	26.3
EAP1_22	40	1.61	7	6.4	23.8
EAP2_31	40	1.64	12	6.8	25.1
EAP1_24	50	1.64	13	4.8	31.7
EAP2_28	50	1.65	8	5.9	29.5
EAP2_24	60	1.65	13	5.2	29.1
EAP2_27	60	1.64	20		26.6
EAP2_23	70	1.65	15	3.3	29.1
EAP1_25	70	1.65	9	4.9	29.2
EAP2_21	80	1.66	16	4.3	29.7
EAP2_22	80	1.63	7	4.6	25.6
EAP1_33	80	1.63	5	10.8	26.5

Table A- XIII: Results of the hydraulic conductivity (k_w) tests at different temperatures for nominal dry density 1.70 g/cm^3 (actual 1.64 g/cm^3)

Test	Temperature (°C)	ρ_d (g/cm^3)	Threshold hydraulic gradient	Hydraulic gradient	k_w (m/s)
EAP2_25	30	1.64	5000	6667-10000	$6.4\cdot10^{-14}$
EAP1_27	30	1.65	10000		
EAP1_31	30	1.64	5000	10000-15000	$1.8\cdot10^{-14}$
EAP1_21	40	1.64	3333	5000	$8.9\cdot10^{-14}$
EAP2_31	40	1.64	5000	10000-15000	$4.1\cdot10^{-14}$
EAP1_24	50	1.63	11667		
EAP2_28	50	1.65	10000	15000	$2.4\cdot10^{-14}$
EAP2_24	60	1.64		5000-8333	$8.7\cdot10^{-14}$
EAP2_27	60	1.64	5000	6667	$4.2\cdot10^{-14}$
EAP2_23	70	1.64	3333	5000	$1.7\cdot10^{-13}$

Test	Temperature (°C)	ρ_d (g/cm^3)	Threshold hydraulic gradient	Hydraulic gradient	k_w (m/s)
EAP1_25	70	1.64	5000	6667	$8.7 \cdot 10^{-14}$
EAP2_21	80	1.65		3333-5000	$6.7 \cdot 10^{-13}$
EAP1_33	80	1.63	5000	15000	$2.8 \cdot 10^{-14}$

Table A- XIV: Results of the swelling under vertical pressure (0.1 MPa) tests at different temperatures with bentonite compacted at nominal ρ_d 1.50 g/cm^3

Temperature (°C)	Initial ρ_d (g/cm^3)	Initial *w* (%)	Final strain (%)	Duration (days)	Final *w* (%)	Final ρ_d (g/cm^3)
20	1.50	14.0	-29.0	52	49.3	1.16
20	1.49	14.8	-28.3	45	50.1	1.16
30	1.50	14.4	-23.0	31	48.0	1.22
40	1.50	13.7	-25.0	67	48.7	1.20
50	1.49	14.4	-25.5	46	49.1	1.19
70	1.50	13.6	-21.1	44	45.8	1.24
80	1.49	14.8	-21.3	46	50.3	1.23

Table A- XV: Results of the swelling under vertical pressure (0.5 MPa) tests at different temperatures with bentonite compacted at nominal ρ_d 1.50 g/cm^3

Temperature (°C)	Initial ρ_d (g/cm3)	Initial *w* (%)	Final strain (%)	Duration (days)	Final *w* (%)	Final ρ_d (g/cm^3)
20	1.50	13.8	-13.4	56	40.9	1.32
30	1.50	11.8	-12.8	97	37.6	1.33
50	1.48	12.8	-14.6	55	38.9	1.29
50	1.53	12.8	-15.9	49	38.5	1.32
60	1.51	12.1	-13.4	53	37.9	1.33
60	1.52	12.1	-14.9	70	38.7	1.33
70	1.49	13.2	-16.7	53	42.3	1.29
80	1.50	13.4	-18.3	85	40.2	1.26
90	1.50	14.8	-13.3	49	38.5	1.33

Table A- XVI: Results of the swelling under vertical pressure (1.5 MPa) tests at different temperatures with bentonite compacted at nominal ρ_d 1.50 g/cm^3

Temperature (°C)	Initial ρ_d (g/cm^3)	Initial *w* (%)	Final strain (%)	Duration (days)	Final *w* (%)	Final ρ_d (g/cm^3)
20	1.49	15.3	-5.5	40	36.9	1.41
30	1.49	13.6	-7.2	42	34.4	1.39
30	1.52	13.1	-5.3	38	34.6	1.44
40	1.51	13.3	-6.1	48	36.6	1.42
50	1.50	13.5	-5.0	45	37.8	1.43
50	1.49	15.0	-7.0	60	34.5	1.39
60	1.48	15.1	-6.2	60	36.0	1.39
70	1.51	13.2	-3.4	51	36.4	1.46
80	1.51	13.4	-2.9	42	33.4	1.46
80	1.51	13.2	-3.2	43	36.2	1.46
90	1.49	14.0	-3.3	38	38.0	1.45

Table A- XVII: Results of the swelling under vertical pressure (3.0 MPa) tests at different temperatures with bentonite compacted at nominal ρ_d 1.50 g/cm^3

Temperature (°C)	Initial ρ_d (g/cm^3)	Initial *w* (%)	Final strain (%)	Duration (days)	Final *w* (%)	Final ρ_d (g/cm^3)
20	1.49	14.4	0.7	39	33.2	1.49
30	1.50	13.6	-2.9	55	32.5	1.46
30	1.51	12.7	-1.5	24	31.6	1.49
40	1.51	14.0	1.6	29	33.7	1.53
40	1.49	12.8	2.1	21	32.7	1.52
50	1.50	15.1	2.0	42	35.4	1.53
50	1.48	15.2	1.3	41	35.0	1.50
70	1.52	12.6	1.6	29	30.0	1.54
70	1.50	13.6	1.1	21	30.9	1.52
80	1.50	13.1	2.2	55	30.3	1.53
80	1.56	10.1	0.7	43	31.8	1.57

Table A- XVIII: Results of the swelling under vertical pressure (0.1 MPa) tests performed at different temperatures with bentonite compacted at nominal ρ_d 1.60 g/cm^3

Temperature (°C)	Initial ρ_d (g/cm^3)	Initial *w* (%)	Final strain (%)	Duration (days)	Final *w* (%)	Final ρ_d (g/cm^3)
20	1.61	13.1	-31.6	79	47.0	1.22
20	1.56	14.0	-35.6	43	49.2	1.15
30	1.63	12.5	-33.5	57	43.6	1.22
40	1.62	13.3	-27.1	70	44.4	1.27
50	1.64	11.3	-32.1	71	43.0	1.24
60	1.62	12.6	-29.8	48	41.7	1.25
70	1.62	12.9	-29.8	36	44.1	1.25
80	1.60	13.3	-24.8	43	45.9	1.19

Table A- XIX: Results of the swelling under vertical pressure (0.5 MPa) tests at different temperatures with bentonite compacted at nominal ρ_d 1.60 g/cm^3

Temperature (°C)	Initial ρ_d (g/cm^3)	Initial *w* (%)	Final strain (%)	Duration (days)	Final *w* (%)	Final ρ_d (g/cm^3)
20	1.62	13.6	-22.1	66	40.0	1.32
30	1.61	13.0	-23.0	49	39.7	1.31
30	1.60	13.7	-23.1	90	40.4	1.30
40	1.59	15.5	-19.9	55	44.8	1.33
40	1.61	13.6	-17.5	32	36.4	1.37
50	1.63	11.5	-18.6	57	39.5	1.37
60	1.61	12.8	-12.2	37	37.9	1.44
60	1.61	13.1	-21.6	43	37.3	1.33
70	1.61	12.8	-20.1	56	37.5	1.34
80	1.62	13.2	-20.2	48	37.6	1.35
80	1.64	10.4	-17.2	26	35.2	1.40

Table A- XX: Results of the swelling under vertical pressure (1.5 MPa) tests at different temperatures with bentonite compacted nominal at ρ_d 1.60 g/cm^3

Temperature (°C)	Initial ρ_d (g/cm^3)	Initial *w* (%)	Final strain (%)	Duration (days)	Final *w* (%)	Final ρ_d (g/cm^3)
20	1.58	14.9	-13.4	39	36.2	1.40
30	1.62	13.1	-15.6	51	35.3	1.40
40	1.60	12.8	-12.1	39	35.7	1.43
50	1.58	14.6	-12.1	36	34.0	1.41
60	1.62	12.8	-11.0	23	32.7	1.46
70	1.61	12.5	-12.5	29	30.8	1.43
70	1.62	12.7	-10.1	34	32.6	1.47
80	1.62	12.4	-10.0	28	31.2	1.47

Table A- XXI: Results of the swelling under vertical pressure (3.0 MPa) tests at different temperatures with bentonite compacted at nominal ρ_d 1.60 g/cm^3

Temperature (°C)	Initial ρ_d (g/cm^3)	Initial *w* (%)	Final strain (%)	Duration (days)	Final *w* (%)	Final ρ_d (g/cm^3)
20	1.60	14.1	-7.1	38	31.8	1.49
30	1.61	13.0	-8.9	44	31.0	1.48
30	1.61	12.7	-5.7	39	31.8	1.53
40	1.60	14.1	-9.6	44	31.7	1.46
50	1.61	12.9	-5.3	30	31.0	1.53
70	1.62	12.9	-7.8	35	28.9	1.51
70	1.61	12.9	-3.2	27	29.6	1.56
80	1.59	13.2	-6.0	57	35.0	1.51
80	1.61	13.2	-5.2	30	28.8	1.53

Table A- XXII: Results of the swelling under vertical pressure (0.1 MPa) tests at different temperatures with bentonite compacted at nominal ρ_d 1.70 g/cm^3

Temperature (°C)	Initial ρ_d (g/cm^3)	Initial *w* (%)	Final strain (%)	Duration (days)	Final *w* (%)	Final ρ_d (g/cm^3)
20	1.70	13.7	-37.7	91	48.1	1.24
60	1.70	13.7	-41.9	39	51.6	1.70
80	1.70	13.5	-39.6	19	53.5	1.22

Table A- XXIII: Results of the swelling under vertical pressure (0.5 MPa) tests at different temperatures with bentonite compacted at nominal ρ_d 1.70 g/cm^3

Temperature (°C)	Initial ρ_d (g/cm^3)	Initial *w* (%)	Final strain (%)	Duration (days)	Final *w* (%)	Final ρ_d (g/cm^3)
20	1.69	13.9	-24.0	91	39.8	1.37
20	1.71	14.5	-25.8	63	40.4	1.36
20	1.68	15.4	-23.3	60	41.1	1.36
40	1.71	12.7	-28.9	19	37.0	1.32
60	1.69	14.1	-23.3	60	38.9	1.37
70	1.71	12.3	-27.8	19	37.2	1.34
80	1.70	14.0	-20.5	67	39.2	1.41

Table A- XXIV: Results of the swelling under vertical pressure (1.5 MPa) tests at different temperatures with bentonite compacted at nominal ρ_d 1.70 g/cm^3

Temperature (°C)	Initial ρ_d (g/cm^3)	Initial *w* (%)	Final strain (%)	Duration (days)	Final *w* (%)	Final ρ_d (g/cm^3)
20	1.70	14.2	-15.9	53	35.2	1.46
20	1.71	14.1	-16.4	63	34.1	1.47
40	1.69	14.3	-16.6	46	34.3	1.45
60	1.72	12.4	-14.9	39	33.0	1.50
70	1.69	14.4	-15.2	46	35.2	1.47
80	1.70	16.0	-12.2	44	32.4	1.52

Table A- XXV: Results of the swelling under vertical pressure (3.0 MPa) tests at different temperatures with bentonite compacted at nominal ρ_d 1.70 g/cm^3

Temperature (°C)	Initial ρ_d (g/cm^3)	Initial *w* (%)	Final strain (%)	Duration (days)	Final *w* (%)	Final ρ_d (g/cm^3)
20	1.69	14.3	-9.4	53	32.6	1.55
20	1.70	15.0	-10.0	30	32.1	1.55
20	1.70	14.9	-10.9	60	31.8	1.53
40	1.68	14.7	-11.0	53	31.8	1.52
50	1.73	13.8	-10.3	52	30.8	1.57
80	1.71	14.8	-6.1	30	31.0	1.61
90	1.68	14.7	-6.4	39	30.6	1.58

Table A- XXVI: Results of the retention curve determined with the cell method at constant volume and at 20°C for different dry densities (1 specimen per density)

Suction (MPa)	1.30 g/cm^3			1.40 g/cm^3			1.50 g/cm^3		
	w (%)	ρ_d (g/cm^3)	S_r (%)	w (%)	ρ_d (g/cm^3)	S_r (%)	w (%)	ρ_d (g/cm^3)	S_r (%)
121	13.8	1.30	35	14.0	1.40	41	13.4	1.50	45
83	15.7	1.30	39	15.6	1.40	45	15.1	1.50	51
31[a]	20.4	1.30	51	20.3	1.40	59	19.7	1.50	67
14	23.1	1.30	58	23.2	1.40	68	22.6	1.50	76
4[a]	25.5	1.30	64	25.5	1.40	74	24.5	1.50	83
0.5	31.4	1.30	79	31.4	1.40	91	28.6	1.50	97
4	31.1	1.30	78	30.7	1.40	89	28.9	1.50	97
14	24.4	1.30	61	24.5	1.40	71	24.0	1.50	81
33	21.3	1.41	63	21.5	1.51	74	21.0	1.59	81
62	17.8	1.45	56	18.5	1.56	68	18.5	1.61	74
127	13.4	1.47	43	14.0	1.59	54	14.2	1.66	61

[a]steps that had not reached stabilisation

Table A- XXVII: Results of the retention curve determined with the cell method at constant volume and at 60°C for different dry densities (2 specimens per density)

Suction (MPa)	1.30 g/cm^3			1.50 g/cm^3		
	w (%)	ρ_d (g/cm^3)	S_r (%)	w (%)	ρ_d (g/cm^3)	S_r (%)
17	21.9	1.30	55	22.0	1.50	74
6[a]	22.7	1.30	57	22.7	1.50	77
21	22.4			22.3		
36	19.2			19.6		
84	15.4			16.0		
100	14.2			14.9		

[a]steps that had not reached stabilisation

Table A- XXVIII: Results of the retention curve determined with the cell method at constant volume and at 70°C for different dry densities (2 specimens per density)

Suction (MPa)	1.30 g/cm^3			1.50 g/cm^3		
	w (%)	ρ_d (g/cm^3)	S_r (%)	w (%)	ρ_d (g/cm^3)	S_r (%)
141	12.4	1.30	31	11.9	1.50	40
112	14.2	1.30	36	13.2	1.50	44
72	16.8	1.30	42	15.2	1.50	51
22	20.6	1.30	52	20.1	1.50	68
7	25.3	1.30	63	25.2	1.50	85
20[a]	21.6			21.9		
35	18.9			18.8		
82	15.2			15.3		
151	11.4			11.6		

[a]steps that had not reached stabilisation

Table A- XXIX: Characteristics of the tests performed with FEBEX bentonite compacted at nominal ρ_d 1.50 g/cm^3 for determination of the retention curve with the sensor/cell method

Test	Initial ρ_d (g/cm^3)	Initial w (%)	Duration (days)	Final w (%)	Final ρ_d (g/cm^3)
150_7	1.50	6.6	73	7.1	1.62
150_11	1.52	11.2	75	11.2	1.51
150_12	1.50	12.9	51	12.7	1.50
150_14	1.48	14.6	40	12.4	1.55
150_17	1.48	17.5	84	12.4	1.58
150_18	1.48	18.5	73	11.6	1.56
150_20	1.55	19.4	70	19.2	1.54
150_21	1.53	21.2	70	21.2	1.52

Table A- XXX: Equilibrium temperatures and suctions measured during heating/cooling of FEBEX bentonite compacted at nominal ρ_d 1.50 g/cm^3 with different water contents (see Table A- XXIX for actual values of ρ_d and *w*)

1.50_7		1.50_11		1.50_12		1.50_14		1.50_17		1.50_18		1.50_20		1.50_21	
T (°C)	*s* (MPa)	*T* (°C)	*s* (MPa)	*T* (°C)	*s* (MPa)	*T* (°C)	*s* (MPa)	*T* (°C)	*s* (MPa)	*T* (°C)	*s* (MPa)	*T* (°C)	*s* (MPa)	*T* (°C)	*s* (MPa)
23	280	26	161	26	122	26	113	24	50	29	40	28	36	27	2
40	275	40	157	40	119	40	108	40	33	40	39	39	34	40	
60	270	60	153	61	119	59	105	60	31	62	40	60	30	60	
80	265	81	146	82	116	80	101	80	28	83	37	80	23	81	
99	260	101	132	101	106	101	92	100	30	100	29	100	13	100	
120	252	121	109	121	94	101	155	120	175	121	154	112	10	122	
99	261	101	129	101	112	78	171	100	168	94	164	60	33	100	
80	268	81	142	81	122	54	182	80	167	81	203	39	39	80	
60	273	60	152	60	128	38	188	60	167	61	216	29	40	59	
40	278	40	158	39	130	23	194	40	178	41	226			40	
27	281	25	164	24	132			24	196	27	235			30	2

Table A- XXXI: Characteristics of the tests performed with FEBEX bentonite compacted at nominal ρ_d 1.60 g/cm^3 for determination of the retention curve with the sensor/cell method

Test	Initial ρ_d (g/cm^3)	Initial *w* (%)	Duration (days)	Final *w* (%)	Final ρ_d (g/cm^3)
160_7_2	1.63	8.0	71	8.0	1.63
160_9	1.61	9.6	85	9.6	1.61
160_11	1.60	11.2	30	11.2	1.60
160_14	1.64	13.7	104	13.7	1.64
160_16	1.58	17.0	51	16.6	1.62
160_19	1.63	18.6	39	18.6	1.63
160_21	1.68	19.8	35	19.8	1.67
160_22	1.64	21.8	39	21.8	1.64

Table A- XXXII: Equilibrium temperatures and suctions measured during heating/cooling of FEBEX bentonite compacted at nominal ρ_d 1.60 g/cm^3 with different water contents (see Table A- XXXI for actual values of ρ_d and *w*)

1.60_7		1.60_9		1.60_11		1.60_14		1.60_16		1.60_19		1.60_21		1.60_22	
T (°C)	*s* (MPa)	*T* (°C)	*s* (MPa)	*T* (°C)	*s* (MPa)	*T* (°C)	*s* (MPa)	*T* (°C)	*s* (MPa)	*T* (°C)	*s* (MPa)	*T* (°C)	*s* (MPa)	*T* (°C)	*s* (MPa)
30	348	24	304	25	156	23	121	25	74	27	55	27	24	28	6
40	336	41	276	39	151	41	116	42	72	40	50	40	23	40	10
58	324	59	250	60	146	62	107	62	70	60		60	22	60	4
79	310	80	223	80	139	84	95	85	62	80	33	80	14	80	
100	288	100	197	101	124	105	80	107	48	100	19	99	4	100	
121	256	119	170	122	101	116	71	122	33	117	7	99	2	119	
99	289	100	203	100	123	105	84	104	49	99	18	81	14	82	
79	312	80	225	80	137	83	100	81	65	79	32	60	23	59	
60	328	60	245	60	145	62	114	62	73	59	43	40	30	40	0
40	343	44	259	40	151	41	124	39	81	39	50	28	35	27	6
28	357	25	283	28	155	28	129	26	84	28	53				

Table A- XXXIII: Characteristics of the tests performed with FEBEX bentonite compacted at nominal ρ_d 1.75 g/cm^3 for determination of the retention curve with the sensor/cell method

Test	Initial ρ_d (g/cm^3)	Initial *w* (%)	Duration (days)	Final *w* (%)	Final ρ_d (g/cm^3)
175_7	1.72	7.0	68	7.0	1.72
175_9	1.73	8.8	94	8.5	1.73
175_12	1.71	12.6	74	11.9	1.73
175_13	1.71	12.8	94	12.8	1.71
175_14	1.72	13.0	40	13.0	1.72
175_18	1.68	17.8	67	16.0	1.72
175_19	1.68	21.4	85	12.4	1.81

Table A- XXXIV: Equilibrium temperatures and suctions measured during heating/cooling of FEBEX bentonite compacted at nominal ρd 1.75 g/cm^3 with different water contents (see Table A- XXXIII for actual values of ρ_d and *w*)

1.75_7		1.75_9		1.75_12		1.75_13		1.75_14		1.75_18		1.75_19	
T (°C)	*s* (MPa)	*T* (°C)	*s* (MPa)	*T* (°C)	*s* (MPa)	*T* (°C)	*s* (MPa)	*T* (°C)	*s* (MPa)	*T* (°C)	*s* (MPa)	*T* (°C)	*s* (MPa)
23	389	20	329	28	162	20	139	24	111	29	61	26	32
38	364	39	309	38	158	41	132	41	106	40	58	40	30
58	347	60	295	68	148	61	126	60	105	60	53	62	27
79	329	83	276	94	133	80	121	78	101	80	45	80	21
96	311	100	257	101	129	100	115	100	91	100	31	100	11
119	278	120	230	120	136	120	99	120	109	120	28	120	137
99	309	101	257	102	163	100	117	100	145	100	61	98	166
78	334	82	278	81	181	81	126	79	156	80	75	76	180
60	350	62	292	57	191	60	132	59	162	60	80	60	186
42	362	40	306	42	196	40	138	40	165	40	85	40	191
27	388	25	318	26	203	27	141	25	169	27	88	26	195